
Electronic Thesis and Dissertation Repository

12-4-2014 12:00 AM


Design of a Haptic Interface for Medical Applications using Magneto-Rheological Fluid based Actuators

Nima Najmaei
The University of Western Ontario

Supervisor
Dr. Rajni V. Patel
The University of Western Ontario Joint Supervisor
Dr. Mehrdad R. Kermani
The University of Western Ontario

Graduate Program in Electrical and Computer Engineering
A thesis submitted in partial fulfillment of the requirements for the degree in Doctor of Philosophy
© Nima Najmaei 2014

Follow this and additional works at: <https://ir.lib.uwo.ca/etd>

 Part of the [Biomedical Devices and Instrumentation Commons](#), [Controls and Control Theory Commons](#), [Electro-Mechanical Systems Commons](#), and the [Robotics Commons](#)

Recommended Citation

Najmaei, Nima, "Design of a Haptic Interface for Medical Applications using Magneto-Rheological Fluid based Actuators" (2014). *Electronic Thesis and Dissertation Repository*. 2534.
<https://ir.lib.uwo.ca/etd/2534>

This Dissertation/Thesis is brought to you for free and open access by Scholarship@Western. It has been accepted for inclusion in Electronic Thesis and Dissertation Repository by an authorized administrator of Scholarship@Western. For more information, please contact wlsadmin@uwo.ca.

Design of a Haptic Interface for Medical Applications using Magneto-Rheological Fluid based Actuators

(Thesis Format: Integrated Article)

by

Nima Najmaei

Graduate Program in Engineering Science
Department of Electrical and Computer Engineering

A thesis submitted in partial fulfillment
of the requirements for the degree of
Doctor of Philosophy

The School of Graduate and Postdoctoral Studies
The University of Western Ontario
London, Ontario, Canada

© Nima Najmaei 2014

Abstract

This thesis reports on the design, construction, and evaluation of a prototype two degrees-of-freedom (DoF) haptic interface, which takes advantage of Magneto-Rheological Fluid (MRF) based clutches for actuation. Haptic information provides important cues in teleoperated systems and enables the user to feel the interaction with a remote or virtual environment during teleoperation. The two main objectives in designing a haptic interface are stability and transparency. Indeed, deficiencies in these factors in haptics-enabled telerobotic systems has the introduction of haptics in medical environments where safety and reliability are prime considerations. An actuator with poor dynamics, high inertia, large size, and heavy weight can significantly undermine the stability and transparency of a teleoperated system. In this work, the potential benefits of MRF-based actuators to the field of haptics in medical applications are studied. Devices developed with such fluids are known to possess superior mechanical characteristics over conventional servo systems. These characteristics significantly contribute to improved stability and transparency of haptic devices. This idea is evaluated and verified through both theoretical and experimental points of view. The design of a small-scale MRF-based clutch, suitable for a multi-DoF haptic interface, is discussed and its performance is compared with conventional servo systems. This design is developed into four prototype clutches. In addition, a closed-loop torque control strategy is presented. The feedback signal used in this control scheme comes from the magnetic field acquired from embedded Hall sensors in the clutch. The controller uses this feedback signal to compensate for the nonlinear behavior using an estimated model, based on Artificial Neural Networks. Such a control strategy eliminates the need for torque sensors for providing feedback signals. The performance of the developed design and the effectiveness of the proposed modeling and control techniques are experimentally validated. Next, a 2-DoF haptic interface based on a distributed antagonistic configuration of MRF-based clutches is constructed for a class of medical applications. This device is incorporated in a master-slave teleoperation setup that is used for applications involving needle insertion and soft-tissue palpation. Phantom and *in vitro* animal tissue were used to assess the performance of the haptic interface. The results show a great potential of MRF-based actuators for integration in haptic devices for medical interventions that require reliable, safe, accurate, highly transparent, and stable force reflection.

KEYWORDS: Haptics, Haptic Interface, Magneto-Rheological Fluids and Actuators, Mechanical Design, Prototyping, Modeling and Control, Needle Insertion, Soft-Tissue Palpation, Artificial Neural Networks, Simulation and Analysis, Virtual Wall

Statement of Co-Authorship

The thesis presented here has been written by me, under the supervision of Dr. Rajni V. Patel and Dr. Mehrdad R. Kermani. Part of the material in the thesis has been published in peer-reviewed journal and conference papers, or are under review for publication. My colleagues, Dr. Ali Asadian and Dr. Peyman Yadmellat have also served as co-authors in some of these papers. In all cases, the key ideas, primary contributions, experimental designs, data analysis, and interpretation, were mine. The research published has been guided, supervised, and supported by my research supervisors, Dr. Patel and Dr. Kermani. Dr. Asadian and Dr. Yadmellat have provided valuable support in preparing and conducting experiments.

I am aware of the University of Western Ontario's policies on authorship and I certify that I have properly acknowledged the contribution of all co-authors to my thesis. I certify that, with the above qualification, this thesis, and the research to which it refers, is the product of my own work.

IEEE copyrighted material in this thesis is used with the permission of the IEEE. The IEEE requires the following statement to be included as part of this permission: The IEEE does not endorse any of Western University's products or services. Internal or personal use of this material is permitted. If interested in reprinting or republishing IEEE copyrighted material for advertising or promotional purposes or for creating new collective works for resale or redistribution, please go to IEEE website to learn how to obtain a License from RightsLink.

The papers included in this thesis are as follow,

- Chapter 2: Effect of Smart Fluid Based Actuators on Transparency and Stability
 - **Najmaei N.**, Yadmellat P., Kermani M.R., Patel R.V., Application of Magneto-Rheological Fluid Based Clutches for Improved Performance in Haptic Interfaces , IEEE International Conference on Robotics and Automation, Hong Kong, June 1-4, 2014.
 - **Najmaei N.**, Kermani M.R., Patel R.V., Suitability of Small-Scale Magneto-Rheological Fluid Based Clutches in Haptic Interfaces for Improved Performance, IEEE/ASME Transactions on Mechatronics, in Press, 2014.

- Chapter 3: Design of Small-Scale MRF-Based Clutch Suitable for a Medical Haptic Interface
 - **Najmaei N.**, Yadmellat P., Kermani M.R., Patel R.V., Application of Magneto-Rheological Fluid Based Clutches for Improved Performance in Haptic Interfaces , IEEE International Conference on Robotics and Automation, Hong Kong, June 1-4, 2014.
 - **Najmaei N.**, Kermani M.R., Patel R.V., Suitability of Small-Scale Magneto-Rheological Fluid Based Clutches in Haptic Interfaces for Improved Performance, IEEE/ASME Transactions on Mechatronics, in Press, 2014.
- Chapter 4: Development, Modeling, Control, and Validation of a Prototype Clutch
 - **Najmaei N.**, Asadian A., Kermani M.R., Patel R.V., Magneto-Rheological Actuators for Haptic Devices: Design, Modeling, Control, and Validation of a Prototype Clutch, Submitted to IEEE International Conference on Robotics and Automation, Seattle WA, May 26-30, 2015.
- Chapter 5: Design and Development of a Prototype Two-DOF Haptic Interface
 - **Najmaei N.**, Asadian A., Kermani M.R., Patel R.V., Design and Evaluation of a Prototype Two-DOF Haptic Interface for Medical Applications based on Magneto-Rheological Actuation, Submitted to IEEE International Conference on Robotics and Automation, Seattle WA, May 26-30, 2015.
 - **Najmaei N.**, Asadian A., Kermani M.R., Patel R.V., Design of a Haptic Interface for Medical Applications using MRF-based Actuators, Submitted to IEEE/ASME Transactions on Mechatronics, 2014.

To the memory of Mansour Najmaei

Acknowledgement

I would like to extend my sincere gratitude and appreciation to all those who made this Ph.D. thesis possible. Special thanks are due to my supervisors, Dr. Rajni V. Patel and Dr. Mehrdad R. Kermani, for their support and guidance during this research. I am very grateful for all the great advice, constructive criticism, stimulating discussions, and their merciless red pen. Beyond all the help with this thesis, Dr. R.V. Patel has been a patient counselor, a trusted confidante, and an inspiring mentor, who always pushed me to become better with his fatherly manner and stood beside his naive son through his hard times. I am so grateful for the countless times he went out of his way to keep this project rolling.

Thanks also go to the members of my research group and my friends: Ali Asadian, Peyman Yadmellat, Chris Ward, Abelardo Escoto, Alex Shafer, Wenjun Li, Mostafa Hadavand, Amir Takhmar, Iman Khalaji, Mahta Khoshnam, Farokh Atshzar, and Mahya Shahbazi. It was truly a pleasure working and learning side by side with them. I really appreciate all their great help and consultations to this work. I would like to extend my special thanks to my true friend, Dr. Mahdi Azizian for his ideas and thoughtful help. Mahdi helped me in my first years of Ph.D. to find my path and he provided me with great advice and knowledge, which I will always hold close in mind through my professional and personal life.

I would like to thank my great friends all around the world for always being there for me. A special thanks goes to my brothers, Behzad Zamani, Ashkan Amirsadri, Saeed Zamani, Iman Shames, Ali Moatadelro, and Koosha Azhie. They were always on my side, no matter how far we were apart. I am so grateful for your true friendships.

I am deeply indebted to my family for their support and encouragement. My mom, Simin and my dad, Naser, have inspired me with their achievements, and instilled in me with confidence to set the bar high, and go for it. They never stopped believing in me and never said no when I needed help. My lovely sister, Dorna and her awesome husband, Hamid, it was a great feeling to know there are two great persons, not so far away, that always support me with their endless love and help my confidence with their great encouragement. Moreover, they gave me one of the best gifts in the world, my nephew, Daniel. The smile on the face of this little dude is worth the whole world to me. I would also like to thank my second parents and sister, Leila, Houshang, and Sheida for being so kind to me. I will never forget your understanding, support, and love throughout these years.

Last, but not least, I would like to thank my honey, lovely Sadaf, for her love, encouragement, help, and unflagging support. We spent many many days far away from each other. For always pushing me to become the best I can be. We have been through thick and thin together. Your love held us side by side and made me a better person. A new chapter has started and I want to make the best out of us. This thesis is dedicated to you.

Nima Najmaei, October 2014

Sources of Funding

I would like to thank all sources of funding for supporting this project.

Financial support for this study was provided by NSERC grants RGPIN-1345 (R.V. Patel) and RGPIN-346166 (M.R. Kermani). The design and construction of the haptic interface described in this thesis is part of a project on haptic devices for medical interventions and training (led by R.V. Patel) that is funded by an Ontario Research Fund Research Excellence Grant (RE-05-049). Financial support for N. Najmaei was also provided by an NSERC CGS-D Scholarship (N. Najmaei), an Ontario Graduate Scholarship (N. Najmaei), and an NSERC Collaborative Research and Training Experience (CREATE) program grant (R.V. Patel) on Computer-Assisted Medical Interventions.

Table of Contents

Abstract	ii
Statement of Co-Authorship	iii
Acknowledgement	vi
Sources of Funding	vii
List of Tables	xiv
List of Figures	xv
Abbreviations	xx
Nomenclature	xxi
1 Introduction	1
1.1 Haptics and the Issues of Stability and Transparency	1
1.2 Haptics in Medicine: Safety Concerns	2
1.3 Effect of Actuators on Stability and Transparency	3
1.4 Paradigm Shift in Actuation	4
1.5 Overview of the Dissertation	4

1.6	Fundamentals of Smart Fluids Based Actuators	6
1.6.1	Discovery and Current Applications	8
1.6.2	Actuators and Operational Modes	8
1.7	State of the Art: Application in Haptic Devices	10
1.7.1	Knobs, Joysticks, and Force Displays	11
1.7.2	Tactile Displays	14
1.7.3	Hand Masters	17
1.7.4	Rehabilitation Devices and Exoskeletons	20
	Bibliography	22
2	Theoretical and Experimental Evaluation of Transparency and Stability	27
2.1	Introduction	28
2.2	Transparency of Smart Fluid Based Force Feedback	30
2.2.1	Shear Stress	30
2.2.2	Actuator Inertia	31
2.2.3	Actuator Mass	31
2.2.4	Frequency Response	32
2.2.5	Hysteresis and Nonlinear Behavior (Disadvantages)	32
2.2.6	MRF vs. ERF	33
2.3	Stability of Smart Fluid Based Haptic Interfaces	34
2.3.1	Small-Gain Theorem	34
2.3.2	Virtual Wall Benchmark	37
2.4	Experimental Validation: Virtual Wall	41
2.4.1	Experimental Setup	41
2.4.2	Results	44

2.5	Concluding Remarks	46
	Bibliography	48
3	Design of a Small-Scale MRF-Based Clutch Suitable for a Haptic Interface	52
3.1	Introduction	53
3.2	Preliminary Design of a Small-Scale MRF-Based Clutch	54
3.3	Proposed Clutch Structure	54
3.4	Figures of Merit	57
3.4.1	Magnetic Reluctance and Flux	58
3.4.2	Actuator Mass and Reflected Inertia	61
3.5	Optimization	63
3.6	Comparison with MRF and Conventional Actuators	64
3.6.1	Comparison with Drum- and Disk-Based Clutches	65
3.6.2	Comparison with Conventional DC Motors	70
3.7	Challenges and Shortcomings	71
3.7.1	Heat Generation	72
3.7.2	Leakage	73
3.7.3	Friction	73
3.7.4	Thickening	74
3.7.5	Nonlinearity and Hysteresis	74
3.8	Concluding Remarks	75
	Bibliography	76

4	Development, Modeling, Control, and Validation of the Prototype Clutch	78
4.1	Introduction	79
4.2	Development of Four Prototype Small-Scale Clutches	80
4.2.1	Design Concept: Review	80
4.2.2	Final Design	81
4.2.3	Development and Construction	82
4.3	Figures of Merit	85
4.4	Comparison with Conventional Electrical Motors	87
4.5	Comparison with Conventional Rheological Actuators	88
4.6	Modeling And Control	89
4.6.1	ANN-Based Modeling Method	91
4.6.2	Torque Control Scheme	93
4.7	Results	93
4.7.1	Experimental Setup	93
4.7.2	Frequency Response	94
4.7.3	Validation of the Modeling Method	95
4.7.4	Evaluation of the Control Technique	97
4.8	Concluding Remarks	99
	Bibliography	101
5	Development and Evaluation of the Prototype Haptic Interface	104
5.1	Introduction	105
5.2	State of the Art	107
5.3	Design of the Two-DoF Haptic Interface	109
5.3.1	MRF-Based Clutch	109

5.3.2	Bidirectional Actuation: Antagonistic Configuration	110
5.3.3	Multi-DoF System: PA-DASA Configuration	111
5.3.4	Two-DoF Prototype Haptic Interface	113
5.3.5	Modeling and Control	114
5.4	Comparison to Off-the-Shelf Haptic Interfaces	115
5.5	Experimental Setups	117
5.5.1	<i>Configuration A</i> : Evaluation of Modeling and Control Methods . .	118
5.5.2	<i>Configuration B</i> : Virtual Wall Experiments	119
5.5.3	<i>Configuration C</i> : Needle Insertion Experiments	119
5.5.4	<i>Configuration D</i> : Tissue Palpation Experiments	120
5.5.5	<i>Configurations C*</i> and <i>D*</i> : Force Feedback Transparency	121
5.5.6	Configurations: Summary	122
5.6	Results: Validation of Antagonistic Control	122
5.7	Results: Evaluation of Force Feedback Stability	123
5.7.1	Virtual Wall Experiments	123
5.7.2	Phantom and <i>In Vitro</i> Needle Insertion and Palpation	125
5.8	Results: Evaluation of Force Feedback Transparency	128
5.8.1	Needle Insertion	129
5.8.2	Tissue Palpation	134
5.9	Concluding Remarks	135
	Bibliography	138
6	Concluding Remarks and Future Work	141
6.1	Summary of Research and Achievements	141
6.2	Contributions	143

6.3	Discussion: Manufacturing Expenses	144
6.4	Discussion: Shortcomings and Drawbacks	145
6.5	Future Work	146
A	Technical Drawings of the Parts	148
B	Kinematics and Dynamics of the Haptic Handle	157
B.1	Kinematics	158
B.2	Inverse Kinematics	159
B.3	Jacobian	159
B.4	Dynamics	160
	Curriculum Vitae	161

List of Tables

2.1	Transparency of the MRF-based clutch and DC Motor for different stiffness	46
3.1	Comparison between torque capacity of Maxon EC-max and MRF-based clutch with same dimensions <i>Note: ECXX YYW = EC-Max XX, YY Watt</i>	71
4.1	MR Clutch Dimensions and Specifications	86
4.2	MR Clutch Mass Specifications	87
4.3	MR Clutch Electromechanical Specifications and Comparison	88
4.4	Clutch Electromechanical Specifications and Comparison (\varnothing = diameter size)	89
5.1	Specifications of MRF-Based Clutches	110
5.2	Haptic Interface Specifications	114
5.3	Comparison to Off-the-Shelf Haptic Interfaces	116
5.4	Summary of Configurations used in the Experiments	122
6.1	List of Expenses for Manufacturing of a Single Clutch	144
B.1	DH Parameters of Haptic Handle	158

List of Figures

1.1	(a) Microscopic view of particles, and (b) schematic view of operation of the MRF and ERF [12]	7
1.2	Operation modes of MRF, (a) flow mode, (b) direct shear mode, and (c) squeeze mode.	9
1.3	A possible arrangement for robot joint actuation using an MRF-based clutch, through which the delivery of output torque at the joints is controlled	10
1.4	(a) An ERF-based joystick [44], and (b) an MRF-based joystick using MRF-based brakes and a gimbal structure [40]	13
1.5	(a) A passive force display using 2 ERF brakes [46], (b) a semi-active force display using two DC motors and four MRF-based clutches.	15
1.6	Haptic Black Boxes (a) Pinch Grasp, (b) HBB-I, (c) HBB-IMP, and (d) HBB-II	17
1.7	(a) MRAGES [59], (b) haptic glove with MRF-based brakes [34]	20
2.1	Interconnection of a master-slave system through a communication channel with time delay.	35
2.2	A simple model of the virtual wall consisting of an encoder, a discrete unilateral spring-damper system, and a Zero-Order Hold (ZOH) [35]	37
2.3	Block Diagram of the virtual wall haptic rendering system; including a haptic interface with physical mass m_p and damping b_p , a virtual wall with virtual stiffness K_W and virtual damping B_W , switching, and zero-order hold [39].	38

2.4	Stability margin of virtual wall display for no additional damping (R_1), additional constant damping (R_2), and controllable damping (R_3).	40
2.5	(a) The experimental setup. The mechanism takes advantage of MRF-based clutches as part of the actuator. (b) Sectional view of the prototype MRF-based clutch	42
2.6	Results of interaction with the virtual wall at 500 Hz with damping $B_w = 10 \frac{\text{Nms}}{\text{rad}}$ and different stiffness for the MRF-based clutch (top row) and the DC motor (bottom row). The virtual wall starts at 0 deg position.	45
2.7	Maximum achievable virtual stiffness $K_w [\frac{\text{Nm}}{\text{rad}}]$ for different virtual damping $B_w [\frac{\text{Nms}}{\text{rad}}]$ at 500 Hz for the MRF-based clutch and DC motor	47
3.1	The structure of (a) disk- [1] and (b) drum-based clutches [6].	55
3.2	(a) Cross-sectional and (b) exploded view of the proposed small-scale MRF-based clutch. (c) Depiction of the proposed clutch operation.	56
3.3	Dimension of the outer casing and a single pole of the clutch	58
3.4	Magnetic circuit model of the armature-based clutch	58
3.5	Figures in the left column show the magnetic field distribution in (a ₁) cross-sectional view of armature-based, and axisymmetric views of (b ₁) drum-based, and (c ₁) disk-based designs, with same volume. Figures in the right column depict the magnitude of the magnetic density in the MRF gap (shown by red dashed lines) perpendicular to the (a ₂) armature surface, (b ₂) cylindrical pole surface, and (c ₂) disk surface.	66
3.6	Comparison between the torque capacity of armature-, drum-, and disk-based designs with comparable volume	67
3.7	Comparison of (a) inertia-torque and (b) mass-torque ratios between armature-, drum-, and disk-based designs with comparable volume	69
3.8	Comparison of zero-field friction torque between armature-, drum-, and disk-based designs with comparable volume	70
3.9	(a) Inertia to torque (with gear reduction) and (b) mass to torque (without gear reduction) ratios for Maxon EC-max and MRF-based clutch	72

4.1	(a) Final version of the armature-based clutch and (b) the internal view	81
4.2	(a) Machined and (b) coiled armature of the system. (c) Silicon molding method used for (d) insulating the coil of the armature. (e) Location of one of the Hall sensors on the pole and routing of the wires through the keyhole. (f) Filling the gap between armature and outer casing with MRF.	83
4.3	The developed armature-based MRF clutch	84
4.4	The architecture of the ANN used for estimating output torque based on Hall sensor readings.	92
4.5	Closed-loop control configuration using embedded Hall sensors and the proposed ANN model	93
4.6	Experimental Setup	94
4.7	Frequency response of the system.	95
4.8	Modeling of hysteretic behavior of the system in response to sinusoidal currents of 1Hz (top row) and 4Hz (bottom row).	96
4.9	Modeling of the inner loops of the hysteresis	97
4.10	Results for the validation of the modeling technique by applying (a) chirp, (b) multi-sinusoidal, (c) damped sinusoidal, (d) cropped sinusoidal, (e) sinusoidal (1Hz), (f) sinusoidal (4Hz), (g and h)step-sequence current, and (i) sawtooth signals.	98
4.11	Results for the validation of the control method by applying (a) damped sinusoidal, (b and c) multi-sinusoidal, sinusoidal of (d) 0.5Hz, (e) 2Hz, (f) 5Hz, (g) 10Hz, and (h and i) step-sequence reference signals.	100
5.1	The developed MRF-based clutch used for actuation of the haptic interface.	109
5.2	(a) Isometric and (b) front views of the antagonistic configuration for bidirectional actuation.	111
5.3	PA-DASA configuration for bidirectional multi-DoF actuation.	112
5.4	Structure of the multi-DoF haptic interface.	113

5.5	Workspace of the multi-DoF haptic interface.	114
5.6	The two-DoF haptic interface.	117
5.7	<i>Configuration C</i> : Block diagram of the master-slave haptic teleoperation.	120
5.8	(a) The needle insertion robot [30, 31]. (b) <i>Configuration C</i> : Needle insertion setup. (c) <i>Configuration D</i> : Tissue Palpation Setup.	121
5.9	<i>Configurations C*</i> and <i>D*</i> : Use of a linear stage and a sensor for assessing accuracy.	121
5.10	Results for validation of the antagonistic control (<i>Configuration A</i>) by applying bidirectional multi-sinusoidal (left) and sinusoidal (right) reference signals	123
5.11	Maximum virtual stiffness that the MRF-based device, PHANTOM Omni, and Haptic Wand can render while remaining stable for (a) variable virtual damping, and (b) variable sampling time (<i>Configuration B</i>).	124
5.12	Results of interaction with the virtual wall (<i>Configuration B</i>) at 1 KHz with damping $B_w = 4 \frac{Ns}{m}$ and different stiffness for PHANTOM Omni, Haptic Wand, and the prototype system. (a-c) Stable interaction and (d-f) unstable interaction.	126
5.13	Results of needle insertion and retraction (<i>Configuration C</i>) on (a-c) an agar sample (10% concentration); and (d-f) an <i>in vitro</i> beef kidney.	127
5.14	Results of tissue palpation (<i>Configuration D</i>) on (a-c) an agar sample (10% concentration) and (d-f) an <i>in vitro</i> beef kidney.	128
5.15	<i>Configuration C*</i> , used for validating haptic feedback transparency using a large variety of samples.	129
5.16	(a) Desired and estimated torques in the clutches during insertion and retraction of a needle inside a homogeneous phantom. (b) Top row: desired and approximated torques of joints. Bottom row: the error between the two variables.	130
5.17	Desired, estimated, and actual force feedback at the end effector during insertion and retraction of a needle (<i>Configuration C*</i>) inside phantoms.	132

5.18	Desired, estimated, and actual force feedback at the end effector during insertion and retraction of a needle (<i>Configuration C*</i>) inside <i>in vitro</i> samples.	133
5.19	Desired, estimated, and actual stiffness at the end effector during palpation (<i>Configuration D*</i>) of phantoms samples.	134
5.20	Desired, estimated, and actual stiffness at the end effector during palpation (<i>Configuration D*</i>) of <i>in vitro</i> organs.	136
6.1	The problem of thickening in MRF-based clutch.	145
A.1	Dimensions of the capstan pulley in [mm]	148
A.2	Dimensions of the Armature in [mm]	149
A.3	Dimensions of the outer casing in [mm]	150
A.4	Dimensions of the outer casing cap in [mm]	151
A.5	Dimensions of the belt pulley in [mm]. Further Info: Fits 12.7 mm belt width, 36.52 mm outer diameter, 10 teeth, 1.94 inch pitch diameter, 9.52 mm pitch of the belt	152
A.6	Dimensions of the frames of the haptic interface in [mm]	153
A.7	Location of clutches with respect to each other in [mm]	154
A.8	Dimensions of the top frame in [mm]	155
A.9	Dimensions of the bottom frame in [mm]	156
B.1	Assigned frames to the haptic handle.	157

Abbreviations

MRF	Magneto-Rheological Fluid
ERF	Electro-Rheological Fluid
DoF	Degrees of Freedom
IOS	Input-to-Output Stability
ISS	Input-to-State Stability
ZOH	Zero-Order Hold
BVP	Bingham Visco-Plastic (model)
HB	Herschel and Bulkley (model)
PID	Proportional, Integral, and Derivative (controller)
RMS	Root Mean Square
FEM	Finite Element Model
FEMM	Finite Element Modeling Method
ANN	Artificial Neural Network
EDM	Electrical Discharge Machining
AWG	American Wire Gauge
DASA	Distributed Active Semi-Active
PA-DASA	Pluralized Antagonistic Distributed Active Semi-Active
UDP	User Datagram Protocol
TCP	Transmission Control Protocol
DH	Denavit-Hartenberg (parameters)

Nomenclature

B_W & K_W	Virtual Damping and Stiffness
b_p & k_p	Physical Damping and Stiffness
γ	IOS Gain of System
Z	Impedance
$T_i(t)$	Variable Time Delay
T_s	Sampling Time
v	Linear Speed
ω	Rotational Speed
\mathcal{R}	Magnetic Reluctance
μ	Magnetic Permeability
ϕ	Magnetic Flux
B	Magnetic Flux Density
H	Magnetic Field Strength
M	Mass
V	Volume
ρ	Mass Density
J	Moment of Inertia
i	Electrical Current
τ	Shear Stress
τ_y	Field-Dependent Shear Stress
η	Newtonian Viscosity
T	Torque
T_0	Zero-Field (Off-state) Torque
R	Radius
\mathcal{A}	Area

Chapter 1

Introduction

This chapter describes the research problem, namely the issue of stability and transparency in haptic devices for medical applications. In addition, an introduction to the proposed solution is given and denotes a paradigm shift in designing the actuation mechanism of haptic devices through the use of Magneto-Rheological Fluid (MRF) based clutches. The state of the art in this field is also reviewed in this chapter.

1.1 Haptics and the Issues of Stability and Transparency

Haptics studies the use of force and tactile feedback to simulate interaction with remote or virtual objects. Such feedback allows the user to perform appropriate force control actions, through the haptic interface, for safe and proper manipulation. In this regard, haptic sensation should be convincing enough to provide the user with a plausible feeling of being directly in contact with the remote or virtual environment. Such a desirable attribute is called transparency. The stability of the haptic system is another crucial issue in designing such systems. However, it is known that transparency and stability are conflicting design criteria [1][2].

1.2 Haptics in Medicine: Safety Concerns

Since its inception, haptics has attracted a great amount of interest from different sectors of the robotics industry. The force and tactile feedback provided by haptic devices can enable the user to adjust force control actions to ensure accuracy and safety of operations. This significantly improved the quality of telerobotic tasks. In recent years, with the rapid growth in applications of minimally invasive medical interventions, the integration of haptics into such applications has been identified as a high-priority objective in major medical robotics roadmaps [3][4]. Motivated by in-depth research, it is not difficult to imagine the benefits of providing a clinician using robotics-based systems with the feeling of being directly in contact with tissues and organs. Such sensation can improve the intuitiveness of minimally invasive interventions. In addition, it enables the clinicians to control the quality of tasks during procedures (*e.g.*, proper suture knot tying, achieving adequate contact during cardiac ablation) and to avoid causing any damage to tissue by exerting too much force [5]. However, the introduction of haptics in minimally invasive applications brings to light a number of safety concerns particularly among standardization bodies, robotic manufacturers, and researchers [6][7]. This is to be expected since the fundamental premise behind existing safety norms is a high level of reliability and safety of medical devices. However, the issue of stability of haptics-enabled telerobotic systems hampered the introduction of haptics into medical environments [4]. Due to the susceptibility of bilateral teleoperation systems to time delays, there is a possibility that such systems can become unstable as a result of the reflected slave force and induced master motion mechanism [8]. Thus, much research has focused on developing reliable control techniques for haptic applications. To this end, the use of passivity-based and small-gain approaches have been reported in [9][10]. However, the conservative nature of such methods results in degraded quality of force reflection. This calls for a long and costly amount of training for the medical staff to enable them to efficiently use the designed devices.

1.3 Effect of Actuators on Stability and Transparency

Another body of work has focused on addressing this issue through redesigning the actuation mechanisms in haptic interfaces. The actuators and mechanisms used in designing a haptic interface play an important role on the quality of force feedback, as well as the stability of the system. This makes the design of a haptic interface twofold challenging. In order to have transparency, it is of utmost importance that while a haptic device is capable of recreating the forces that occur during contact with stiff objects, it exhibits low friction, damping, and inertia to sustain transparency during motion in free space. Poor dynamics and control of manipulation can affect the sense of touch, in particular when rigid instruments or actuators are used [11]. Heavy and/or cumbersome haptic systems generate artifacts which negatively affect the quality of the virtual presence [12]. The use of electrical motors in haptic devices, especially for medical applications, has proved to be challenging for several reasons. The poor dynamics of electrical motors, imposed by the need for gear reduction, can significantly reduce the transparency of the system by increasing the damping, inertia, and friction of the haptic device [13]. This is highly problematic in medical applications that require high-fidelity and accurate force reflection. Moreover, their active nature (which may be exhibited in the form of oscillations and jerks) can result in degradation of stability, which is unacceptable in medical applications [8][14]. In addition, such actuators can exhibit oscillations and jerks [14], which can not only cause uncomfortable forces for the user, but are highly problematic in delicate operations [15]. While control-based methods [9][10] can alleviate these problems to a great extent, they significantly degrade the quality of haptic telepresence. As a result of the aforementioned safety concerns and their inadequate efficiency in terms of transparency, the application of haptics in medicine is almost nonexistent and is highly limited to research. This work looked into the use of a semi-active actuation mechanism to mitigate the safety and stability concerns, with the hope of easing (*to a small extent*) the entry of haptics into medicine.

1.4 Paradigm Shift in Actuation

Actuators based on Magneto-Rheological Fluids (MRFs) have been proposed as an alternative for use in haptic devices [11]. MRFs exhibit a very unique characteristic: the viscosity and shear stress of these fluids can be intelligently controlled using an applied magnetic field. Several passive and semi-active actuators have been developed by taking advantage of this feature. Such systems exhibit remarkable characteristics, including high yield stress, low mass-torque and inertia-torque ratios, compact size, intrinsic passivity, and precision controllability [16, 17]. It is expected that the superior characteristics of MRF-based actuators in comparison with active actuators will enable the design of a more transparent and stable haptic interface.

An investigation of this idea is carried out in this work. To this end, several theoretical and experimental studies have been performed to study the effect of MRF-based actuators on the performance of a haptic interface. The end result of this work is a prototype two-DoF MRF-based haptic interface developed for medical applications. The performance of this system is validated through rigorous tests conducted in needle insertion and soft-tissue palpation applications from medical robotics. While further investigations are required, the promising results show the great potential of MRF-based actuators to be used in haptic devices for medical applications that require accurate, stable, reliable, high fidelity, and transparent force feedback.

1.5 Overview of the Dissertation

An overview of the presentation and contribution of each chapter of this thesis is as follows;

Chapter 1: Introduction

The research problem is described and the proposed solution is discussed. The fundamentals of smart-fluids based actuators are briefly introduced. A review of the state-of-the-art (application of smart fluid-based actuators in haptics) concludes this chapter.

Chapter 2: Study of Transparency and Stability

The physical characteristics of the MRF-based actuators, which contribute to transparency of the system are reviewed. The results of applying the small-gain theorem and virtual wall benchmark are employed to describe the effect of MRF-based actuators on stability of a teleoperation system. Next, a large-scale 1-DoF MRF-based haptic interface is used to study the stability of the system in comparison to a haptic device based on electrical motors.

Chapter 3: Design of a Small-Scale MRF-based Clutch

A novel design for a small-scale actuator, called an armature-based design, is proposed, which exhibits superior mechanical characteristics and is suitable for use in a medium-size haptic interface. Simulation and analysis of the mechanical characteristics of the designed clutch are performed and its output torque, mass, and reflected inertia are derived. These properties are then compared with those of conventional small-scale electrical motors and conventional MRF-based clutch designs.

Chapter 4: Development and Evaluation of the Small-Scale MRF-based Clutch

The development and construction of four MRF-based clutches based on the proposed design are reported. The properties of the developed system are compared with those of conventional electrical motors and existing MRF-based actuators used for haptic applications. A modeling method based on artificial neural networks is provided to predict the nonlinear behavior of the clutch. In addition, a sensor-less control scheme is proposed for efficient control of the output torque of the clutch. Several experiments are performed to

validate the performance of the clutch, and the modeling and control technique.

Chapter 5: Development and Evaluation of the Haptic Interface

A prototype haptic device is developed based on a distributive antagonistic configuration. The performance and specifications of this system are compared with those of a PHANTOM Omni, a PHANTOM Desktop, and a Quanser Haptic Wand. Several experiments are performed to assess the improvement of stability using the developed system in comparison with the PHANTOM Omni and the Quanser Haptic Wand. To this end, needle insertion and tissue palpation on phantom and *in vitro* animal tissues are considered. Furthermore, the accuracy of the system in providing transparent force feedback to the user is studied through the same medical applications.

Chapter 6: Conclusion and Future Work

An overview of the cost of developing the haptic interface and future approaches to reduce this cost are given. The disadvantages and drawbacks of the proposed system are reviewed and potential solutions are outlined. Possible future steps of the project conclude the thesis.

REMARK 1. Electro-Rheological Fluids (ERF) are another type of smart fluids, which have several similarities to MRF. In this chapter and in a portion of Chapter 2, ERF-based systems are also considered for the sake of comparison. However, as explained in the next chapter, this research is only focused on MRF-based actuators because of their superior characteristics and potential for use in a medical haptic device.

1.6 Fundamentals of Smart Fluids Based Actuators

MRF is a suspension of micrometer-sized ferrous particles in an oil-like carrier fluid. ERF consists of extremely fine non-conducting particles suspended in an electrically insulating

fluid. When these fluids are subjected to an externally applied field (magnetic field for MRF, and electric field for ERF) the particles aggregate into columns aligning themselves in the direction of the applied field (Fig. 1.1). Consequently, the columns act to resist shearing or flow of the fluid. The apparent yield stress of the fluid is dependent on, and increases, with the intensity of the applied field. [18]. In the absence of a field, these fluids act as Newtonian fluids, whose viscosity changes proportionally to the shear rate.

MRF consists of three main components: magnetizable particles (20% to 45% of total volume), a carrier fluid, and additives [19]. The variety in selection and combination of these components defines all the characteristics of the fluid, *e.g.*, viscosity, shear stress, operating temperature range, etc. ERF consists of suspended particles in a liquid whose dielectric constant or conductivity is mismatched to create dipolar particle interactions in the presence of an electric field [20].

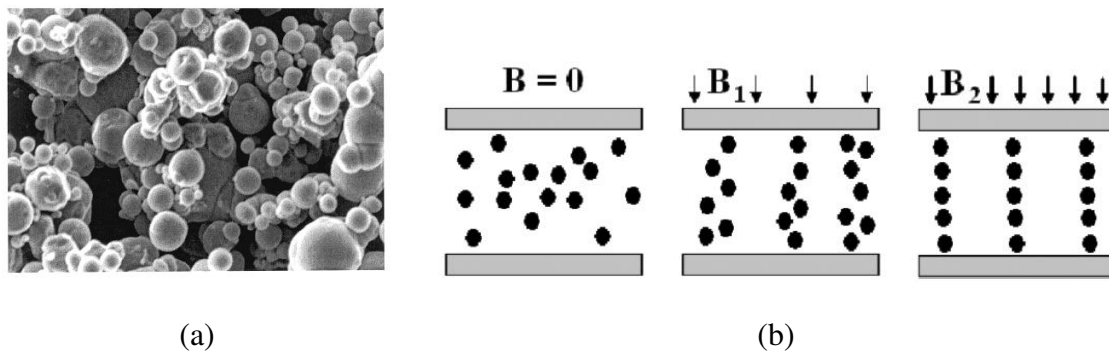


Figure 1.1: (a) Microscopic view of particles, and (b) schematic view of operation of the MRF and ERF [12]

1.6.1 Discovery and Current Applications

Since the discovery of ERF in 1949 by W.M. Winslow, a large number of studies have been performed on this fluid, mainly motivated by potential automotive applications [19]. Despite these major efforts, ERF-based devices failed to reach the commercialization stage, due to their numerous limitations. Vibration control remains as their main application area where such devices provide industrially-suitable damping force ranges. Their current applications are limited to prototypes of engine mounts, vehicle shock absorbers, and shock struts [21]. The need for ERF-based systems to have high voltage power supplies, expensive wires and connectors, their temperature dependence, and their high sensitivity to impurities hampered their commercialization [22].

J. Rabinow discovered MRF shortly after the discover of ERF. However, there were no substantial studies on this type of fluids until the 1990s when it was realized that they are capable of producing ten to twenty times greater shear stress in comparison to ERF, which led to devices with much smaller volumes and weight for comparable performance. In addition, their simple and inexpensive electronics, much lower temperature dependency, and insensitivity to impurities enabled real-time applications of MRF-based devices [22]. In comparison to ERF-based devices, researchers have been more successful in developments and commercialization of MRF-based devices, especially in the automotive industry. More details will be given in Chapter 2.

1.6.2 Actuators and Operational Modes

Using MRFs or ERFs, an actuation system can be constructed such that the amount of transmitted torque/force can be controlled by the intensity of an applied field. MRFs and ERFs exhibit such behavior in three operational modes, namely shear, flow, and squeeze

modes [23] (Fig. 1.2). In shear and squeeze modes, the fluid resists the motion of plates perpendicular to and along the applied field, respectively, while in flow mode, the flow of the fluid itself is resisted due to the formed particle columns [23, 24]. In shear mode, the force required to cause the fluid to shear depends on the intensity of the applied field. In squeeze mode, for a given force, the displacement of the moving pole is controlled by the intensity of the field. Displacement amplitudes are very small but resistive forces are very high. Brakes and clutches have been developed based on the shear mode of MRFS and ERFS. Dampers and shock absorbers take advantage of the flow mode [25], while several compliance-mimicking tactile displays with limited torque/force capacity have been developed using the squeeze mode [26].

Actuators based on such fluids have several advantages over conventional actuators including fast time response, high torque density, low power consumption, and intrinsic passivity [27]. The insensitivity to contamination, durability, and long service life of MRF further empower their commercial utilization. The characteristics of smart fluids based actuators depend on the mode in which the actuator operates, and differ from one type to another. Our focus in this study is only on shear mode in the form of clutches and their application in haptic interfaces. Clutches can be employed in the actuation mechanism of robot manipulators to control the delivery of output torque at the joints. Fig. 1.3 depicts a possible

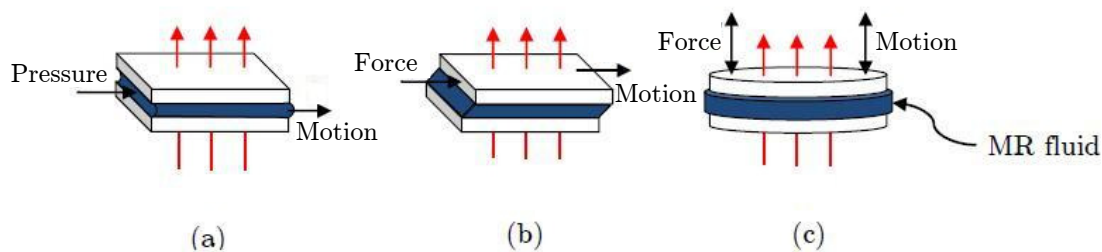


Figure 1.2: Operation modes of MRF, (a) flow mode, (b) direct shear mode, and (c) squeeze mode.

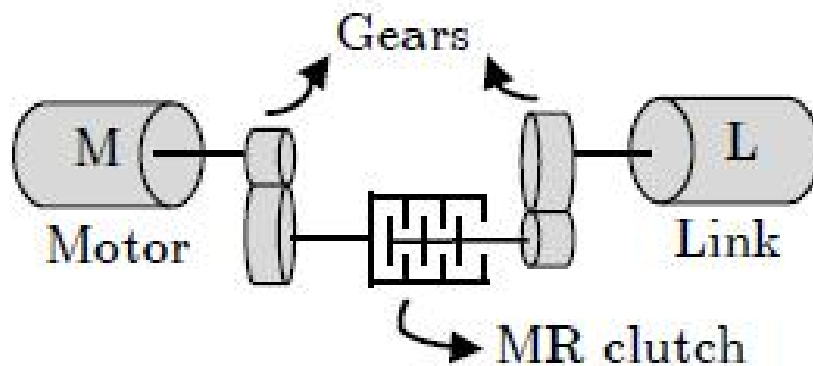


Figure 1.3: A possible arrangement for robot joint actuation using an MRF-based clutch, through which the delivery of output torque at the joints is controlled

arrangement for actuating a robot joint. The active drive (*i.e.*, motor) provides power to the joint via a clutch that controls the output torque. The justification for such a choice is discussed in Chapter 2.

1.7 State of the Art: Application in Haptic Devices

Several haptic devices have been developed based on MRF- and ERF-based actuators. These devices can be roughly categorized into four types, namely,

1. Force Displays: knobs, joysticks, and parallel-link displays [14, 28, 29]
2. Tactile Displays: pinch grasps, haptic black boxes, etc. [11, 12, 30, 31]
3. Hand Masters: ground-mounted mouse, haptic gloves [32–34]
4. Rehabilitation Devices and Exoskeletons [35–37]

1.7.1 Knobs, Joysticks, and Force Displays

These are the simplest types of haptic devices. Several studies have taken advantage of MRF- or ERF-based brakes, dampers, and even clutches in developing single- and multi-DoF force displays. These systems are applicable to a wide range of applications, from virtual reality to space exploration and from vehicular instrument control to minimally invasive surgery.

Knobs

The application of MRF and ERF-based knobs in virtual reality and vehicular instrument control has been reported in the literature. In [38], a disk-type MRF-based brake was used as a control knob to perform a simple 1-DoF task in virtual reality. In this device, by controlling the stiffness of the brake, a simulated feel for events happening on the display was provided to the user. This control knob consisted of a shaft with a flat circular plate in the middle enclosed in a magnetic soft iron core containing MRF. On the lower part of the actuator a rotor-type potentiometer is attached to measure the displacement of the knob. The knob is capable of providing resistive (passive) torque ranges from 0.01 to 0.17 Nm. In another study, a 1-DoF joystick was developed [39, 40] in the same fashion. This system is capable of generating a maximum of 0.8 Nm resistive torque.

An MRF-based damper was developed by Ahmadkhanlou et al. in [28, 41]. This damper was used in a steer-by-wire vehicle to provide haptic feedback to the driver. A system that controls automotive steering by means of computer-controlled electronic signals instead of a direct mechanical linkage through the steering column is called steer-by-wire system. The main problem with these systems lies in the fact that without the steering columns, there is no mechanism for tactile feedback for the driver. Hence, the driver suffers from

the lack of meaningful information about what is happening on the road. In this study, an MRF-based damper was developed, which can apply 15 Nm of torque and was coupled to the steering wheel. By applying a current to the damper, it is possible to generate resistance torque when the driver rotates the steering wheel.

In another work [42], Vitrani et al. developed a disk-type ERF-based brake with application in vehicular instrument control. It was shown in this paper that an ERF-based brake used in conjunction with a nonlinear PI controller (with feed-forward) exhibits a precise and accurate response, compatible with use in a haptic application. The maximum applicable torque with this device is about 0.05 Nm. Another 1-DoF ERF-based joystick was developed by Bose et al. in [43] which is capable of generating torques of up to 1.2 Nm (at field strength of 3 Kv/mm).

Joysticks

A 2-DoF ERF-based joystick was developed in [44] (Fig. 1.4(a)). This device takes advantage of 2 ERF-based disk-type brakes. The actuators were mounted at right angles to each other. In the center was a two-degree of freedom joint on which the joystick handle is mounted. The shafts from the actuators extend towards the joint where they are attached. The joint itself was mounted with four bearings, to reduce any bending moment on the shafts. A low-profile rotary encoder is attached to each shaft to measure angular displacement. This device was capable of generating passive torques in range of 0.15-1.35 Nm.

In another work, The same brakes as in [39] were used in a 2-DoF MRF-based joystick for virtual reality applications [40]. This joystick was constructed of two disc-shaped MRF-based brakes positioned perpendicularly with a gimbal structure, which transfers the movement of the joystick handle into two actuator rotary motions (Fig. 1.4(b)). The handle can

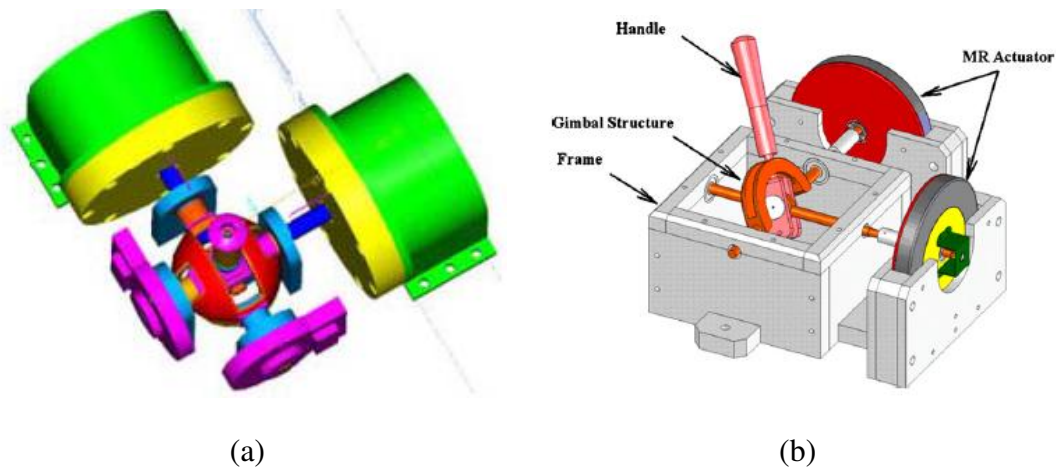


Figure 1.4: (a) An ERF-based joystick [44], and (b) an MRF-based joystick using MRF-based brakes and a gimbal structure [40]

rotate for 120 degrees in each direction. The joystick provides wide resistive torque in range of 0.5-10 Nm. The device was used in 2D and pseudo-3D virtual experiments and was proven successful. The novel characteristics of this system makes the force control come true, which enlarges the application of such joystick in the field of virtual surgery.

Force Displays

Force display systems are large-scale robotic systems that display sensed forces to the users in industrial settings. In conventional force displays, strong active actuators have been used. These types of actuators could be dangerous, because they are capable of creating large forces, which may harm human users. Hence, the interest in passive and dissipative actuators (*e.g.*, MRF- and ERF-based) for such purposes is increasing rapidly.

Furusho et al. [45] developed a low inertia cylindrical type ERF-based actuator and used these actuators within a 2-DoF force display. The force display is capable of generating about 0.7 Nm passive torque at a field strength of 3 kV/mm .

In another work [46], the same authors developed a stronger ERF-based brake which can apply 2 Nm of passive torque at field strength of 3 kV/mm . They then used two such brakes and developed a 2-DoF force display by taking advantage of a belt-pulley mechanism connected to a parallel-link manipulator (Fig. 1.5(a)). Each ERF-based manipulator independent controls the motion of a link. Experimental results for contact with a virtual wall, and tracing over a virtual wall demonstrated the effectiveness and stability of this display system in providing passive force feedback.

Reed et al. [15], proposed a 2-DoF dissipative force display. This device was in the form of a parallel five-bar linkage actuated by commercial MRF-based brakes. Two configurations were proposed, namely, three-brake and four-break configurations. Although the results improved in both cases, the former configuration results in improved intuitiveness, while the latter improves the workspace of the display. Models of both configurations of the device were obtained. The force display was tested by using a virtual environment. Primary results were promising and proposed several potential benefits for the area of obstacle avoidance.

Yamaguchi et al. [47] developed a semi-active high-performance 2-DoF MRF-based force display (Fig. 1.5(b)). In this design, 2 DC motors and four MRF-based clutches were used. The output torque of the system is transferred throughout a belt-pulley mechanism to the parallel links. This design resulted in a low inertia, high torque/inertia ratio, and high responsibility. The maximum generated torque is about 10 Nm.

1.7.2 Tactile Displays

A tactile display is a programmable device, which can artificially stimulate the skin to generate sensation of touch in the form of shape, vibration, pressure, pressure distribution,

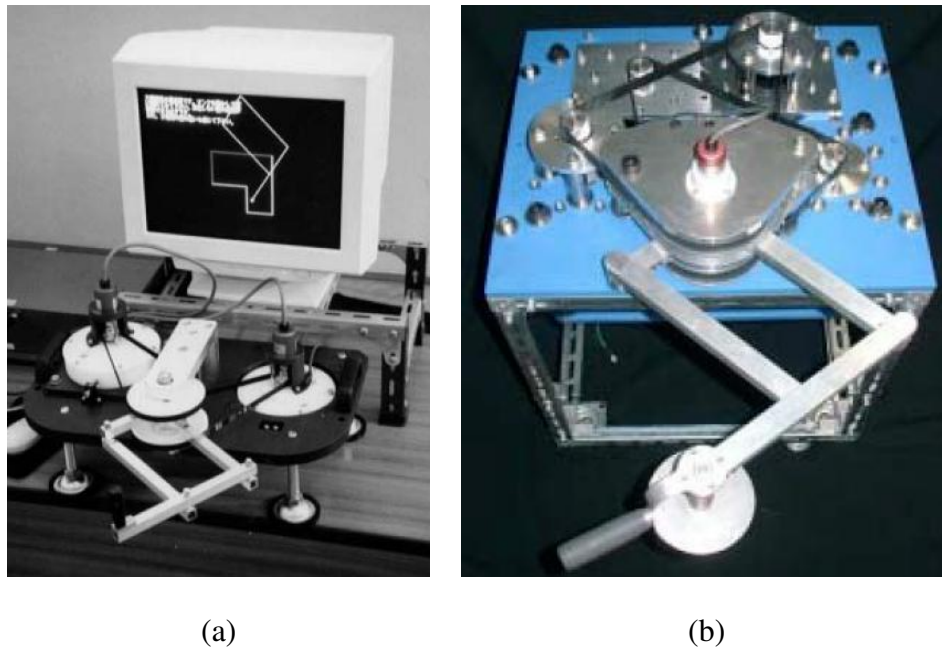


Figure 1.5: (a) A passive force display using 2 ERF brakes [46], (b) a semi-active force display using two DC motors and four MRF-based clutches.

and compliance [48].

Historically, one of the first tactile devices made using ERF was an I/O tablet for a blind user [49] which was developed by Fricke et al. This tablet consisted of an array of ERF elements, which can be activated selectively to create Braille alphabets. The main advantage of such a tablet in comparison to its conventional counterparts was that there is no moving mechanical part and the final price was almost half of the competition.

More recently, in another work, two MRF [50, 51] and ERF [52] based tactile displays using a 5×5 array of coils and electric cells, respectively, were developed. When a field is applied to an element of these systems, a small bump can be easily felt by dragging a finger over the display surface. Surface force responses of these displays under various magnetic/electric fields were measured while a sensorized probe was moved across the

upper surface. The results showed that exact image information of the object could be displayed using these tactile displays. In addition, it was shown that the displayed surfaces are stable and repeatable.

Bicchi et al. developed several instruments capable of suitably energizing MRF with a magnetic field to build shapes that can be directly felt and explored by hand. These devices include, (i) Pinch Grasp (PG) [26], (ii) Haptic Black Box (HBB-I) [11], (iii) HBB-IMP [12], and (iv) HBB-II [30] (Fig. 1.6).

The PG was built to verify the ability of using MRF to mimic the compliance, damping, and creep of some materials (*e.g.*, body tissues), and reproducing virtual object softness. In this device a flexible balloon filled with MRF was placed in the air gap of a magnetic circuit. The compliance of the balloon was intelligently controllable by varying the intensity of the magnetic field. Experimental results demonstrated good agreement between compliance of liver, spleen, and brain with that of an MRF-filled balloon. However, unacceptable results were obtained for bone, muscle and lung. This is due to the fact that the magnetic field intensity required to induce a compliance similar to these biological tissues is beyond the saturation limit of the MRF used [26]. Nevertheless, this system proposed a beneficial tactile device that can be mounted on the handle of minimally-invasive surgical tools, to give the surgeon a sense of the touched tissues.

The next three devices built by Bicchi et al. are called Haptic Black Boxes. These MRF based haptic devices were built based on a freehand concept, in which users can put their hand (covered with a latex glove) within an MRF-filled box and freely interact with suitably controlled fluids. The first prototype was called HBB-I [11]. This device consisted of a rectangular plastic box containing MRF and a series of magnetic coils placed under the box. Applying a proper magnetic field (by tuning the current of the coils) allowed to materialize 2-D objects with a given shape and compliance in the fluid. Due to the placement

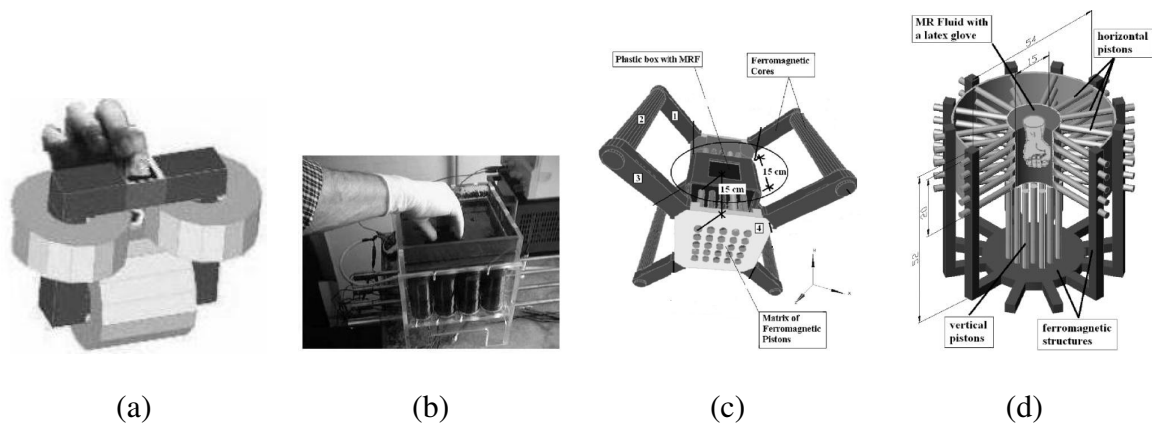


Figure 1.6: Haptic Black Boxes (a) Pinch Grasp, (b) HBB-I, (c) HBB-IMP, and (d) HBB-II of the coils, the generated magnetic circuit included a large air gap, which resulted in reduction of the magnetic intensity, which was the main drawback of this device. In the next generation of haptic black boxes, HBB-IMP was developed [12]. This system included two magnetic systems composed of a series of ferromagnetic pistons symmetrically positioned with respect to the center of the plastic box. Each piston pair was able to move back and forth to dynamically address the magnetic flux in different regions of the MRF. In this way a quasi-3D object can be mimicked inside the MRF box. In order to increase the resolution of the haptic box, HBB-II was developed [30]. It has a cylindrically shaped plastic box containing MRF, and a series of ferromagnetic cores are positioned around and underneath the box. Twenty two pistons are arranged in a circular matrix around the box, while, the other fifty are placed around the lateral surface of the box. The modulus of the magnetic field in a specified portion of the MRF and its spatial resolution can be controlled in this way. Hence, it was possible to reconstruct many objects of different shapes in different zones within the box containing the fluid.

1.7.3 Hand Masters

Three important properties are identified for haptic gloves so as to immerse the human in virtual reality manipulations [53]. These are that: (i) free space must feel free, (ii) a solid

virtual object must feel stiff, and (iii) physical constraints must not be easily saturated. Also, to truly immerse the user in the virtual (remote) environment, she/he must forget the real world. This is a major challenge, which is very demanding when considering the number of actuators needed. Also, the user must not have any constraints to the natural movement of his/her hand [54] [55].

Hence, the requirements for actuators in a haptic glove are many. The actuators must have very low friction when they are in the off-state, a high enough force in the on-state to convince a person when she/he is touching a solid object, as well as a low weight. Finally, the actuators used must be safe especially since their application is in proximity to human skin. A number of technologies have been applied to power previous hand master projects. The most common are electric actuators and pneumatic actuators. Due to the active nature of such actuation, these gloves can cause discomfort or even injury in case of oscillation and instability [32]. In order to overcome these problems, several studies have considered the use of MRF- and ERF-based actuators in the development of feedback gloves. The small weight and size, low inertia, high passive torque capacity, and intrinsic passivity of these types of actuators make them suitable for use in safe and highly transparent (in terms of force reflection accuracy) haptic gloves which are light and compact.

Bar-Cohen et al. [56, 57] conceived a haptic glove called MEMICA (MEchanical MIRRORing using Controlled stiffness and Actuators) that has high dexterity, rapid response, and large workspace. The MEMICA gloves were designed to provide intuitive mirroring of the conditions at a virtual site where a robot simulates the presence of a human operator. The key components of this device are electrically controlled force and stiffness actuators that work based on ERF brakes. This is a semi-active configuration which can provide both active and resistive actuation [57]. The actuators are placed in the back of the hand, and due to their small size they do not cause any obstruction in the grasping motion. Further

results on the performance of the device were not found.

In another study [58, 59], Winter et al. took advantage of MRF-based dampers and developed MRAGES (MRF-based actuated glove electronic system, Fig. 1.7(a)). Five MRF-based dampers (weighing only 0.035 lb) which can exert passive force up to 6 N were placed on the back of the hand. A novel exoskeleton mechanical power transmission system was designed to transmit the resistive forces of the dampers to the user's fingertips. This system acted as a push/pull control cable. The whole system is very lightweight and only weighs less than 0.45 lb. The main drawback of the actuator design is that the actuator produces a large amount of force, even in the off-state. Those used in the final version of the glove had static forces ranging from 1.4 N to 1.9 N (36% of the maximum applicable force). Such a high static force creates hand fatigue and reduces the transparency of the system.

Other authors have discussed the use of MRF-based dampers in haptic gloves. As an example, Cassar et al. [54] proposed such a glove using 2 MRF-based dampers for two fingers. The applied passive force can be as high as 25 N, while the off-state force is about 3.6 N. The glove weighs about 1 lb.

Blake et al. [34], developed a haptic glove by taking advantage of six MRF-based brakes. The developed brakes are compact (25 mm diameter, 14 mm thickness, 0.18 lb weight) and can apply up to 0.899 Nm of passive torque (Fig. 1.7(b)). The glove weighs about 1.4 lb. The system applies passive forces only to 3 fingers. The main advantage of this glove is that it only applies 0.005 Nm of torque (1.2% of the maximum torque) in the off-state. Hence it has better transparency compared to MRAGES. However, it is heavier, bulkier, and less dexterous.

Nam et al. [32] developed an MRF-based glove, called Smart Glove. It takes advantage

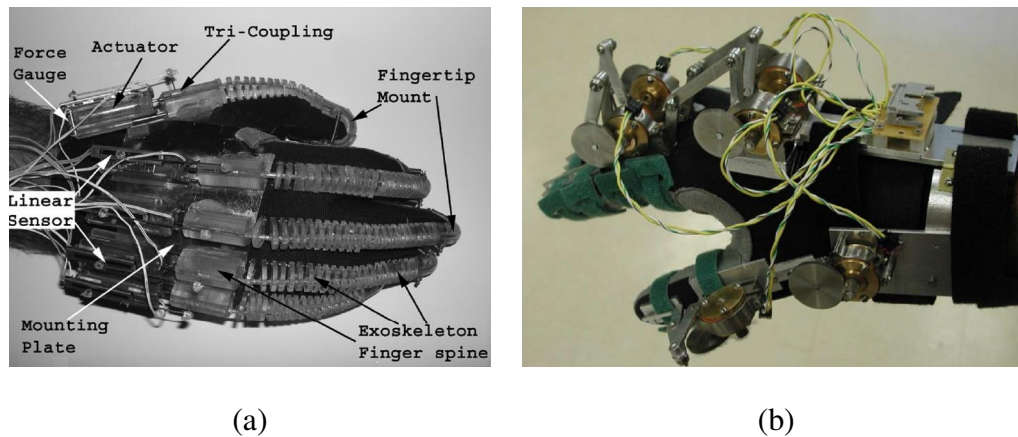


Figure 1.7: (a) MRAGES [59], (b) haptic glove with MRF-based brakes [34]

of 5 MRF-based dampers placed on the wrist of the human, each of which can apply up to 26 N of passive force. Each actuator houses a Hall sensor to measure the position of the piston. It weighs 0.114 lb and has a 20 mm stroke. A tendon-type flexible link was designed to connect the fingertips to the MRF actuators. This resulted in effective force-position transmission, as well as fewer actuators and a low-weight design of this glove (about 0.6 lb). In this design the actuator friction was stated to be a major concern to improve the transparency of the haptic interface. They also developed a 5-DoF ground-based haptic hand master called Smart Mouse [33]. Five passive MRF-based dampers were used in this device, which apply passive forces to the fingers of the user. The mouse-like (ground-based) structure of this device results in elimination of unnecessary reaction forces and reduction of muscular fatigue during operation.

1.7.4 Rehabilitation Devices and Exoskeletons

Force feedback is an essential part of rehabilitation. Fujisawa et al. [35] developed an upper limb patient simulator by taking advantage of two MRF-Based brakes. A physical therapist trainee can use this system to provide the experience, which can only be obtained

through practice. This simulator is capable of reproducing the stiffness of spasticity that is often seen in stroke patients. The symptoms of spasticity can be reproduced by controlling the reaction force given by the physiotherapist passively through controlling the viscosity of the MRF. The results were promising: however periodic vibration was observed which could cause discomfort for the user.

In another work [60], a versatile rehabilitation device, in the form of an exoskeleton, was developed that can be used to strengthen different muscle groups based on the torque generating capability of the muscle. The core of the device is an MRF-based damper, which provides passive exercise force. The device is low cost, smaller than other commercially available machines, and can be programmed to apply resistance that is unique to a particular patient and will optimize strengthening.

Weinberg et al. [36] presented a novel, smart and portable Active Knee Rehabilitation Orthotic Device (AKROD), in the form of an exoskeleton, designed to train stroke patients to correct knee hyperextension during stance and stiff-legged gait. The knee brace provides variable damping controlled in ways that helps motor recovery in stroke patients. A resistive, variable damper, ERF-based component is used to facilitate knee flexion during stance by providing resistance to knee buckling. Initial results from human testing demonstrated that AKROD is able to accurately produce desired torque and velocity profiles while ensuring an adequate level of comfort for patients.

Bibliography

- [1] D. Lawrence, "Stability and transparency in bilateral teleoperation," *IEEE Transactions on Robotics and Automation*, vol. 9, pp. 624–637, Oct 1993.
- [2] M. Lin and M. Otaduy, *Haptic Rendering: Foundations, Algorithms and Applications*. A K Peters, 2008.
- [3] T. Coles, D. Meglan, and N. John, "The role of haptics in medical training simulators: A survey of the state of the art," *IEEE Transactions on Haptics*, vol. 4, pp. 51–66, Jan 2011.
- [4] A. Okamura, C. Basdogan, S. Baillie, and W. Harwin, "Haptics in medicine and clinical skill acquisition [special section intro.]," *Haptics, IEEE Transactions on*, vol. 4, pp. 153–154, May 2011.
- [5] R. Robison, C. Liu, and M. Apuzzo, "Man, mind, and machine: The past and future of virtual reality simulation in neurologic surgery," *World Neurosurgery*, vol. 76(5), pp. 1750–78, 2011.
- [6] A. Hamed, S. Tang, and H. Ran, "Advances in haptics, tactile sensing, and manipulation for robot-assisted minimally invasive surgery, noninvasive surgery, and diagnosis," *Journal of Robotics*, vol. 12, pp. 1–14, 2012.
- [7] K. Ohnishi, "Real world haptics and telehaptics for medical applications," in *Industrial Electronics (ISIE), 2010 IEEE International Symposium on*, pp. 11–14, July 2010.
- [8] K. Kuchenbecker and G. Niemeyer, "Induced master motion in force-reflecting teleoperation," *Journal of Dynamic Systems, Measurement, and Control*, vol. 128, no. 4, pp. 800–810, 2006.
- [9] R. Lozano, N. Chopra, and M. Spong, "Passivation of Force Reflecting Bilateral Teleoperation with Time Varying Delay," *Journal of Mechatronics*, vol. 12, pp. 215–223, 2002.
- [10] I. Polushin, X. Liu, and C. Lung, "Stability of bilateral teleoperators with generalized projection-based force reflection algorithms," *Automatica*, vol. 48-6, pp. 1005–1016, 2012.
- [11] A. Bicchi, M. Raugi, R. Rizzo, and N. Sgambelluri, "Analysis and design of an electromagnetic system for the characterization of Magneto-Rheological fluids for haptic interfaces," *IEEE Transactions on Magnetics*, vol. 41, pp. 1876 – 1879, may 2005.
- [12] R. Rizzo, N. Sgambelluri, E. Scilingo, M. Raugi, and A. Bicchi, "Electromagnetic modeling and design of haptic interface prototypes based on Magneto-Rheological fluids," *IEEE Transactions on Magnetics*, vol. 43, pp. 3586 –3600, Sep 2007.

- [13] A. Shafer and M. Kermani, "Design and validation of a MR clutch for practical control applications in human-friendly manipulation," in *International Conference on Robotics and Automation*, 2011.
- [14] D. Senkal and H. Gurocak, "Haptic joystick with hybrid actuator using air muscles and spherical MR-brake," *Mechatronics*, vol. 21-6, pp. 951–60, 2011.
- [15] M. Reed and W. Book, "Modeling and control of an improved dissipative passive haptic display," in *IEEE International Conference on Robotics and Automation*, vol. 1, pp. 311 – 318, Apr 2004.
- [16] A. Shafer and M. Kermani, "On the feasibility and suitability of MR fluid clutches in human-friendly manipulators," *IEEE/ASME Transactions on Mechatronics*, vol. 16-6, pp. 1073 – 82, Dec 2010.
- [17] A. Grunwald and A. Olabi, "Design of Magneto-Rheological (MR) valve," *Journal of Sensors and Actuators*, vol. 148, no. 1, pp. 211 – 223, 2008.
- [18] M. Jolly, J. Bender, and J. Carlson, "Properties and applications of commercial Magneto-Rheological fluids," in *SPIE International Symposium on Smart Structures and Materials*, 1998.
- [19] M. Avraam, *MR-fluid brake design and application to a portable rehabilitation device*. PhD thesis, Univ Libre de Bruxelles, 2009.
- [20] J. Martin and J. Odinek, "Structure and dynamics of Electro-Rheological Fluids," *PHYSICAL REVIEW*, vol. 57, pp. 756–775, 1998.
- [21] J. Sproston, L. Yanyo, J. Carlson, and A. El Wahed, "Controllable fluids in 2002 - status of er and mr fluid technology," in *Proceedings of Actuator*, pp. 333–338, 2002.
- [22] T. Black and J. Carlson, *Synthetic, Mineral Oils and Bio-Based Lubricants*, ch. Magnetizable Fluids, pp. 565–583. Taylor and Francis, 2006.
- [23] P. Rankin, J. Ginder, and D. Klingenberg, "Electro- and Magneto-Rheology," *Current opinion in colloid and interface science*, vol. 3, pp. 373–381, Jul 1998.
- [24] A. Khanicheh, D. Mintzopoulos, B. Weinberg, A. Tzika, and C. Mavroidis, "Evaluation of Electro-Rheological fluid dampers for applications at 3-t MRI environment," *IEEE/ASME Transactions on Mechatronics*, vol. 13, pp. 286–294, Jun 2008.
- [25] A. Olabi and A. Grunwald, "Design and application of Magneto-Rheological fluid," *Materials and Design*, vol. 28, pp. 2658–64, Nov 2007.

- [26] E. Scilingo, N. Sgambelluri, D. De Rossi, and A. Bicchi, "Haptic displays based on Magneto-Rheological fluids: design, realization and psychophysical validation," in *Symposium on Haptic Interfaces for Virtual Environment and Teleoperator Systems*, pp. 10–15, 2003.
- [27] J. Carlson, D. Catanzarite, and K. Clair, "Commercial Magneto-Rheological fluid devices," in *5th International Conference on Electro-Rheological, Magneto-Rheological Suspensions and Associated Technology*, 1995.
- [28] F. Ahmadkhanlou, G. Washington, and S. Bechtel, "Modeling and control of single and two degree of freedom Magneto-Rheological fluid-based haptic systems for telerobotic surgery," *Journal of Intelligent Material Systems and Structures*, vol. 20, pp. 1171–86, May 2009.
- [29] D. Lee, Y. Nam, M. Park, and R. Yamane, "Transparency improvement of a 1-DOF hybrid haptic device with wide-ranged torque reflection," *International Journal of Applied Electromagnetics and Mechanics*, vol. 33, pp. 47–53, 2010.
- [30] N. Sgambelluri, R. Rizzo, E. Scilingo, M. Raugi, and A. Bicchi, "Free hand haptic interfaces based on Magneto-Rheological fluids," in *Symposium on Haptic Interfaces for Virtual Environment and Teleoperator Systems*, 2006.
- [31] R. Rizzo, "A permanent-magnet exciter for Magneto-Rheological fluid-based haptic interfaces," *IEEE Transactions on Magnetics*, vol. 49, pp. 1390–1401, Dec 2013.
- [32] Y. Nam, M. Park, and R. Yamane, "Smart Glove: Hand master using Magneto-Rheological fluid actuators," in *Proceedings of SPIE*, vol. 6794, pp. 679434–679434–6, 2007.
- [33] K. Kim, Y. Nam, R. Yamane, and M. Park, "Smart Mouse: 5-DOF haptic hand master using Magneto-Rheological fluid actuators," *Journal of Physics: Conference Series*, vol. 149, pp. 1–6, 2009.
- [34] J. Blake and H. Gurocak, "Haptic glove with MR brakes for virtual reality," *IEEE/ASME Transactions on Mechatronics*, vol. 14, pp. 606–615, oct. 2009.
- [35] T. Fujisawa, M. Takagi, Y. Takahashi, K. Inoue, T. Terada, Y. Kawakami, and T. Komeda, "Basic research on the upper limb patient simulator," in *IEEE International Conference on Rehabilitation Robotics*, pp. 48–51, 2007.
- [36] B. Weinberg, J. Nikitczuk, S. Patel, B. Patrilli, C. Mavroidis, P. Bonato, and P. Canavan, "Design, control and human testing of an Active Knee rehabilitation Orthotic device," in *IEEE International Conference on Robotics and Automation*, pp. 4126–4133, 10-14 2007.

- [37] T. Bulea, R. Kobetic, C. To, M. Audu, J. Schnellenberger, and R. Triolo, "A variable impedance knee mechanism for controlled stance flexion during pathological gait," *IEEE/ASME Transactions on Mechatronics*, vol. 17, pp. 822–832, Oct 2012.
- [38] W. Li, H. Du, N. Guo, and P. Kosasih, "Magneto-Rheological fluids based haptic device," *Sensor Review*, vol. 24, pp. 68–73, 2004.
- [39] B. Liu, W. Li, P. Kosasih, and X. Zhang, "Development of an MR-brake-based haptic device," *Smart Materials and Structures*, vol. 15, pp. 1960–1966, 2006.
- [40] W. Li, B. Liu, P. Kosasih, and X. Zhang, "A 2-DOF MR actuator joystick for virtual reality applications," *Sensors and Actuators*, vol. 137, pp. 308–320, 2007.
- [41] F. Ahmadkhanlou, G. N. Washington, S. E. Bechtel, and Y. Wang, "Magneto-Rheological fluid based automotive steer-by-wire systems," in *Proceedings of SPIE*, vol. 6171, p. 61710I, SPIE, 2006.
- [42] M. A. Vitrani, J. Nikitzuk, G. Morel, C. Mavroidis, and B. Weinberg, "Torque control of Electro-Rheological fluidic resistive actuators for haptic vehicular instrument controls," *Journal of Dynamic Systems, Measurement, and Control*, vol. 128, no. 2, pp. 216–226, 2006.
- [43] H. Bose and H. Berkemeier, "Haptic device working with an Electro-Rheological fluid," *Journal of Intelligent Material Systems*, vol. 10, pp. 714–718, 1999.
- [44] J. Melli-Huber, B. Weinberg, A. Fisch, J. Nikitzuk, C. Mavroidis, and C. Wampler, "Electro-Rheological fluidic actuators for haptic vehicular instrument controls," in *Symposium on Haptic Interfaces for Virtual Environment and Teleoperator Systems*, 2003.
- [45] J. Furusho and M. Sakaguchi, "New actuators using ER fluid and their applications to force display devices in virtual reality and medical treatments," *International Journal of Modern Physics*, vol. 13, pp. 2151–2159, 1999.
- [46] J. Furusho, M. Sakaguchi, N. Takesue, and K. Koyanagi, "Development of ER brake and its application to passive force display," *Journal of Intelligent Material Systems and Structures*, vol. 13, pp. 425–429, 2002.
- [47] Y. Yamaguchi, S. Furusho, S. Kimura, and K. Koyanagi, "Development of high-performance MR actuator and its application to 2D force display," *International Journal of Modern Physics B*, vol. 19, pp. 1485–1491, 2005.
- [48] M. Benali, M. Hafez, J. Alexandre, and A. Kheddar, "Tactile interfaces: a state-of-the-art survey," in *Symposium on Robotics*, 2004.

- [49] J. Fricke and H. Baehring, "Design of a tactile graphic I/O tablet and its integration into a personal computer system for blind users," *Journal of Microcomputers Applications*, vol. 16, pp. 259–269, 1993.
- [50] Y. Liu, R. Davidson, P. Taylor, J. Ngu, and J. Zarraga, "Single cell Magneto-Rheological fluid based tactile display," *Displays*, vol. 26, no. 1, pp. 29 – 35, 2005.
- [51] Y. Liu, R. Davidson, and P. M. Taylor, "Tactile display based on smart fluids," in *International Conference on Smart Materials and Nanotechnology in Engineering*, 2007.
- [52] P. M. Taylor, D. M. Pollet, A. Hosseini-Sianaki, and C. J. Varley, "Advances in an Electro-Rheological fluid based tactile array," *Displays*, vol. 18, no. 3, pp. 135 – 141, 1998. Tactile Displays.
- [53] M. Bouzit, G. Burdea, G. Popescu, and R. Boian, "Phantom haptic interface: a device for probing virtual objects," in *International Mechanical Engineering Congress and Exposition*, 1994.
- [54] D. Cassar and M. Saliba, "A force feedback glove based on Magneto-Rheological fluid: Preliminary design issues," in *IEEE Mediterranean Electrotechnical Conference*, pp. 618–623, 26-28 2010.
- [55] M. Seong, K. Sung, and S. Choic, "The Rutgers Master II: New design force-feedback glove," *IEEE/ASME Transactions on Mechatronics*, vol. 7, pp. 256–263, 2002.
- [56] C. Pfeiffer, C. Mavroidis, Y. Bar-Cohen, and B. Dolgin, "Electro-Rheological fluid based force feedback device," in *SPIE International Society for Optical Engineering*, 1999.
- [57] Y. Bar-Cohen, C. Mavroidis, M. Bouzit, B. Dolgin, D. Harm, and W. R. Kopchok, G.E., "Virtual reality robotic telesurgery simulations using MEMICA haptic system," in *SPIE Smart Structures Conference*, 2001.
- [58] S. Winter and M. Bouzit, "Testing and usability evaluation of the MRAGES force feedback glove," in *International Workshop on Virtual Rehabilitation*, pp. 82 –87, 2006.
- [59] S. Winter and M. Bouzit, "Use of Magneto-Rheological fluid in a force feedback glove," *IEEE Transactions on Neural Systems and Rehabilitation Engineering*, vol. 15, pp. 2 –8, Mar 2007.
- [60] S. Dong, K.-Q. Lu, J. Q. Sun, and K. Rudolph, "Adaptive force regulation of muscle strengthening rehabilitation device with Magneto-Rheological fluids," *IEEE Transactions on Neural Systems and Rehabilitation Engineering*, vol. 14, pp. 55 –63, Mar 2006.

Chapter 2

Theoretical and Experimental Evaluation of Transparency and Stability

The two main objectives in designing a haptic interface are stability and transparency. The dynamics of the actuators employed in a haptic interface have a significant effect on these goals. In this chapter, the potential benefits of Smart Fluid based actuators, *i.e.*, Magneto-Rheological Fluid (MRF) and Electro-Rheological Fluid (ERF) based systems, to the field of haptics are discussed from both theoretical and experimental points of view. Devices developed with such fluids are known to possess superior mechanical characteristics over conventional servo systems. This contributes significantly to improved stability and transparency of haptic devices. Conclusions drawn from this investigation indicate that MRF clutch actuation approaches can indeed be developed to design haptic interfaces with improved stability and transparency.

This chapter contains material published in (1) "Application of Magneto-Rheological Fluid Based Clutches for Improved Performance in Haptic Interfaces", presented at the IEEE Int Conf on Robotics and Automation, Hong Kong, June 1-4, 2014. and (2) "Suitability of Small-Scale Magneto-Rheological Fluid Based Clutches in Haptic Interfaces for Improved Performance", accepted for publication in the IEEE/ASME Transactions on Mechatronics, August 2014.

2.1 Introduction

The actuators and mechanisms used in designing a haptic interface play an important role on the quality of force feedback, as well as the stability of the system. This fact makes the design of a haptic interface twofold challenging. In order to have a transparent system, it is of utmost importance that while a haptic device is capable of recreating the forces that occur during contact with stiff objects, it exhibits low friction, damping, and inertia to sustain transparency during motion in free space. Poor dynamics and control of manipulation can affect the sense of touch, in particular when rigid instruments or actuators are used [1]. Heavy and/or cumbersome haptic systems generate artifacts which negatively affect the quality of the virtual presence [2]. Furthermore, the use of active actuators (*e.g.*, electrical motors) in haptic devices may degrade the problem of stability [3] due to generation of energy, the problem of reflected slave forces, and induced master motion mechanisms, especially in systems with time delay [4]. In addition, such actuators can exhibit oscillations and jerks [5], which not only can cause uncomfortable forces for the user, but are highly problematic in delicate operations [6]. Most current haptic systems take advantage of passivity-based and small-gain approaches to guarantee the stability [7, 8]. However, such approaches are considered to be conservative and in turn result in degraded transparency. Hence, to effectively operate such systems, long and costly amount of training is required.

Actuators based on MRF and ERF have been proposed as an alternative for use in haptic devices [1]. These fluids exhibit a very unique characteristic: the viscosity and shear stress of these fluids can be intelligently controlled using an applied magnetic field. Several passive and semi-active actuators have been developed by taking advantage of this feature. Such systems exhibit remarkable characteristics, including high yield stress, low mass-torque and inertia-torque ratios, compact size, intrinsic passivity, and precision controllability [9].

It is expected that the superior characteristics of MRF- and ERF-based actuators in comparison to active actuators will enable the design of a more transparent and stable haptic interface. An investigation into this idea is presented in this chapter.

To this end, first, intrinsic properties of such actuators, which have an impact on transparency, are discussed in Section 2.2. Next, their effect on the stability of a bilateral teleoperation system is discussed from a theoretical point of view in Section 2.3. This chapter takes advantage of the results of small-gain theorem and virtual wall benchmark, to study the effect of smart fluid based actuators characteristics on the stability of a system.

Another important contribution of this chapter is that it shows the effect of MRF-based actuators in improving stability and transparency of haptic interfaces from a practical point of view, by taking advantage of a large-scale setup. Experimental evaluation on the performance of a 1-DoF haptic interface which takes advantage of an MRF-based clutch is presented in Section 2.4. The well-known virtual wall benchmark is used for this purpose and the results are compared with another 1-DoF haptic device with a DC motor at its core. Although the clutch used in Section 2.4 is bulky, it serves as a proof of concept. Conclusions drawn from these results indicate that indeed the haptic interface with an MRF clutch exhibit improved stability and transparency in comparison to its standard counterpart. The results show the promising potential of these actuators for integration in a multi-DoF haptic interface with improved stability and transparency.

This motivated us to move toward design of a small-scale MRF-based clutch suitable for haptic interface, which is discussed in Chapter 3.

2.2 Transparency of Smart Fluid Based Force Feedback

In this section, the advantages and disadvantages of MRF- and ERF-based actuators in improvement of transparency in a haptic systems are studied from mechanical and physical points of view. Overall, such actuators can be used to design compact, light weight, low inertia, low friction, high bandwidth, and high torque haptic devices which can contribute to transparency of a haptic interface. Although the main focus of this research is on MRF-based systems, in this section, the properties of ERF-based actuators are also briefly reviewed to provide a comparison between the two types of smart fluids and the reasoning behind selecting MRF-based actuators over ERF-based actuators for developing the haptic interface in this thesis (Section 2.2.6).

2.2.1 Shear Stress

A haptic device should be capable of generating large forces/torques to mimic interaction with stiff objects. MRF are capable of producing high shear stress. The produced shear stress by MRF though is bounded and is limited to the physical properties of the fluid, *e.g.*, its magnetic saturation [10]. Nevertheless, MRF can produce high yield stresses typically in the range of 50 to 100 kPa, depending on their chemistry. Consequently, these fluids can be used in designing actuators with high torque capacity, suitable for transparent haptic interfaces. Alternatively, the value of shear stress for ERF does not typically exceed 10 kPa which is limited by electrical breakdown at high electrical field strengths [11]. However, it should be noted that more recent research into the field of ERF has produced materials exhibiting higher yield stress [12]. Hence, these fluids can also be used to design actuators capable of transmission or generation of high passive/semi-active force and torque.

2.2.2 Actuator Inertia

While a haptic device should be able to generate high torques, it is highly desirable that it exhibits low inertia. The use of gear reduction for increasing the torque capacity of electrical motors results in a significant increase of reflected inertia. The reflected actuator inertia can in fact be much larger than that of the link inertia due to the use of gear reduction [13]. On the other hand, in an MRF- or ERF-based actuator the reflected rotor inertia of the motor is replaced with the reflected inertia of the clutch output shaft [9]. It has been shown that MRF-based clutches can demonstrate superior output inertia characteristics over the low-inertia servo motors [10, 14].

2.2.3 Actuator Mass

Heavy and cumbersome haptic interfaces affect the quality of force feedback. It is highly desirable that a haptic device has low mass-torque ratio. Light weight and compact size of MRF- and ERF-based actuators allow the user to experience a more realistic interaction [15]. Ferromagnetic materials (*i.e.*, steel) must be used in MRF-based actuators in order to create magnetic circuits. However, in ERF-based actuators much lighter materials (*i.e.*, aluminum) can be used which result in a relatively lighter weight of the system [10]. On the other hand, due to their large shear stress, MRF-based devices can be made substantially smaller than ERF-based devices (10-100 times smaller in volume for comparable performance [11]). Furthermore, MRF-based devices can be made substantially more compact and lighter in comparison to electrical motors for comparable performance [16]. In fact, such actuators exhibit superior mass-torque ratio over the commercially available servo motors as shown in [10].

2.2.4 Frequency Response

High bandwidth of the actuation system is essential for the transparency of a haptic device. MRF respond to an applied field in the order of few milliseconds [17]. However, the actuation response can become delayed due to the field propagation [18]. As the magnetic field propagates from the coil, it is met by an opposing field produced by induction currents in the magnetic circuit. The response delay produced by this effect is exacerbated by the use of conductive material in the magnetic circuit. Nevertheless, MRF-based actuators are considered as high bandwidth systems which can permit high bandwidth control, essential for mirroring fast motions [15]. ERF-based actuators have higher bandwidth since there is no delay in propagation of the electrical field.

2.2.5 Hysteresis and Nonlinear Behavior (Disadvantages)

The main problems with MRF-based devices is their nonlinear behavior and temperature dependency. MRF-based actuators exhibits hysteresis due to the use of ferromagnetic materials. This translates to a hysteresis relationship between the input current and the output torque which leads to tracking errors, unwanted harmonics, and undesired stick-slip motions [19, 20]. To develop accurate output torque to input current relationships, it is important to both understand and model the actuator hysteresis [19, 21]. This is still an open area of research. Same as MRF-based actuators, ERF-based actuators can display hysteric behavior as well. However, in the case of ERF-based actuators, it is the ERF itself and not the surrounding material that displays the field dependent hysteric behavior [16].

2.2.6 MRF vs. ERF

ERF exhibit several additional undesirable characteristics, including temperature dependency, sensitivity to impurities in the fluid, electrical breakdown, and high voltage requirements. The properties of ERF are known to change with temperature [11]. Particularly, the yield stress of ERF drastically varies with respect to temperature. Although MRF properties also vary with temperature, such deviations are minimal in comparison to ERF [10]. On the other hand, the existence of impurities inside the ERF can prove disastrous as it results in the instability of the system and may cause electrical breakdown [11]. Regarding the power consumption, MRF-based actuators requires low voltages (2-24 V) and high currents (1-2 A), while ERF-based actuators requires very high voltages (2-10 kV) and very low currents (1-10 mA) [22]. One finds that the field energy requirements for comparable MRF- and ERF-based devices are approximately equal [11]. In ERF devices power losses are mainly due to electric conduction through the fluid, while in MRF devices such losses are present in the coil used to produce the magnetic field [11]. Losses in the coil used to activate the MRF will vary depending on the specifics of how coil is wound and the materials used. Overall, these systems are considered as low power consumption systems. As an example, in case of an MRF-based clutch developed in [9], the power of a USB port suffices to power this system. However, the high voltage requirement of an ERF-based actuator asks for complex circuitry systems capable of feeding such voltage (this is the main reason for high price of ERF-based actuators in comparison to MRF-based actuators) [23]. In addition, such high voltage requirements can be highly dangerous when operator is using the haptic device.

Hence, as discussed, MRF provides superior properties, higher reliability, and safer operation in comparison to ERF. Thus, in this work, MRF-based actuators are selected as the more suitable smart fluid actuator for use in a haptic interface with medical application.

2.3 Stability of Smart Fluid Based Haptic Interfaces

In order to study the effect of MRF-based actuators on the stability of teleoperation systems, two theoretical approaches are considered, namely, (1) small-gain theorem and (2) virtual wall benchmark.

2.3.1 Small-Gain Theorem

The small-gain theorem, which is one of the main results in control system theory, implies that a feedback system is stable if the product of the IOS (Input-Output Stability) gains [24] of the subsystems is less than one [25–29]. In a teleoperation system, two (or more) manipulators called master and slave are connected over a network. In the presence of communication delays in the network, as a result of the time-varying delays, the teleoperation system can become active, and hence unstable [30, 31]. Polushin et al. [32] presented a version of the IOS Small-Gain Theorem that is designed specifically for interconnections where the subsystems communicate asynchronously over multiple channels, and the communication is subject to multiple time-varying possibly unbounded communication delays. They demonstrated that a multi-dimensional version of the small-gain condition guarantees the stability of the interconnection of IOS subsystems under certain mild assumptions imposed on communication process [8, 32, 33]. This result is applicable to a wide range of dynamical systems whose parts communicate over networks. A review of this theorem is given in this section and by taking advantage of its result the potential impacts of MRF-Based actuators on the stability of the system will be discussed.

Let's consider the system depicted in Fig. 2.1. A master device, with impedance Z_m , is interconnected to a slave device and environment, with combined impedance of Z_{se} , through a communication channel with time-varying delays of $T_1(t)$ and $T_2(t)$. A filter

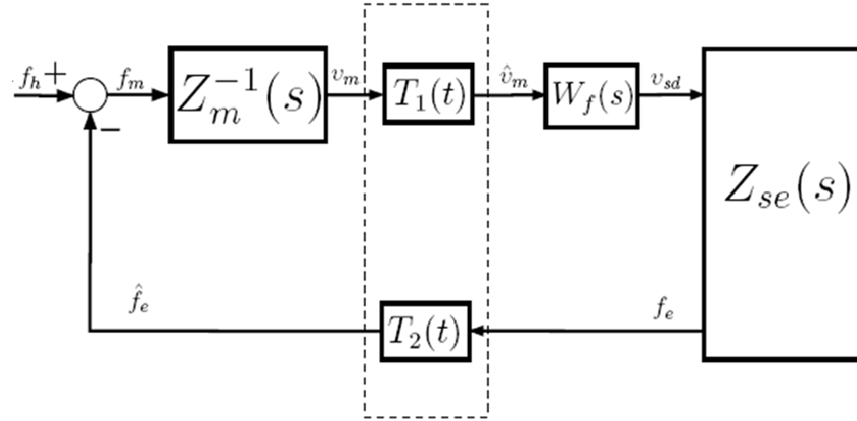


Figure 2.1: Interconnection of a master-slave system through a communication channel with time delay.

$W_f(s)$ is used to guarantee the stability of the system. One should note that in order to have ideal transparency the gain of this filter should be close to one, *i.e.*, $\gamma_f = \|W_f(s)\|_{\mathcal{L}_1} = 1$, where γ_f is the IOS gain of the filter which is equal to its \mathcal{L}_1 -norm [34].

One immediate result of the findings by Polushin et al. in [32, 33] is the condition of stability for the system in Fig. 2.1. The master-slave device interconnected through network with communication delay is stable if,

$$\gamma_m \gamma_{se} \gamma_f < 1 \quad (2.1)$$

where $\gamma_m = \|Z_m^{-1}(s)\|_{\mathcal{L}_1}$ and $\gamma_{se} = \|Z_{se}(s)\|_{\mathcal{L}_1}$ are gains of master and the slave subsystems, respectively, AND the following two assumptions hold [32, 33],

- **Assumption 1:** There exist an upper bound for communication delays $T_1(t)$ and $T_2(t)$ that does not grow faster than the time itself
- **Assumption 2:** $t - \max\{T_1(t), T_2(t)\} \rightarrow +\infty$ as $t \rightarrow +\infty$

These assumptions can always be guaranteed by taking advantage of certain features of the underlying communication protocol, and is not dependent on the communication channels properties [32, 33]. As an example, the first assumption always holds in real world networks as a result of sequence numbering and time-stamping. Also, the second assumption is always satisfied unless the communication between the subsystems is totally lost.

The small-gain stability condition in Eq. (2.1) can be rewritten as,

$$\gamma_f < \frac{\|Z_m(s)\|_{\mathcal{L}_1}}{\|Z_{se}(s)\|_{\mathcal{L}_1}} \quad (2.2)$$

The importance of the characteristics of a master device (haptic interface) becomes evident in this equation. When the slave device is in contact with a rigid environment, the value of $\|Z_{se}(s)\|_{\mathcal{L}_1}$ can become very large. As a result, in order to both satisfy stability, *i.e.*, Eq. (2.1), and transparency, *i.e.*, $\gamma_f \approx 1$, the haptic interface should be capable of producing large impedance $\|Z_m(s)\|_{\mathcal{L}_1}$. If the master is incapable of creating such a high impedance, then the filter gain should be decreased $\gamma_f \ll 1$ which in turn results in a conservative design and degraded transparency [33]. As discussed in this chapter and as will be shown in the upcoming chapters, the MRF-based actuators are capable of creating larger force/torques than that of conventional servo systems with comparable size and weight which enables us to have improved transparency, while guaranteeing stability. In other words, by creating larger impedances $\|Z_m(s)\|_{\mathcal{L}_1}$, we are capable of simulating contact with more rigid environments $\|Z_{se}(s)\|_{\mathcal{L}_1}$, while keeping γ_f close to 1 for better transparency.

2.3.2 Virtual Wall Benchmark

In this section, the effect of MRF-Based actuators on the stability of a teleoperation system is studied from another theoretical point of view. To this end, the virtual wall experiment is considered. A simple model of the virtual wall was proposed in [35], which consisted of an encoder, a discrete unilateral spring-damper system, and a zero-order hold (ZOH), *i.e.*, Fig. 2.2. A virtual wall can generate energy which subsequently results in the system becoming active and unstable. This is due to the delay that is caused by the zero-order hold and asynchronous switching time [36]. Thus, a virtual wall provides a proper ground for studying the stability of a teleoperation system and as a result it is considered as one of the most efficient benchmarks in telerobotics for stability evaluation [37, 38].

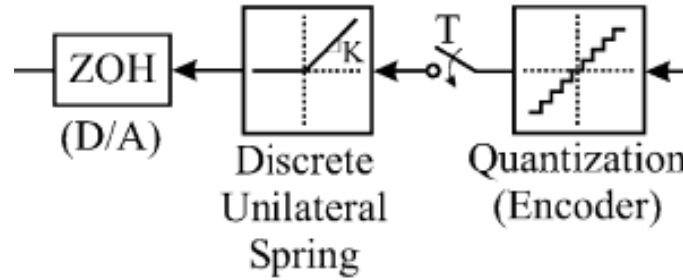


Figure 2.2: A simple model of the virtual wall consisting of an encoder, a discrete unilateral spring-damper system, and a Zero-Order Hold (ZOH) [35]

Using the passivity theorem [34], a necessary and sufficient condition for the stability of a haptic interface with physical damping of b_p interacting with a virtual wall with virtual stiffness K_w and virtual damping B_w (Fig. 2.3), can be derived. Such a condition, known as *Z-width*, implies the maximum achievable virtual stiffness and virtual damping [39] and is given by,

$$b_p > \frac{K_w T_s}{2} + B_w \quad (2.3)$$

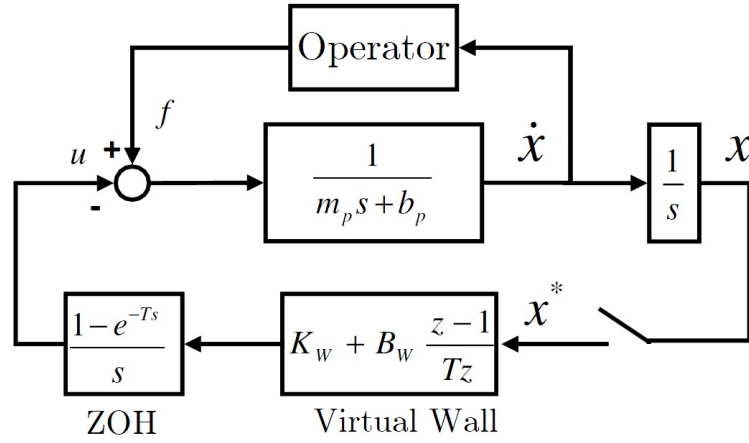


Figure 2.3: Block Diagram of the virtual wall haptic rendering system; including a haptic interface with physical mass m_p and damping b_p , a virtual wall with virtual stiffness K_W and virtual damping B_W , switching, and zero-order hold [39].

where T_s is the sampling period of the system. Fig. 2.4 depicts the stability region of the system in the current and future cases. In this figure, region (R_1) shows the stability margin of the system. The most significant conclusion drawn from (2.3) is that physical damping b_p is essential to achieve stability and it cannot be substituted with virtual damping. As a result, an active haptic device cannot simulate a virtual wall beyond the extent of its physical damping while guaranteeing stability [40]. One approach to relax such limitation is to add a constant physical damping b_c to the haptic interface [39]. In this case the Z -width will be modified as,

$$b_p + b_c > \frac{K_w T_s}{2} + B_w \quad (2.4)$$

Region (R_2) in Fig. 2.4 presents the stability margins after such modification. Although the haptic device is more stable in this case, the addition of the constant physical damping deteriorates the transparency of the teleoperation. This is due to the fact that the user feels

additional damping forces, even if the slave is moving in free space. As a result, damping cancelation is required to remedy this issue.

Another approach to increase the *Z-width*, while sustaining transparency, is to use a controllable physical damping, as opposed to a constant one [41]. In this case, the *Z-width* is modified as,

$$b_p + b_{cont}(\mathbf{H}) > \frac{K_w T_s}{2} + B_w \quad (2.5)$$

where $b_{cont}(\mathbf{H})$ is the controllable physical damping variable of the passive actuator which in the case of MRF-based actuators is a function of \mathbf{H} , the strength of the magnetic field. The system can now exhibit low damping, with no need for damping cancelation, when in free space motion, and consequently have better transparency. On the other hand, the system can have high damping when in contact with stiff objects, hence better stability. In this way, the passivity bounds are extended to the limits of the achievable physical damping variable (*e.g.*, magnetic saturation in MRF actuators) [14], *i.e.*, region (R_3) in Fig. 2.4.

Some passive devices, such as MRF-based brakes and dampers, are capable of creating a controllable damping. The idea is to use the controllable physical damping of such devices to simulate the virtual damping. It is shown in [40] that the passive force exerted using such devices f_c can be modeled as a viscous friction which is a function of the strength of the magnetic field \mathbf{H} and the speed v ,

$$f_c = b_{cont}(\mathbf{H})|v|sgn(v) \quad (2.6)$$

In other words, MRF-based devices can display virtual damping by regulating the magnitude of the viscous friction [40]. However, an MRF-based brake or damper, on its own (as

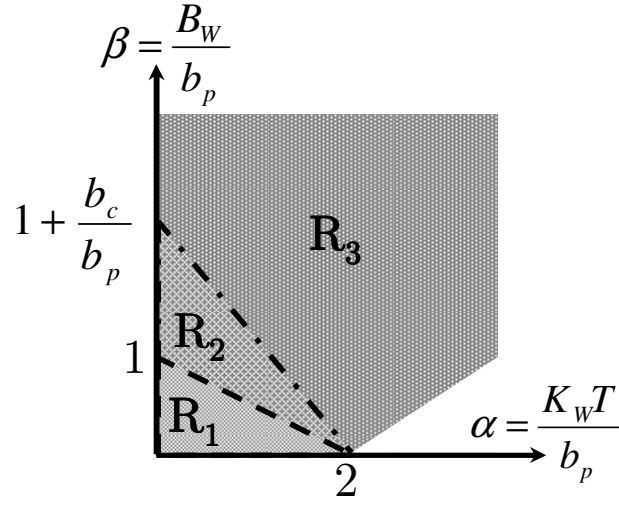


Figure 2.4: Stability margin of virtual wall display for no additional damping (R_1), additional constant damping (R_2), and controllable damping (R_3).

a passive actuator), is not capable of simulating both stiffness and damping of the virtual wall. In fact, a hybrid semi-active combination of a motor (as an active system) and an MRF-based brake (as a passive system) is required. In this regard, MRF-based clutches are the most useful type among such devices for use in haptic interfaces [42]. The structure and design of an MRF-based clutch are described in detail in previous works in our lab, *e.g.*, [17]. A brief review is given in the next section. The advantage of the configuration proposed in [17], is that both K_W (displayed by motor) and B_W (displayed by the MRF-based clutch) can be controlled using the strength of the magnetic field in the clutch. In other words, in this configuration, the motor rotates at a constant velocity while the MRF-based clutch controls the output torque. By controlling the magnetic field, the MRF-based clutch simulates B_W through controlling the magnitude of the viscous friction in the clutch [40] and mimics K_W by regulating the portion of the motor torque derived to the output.

2.4 Experimental Validation: Virtual Wall

In order to evaluate the effect of MRF-based actuators on the transparency and stability of haptic devices, experimental results from virtual wall display obtained by using two single-DoF haptic displays are presented and compared in this section. The first haptic interface consists of a prototype MRF-based clutch (designed and constructed in our research group [17]) that couples a brushless DC motor to the haptic interface handle. The result of this system is then compared with an equivalent haptic interface that is directly coupled to a brushless DC motor (Maxon EC-60).

REMARK 2. One should note that the prototype clutch used for this experimental validation was previously designed for industrial applications and not specifically for haptic interface. Nevertheless, the setup provides a good ground to study the benefits of MRF-based actuators in haptic systems. The prototype clutch only serves as a proof-of-concept setup to validate the advantages of MRF-based devices highlighted in previous sections. In fact, in Chapter 3, the design and analysis of a small-scale MRF-based clutch, specifically designed for haptic applications, is presented.

2.4.1 Experimental Setup

As mentioned earlier, two single-DoF haptic devices were considered. The experimental setup is shown in Fig. 2.5(a). A brief overview of this setup is given here. Further details can be found in [17, 43].

MRF-Based Haptic Interface: The mechanism uses an MRF-based clutch at its core [17]. Fig. 2.5(b) shows the cross-section of a typical multi-disk MRF-based clutch. The input shaft breaks out into a set of input disks which are aligned in parallel to a set of output disks

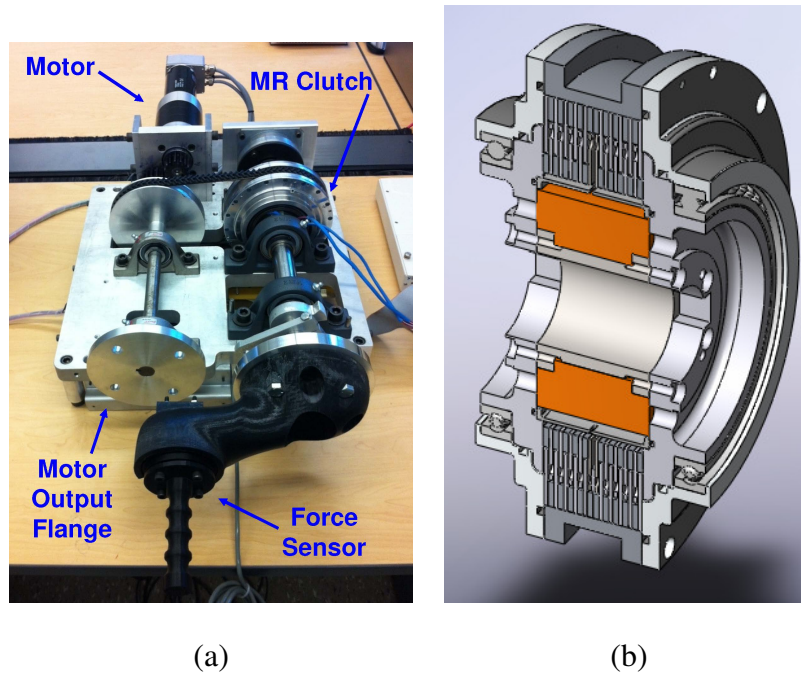


Figure 2.5: (a) The experimental setup. The mechanism takes advantage of MRF-based clutches as part of the actuator. (b) Sectional view of the prototype MRF-based clutch

attached to the output shaft. MRF fills the volume between input and output disks. A driver motor applies a constant torque to the input shaft. By energizing the electromagnetic coil, the viscosity of MRF, thereby the compliancy of the clutch are controlled. As a result, the output torque of the clutch can be controlled.

In this setup, the coil of the clutch is driven by a servo amplifier (Maxon 4-Q-DC Servo-amplifier ADS 50/5) set up in torque mode. A servo motor (Maxon EC-60) provided the rotational input to the clutch. A handle is connected to the output shaft of the clutch and the user can interact with the interface using this handle. An ATI Force/Torque sensor is placed inside the handle to measure the forces/torques applied by and to the human's hand. Although this setup is only capable of generating forces in one direction [17], it is suitable for our experimental validations since all the forces experienced from the wall are in the same direction. The clutch is mounted on an experimental platform that incorporates

an angular encoder (Renishaw RM22I) to read the position of the output shaft. Embedded Hall sensors measure the magnetic field inside the clutch. A National Instruments (NI USB-6229) multifunction I/O device is used to read the measured parameters and to implement a closed-loop control for the output torque of the clutch.

One should note that, the output torque of the clutch is only controlled through regulating the magnetic field of the clutch. The Maxon motor plays no role in controlling the output torque except providing the input motions in constant velocity (refer to Section 2.3 for more details). In order to control the output torque of the clutch, first, a Hall sensor is used to measure magnetic field density inside the clutch. Next, the Bingham Visco-Plastic (BVP) model [19, 44, 45] is used to estimate the shear stress by using magnetic field flux density, and consequently output torque. Based on this calculation a PID controller generates the current required to control the output torque.

Electrical Motor-Based Haptic Interface: The setup in Fig. 2.5 can also be used to study the performance of direct and rigid coupling of a motor in a haptic device. The handle, connected to the output shaft of the clutch, can be removed and attached to the output flange of Maxon EC-60 motor directly (Fig. 2.5). In this way, the motor can be used as a 1-DoF haptic interface. During these tests, the belt coupling of the gears to the clutch was removed. The built-in PID controller in the EPOS motion controller was used to control the output torque.

REMARK 3. Application of Herschel and Bulkley (HB) method [46] for estimating the shear stress, instead of BVP, has also been reported in the literature. However, one should note that the HB model is more useful in applications with high shear rate, *e.g.*, MRF-based dampers. In the current application, the shear rate is low and as a result the BVP model is sufficiently accurate [47]. Another concern is that Hall sensors can alter the flux lines inside the system. The motivation for using Hall sensors is the fact that it enables us to

bypass the main hysteresis of the system. In fact, our previous study demonstrated that the error due to the sensor was minimal and the considered torque estimation method (Hall sensor + BVP) showed high accuracy [47].

2.4.2 Results

Using the aforementioned setup, several experiments were performed to compare the stability and transparency of MRF-based clutches with electrical motors when implemented in a 1-DoF haptic interface of virtual wall. The virtual wall was implemented as a virtual torsional spring with stiffness K_w and a virtual rotational damper with damping coefficient B_w . At the frequency of 500 Hz (maximum achievable frequency using the current setup), interaction with a virtual wall with different stiffness and damping was tested using both types of couplings, *i.e.*, direct vs. MRF-based Clutch. The user held the handle and made several contacts with the virtual wall in each case.

First, a virtual wall with stiffness of $K_w = 10 \frac{\text{Nm}}{\text{rad}}$ and damping of $B_w = 10 \frac{\text{Nms}}{\text{rad}}$ was considered. In this case, due to the low stiffness, the wall exhibited high compliancy and it deformed substantially. Fig 2.6(a) presents the results of the interaction with the wall using the clutch and then using the motor as haptic devices. These plots depict the torque applied by the wall and the torque generated by the actuator. In addition, it depicts the position of the handle with respect to the wall (the wall starts at 0 deg). As seen, the clutch exhibited much higher transparency when the user makes contact with the wall. In fact, the root mean square (RMS) of the errors between the torque of the virtual wall and the torque felt by the user hand are 0.119 Nm and 0.667 Nm for the clutch and the DC motor, respectively. Then, a wall with higher stiffness was considered (*i.e.*, $K_w = 400 \frac{\text{Nm}}{\text{rad}}$ and $B_w = 10 \frac{\text{Nms}}{\text{rad}}$). The results are presented in Fig. 2.6(b). Once more, the clutch exhibits better transparency. The

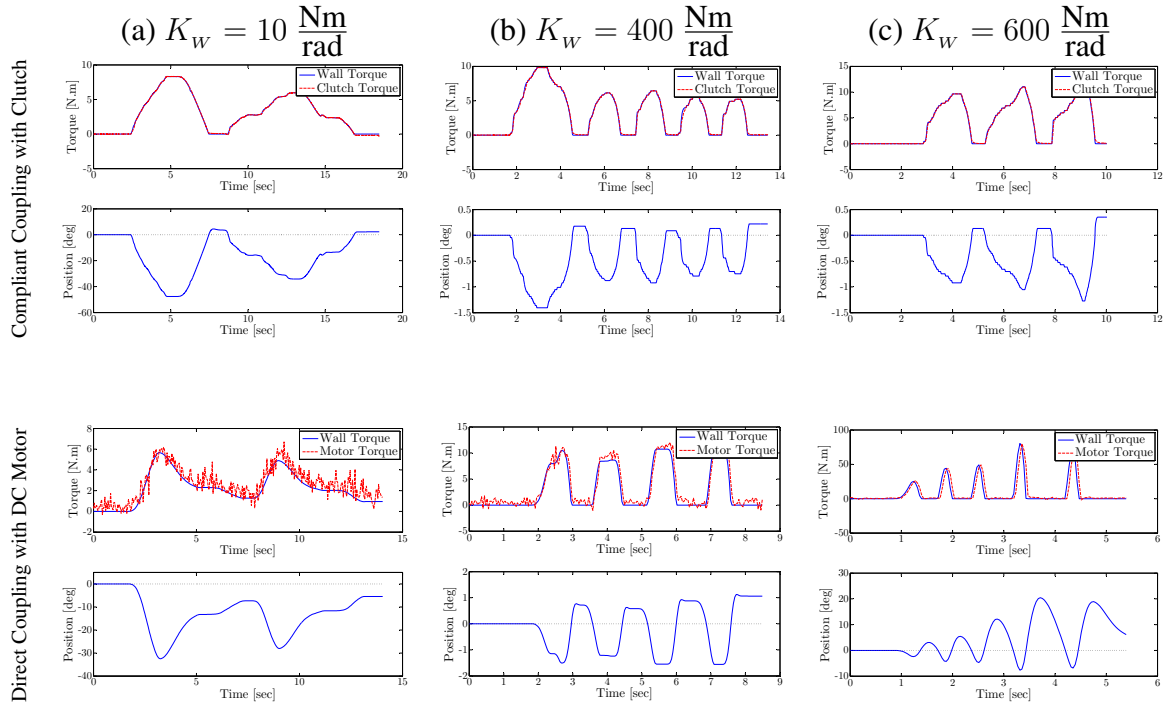


Figure 2.6: Results of interaction with the virtual wall at 500 Hz with damping $B_w = 10 \frac{\text{Nms}}{\text{rad}}$ and different stiffness for the MRF-based clutch (top row) and the DC motor (bottom row). The virtual wall starts at 0 deg position.

RMS errors for the torque in this case are 0.137 Nm and 0.94 Nm for the clutch and the DC motor, respectively. The advantages of the MRF-based clutch become more evident when the virtual wall becomes stiffer (*i.e.*, $K_w = 600 \frac{\text{Nm}}{\text{rad}}$ and $B_w = 10 \frac{\text{Nms}}{\text{rad}}$). The results for this case are depicted in Fig. 2.6(c). In this case, the clutch exhibits a few ripples in the output torque when a contact is made with the wall. However, these ripples are damped out after a few cycles. The RMS error of the torque is 0.185 Nm for the clutch. As it can be seen, the user is capable of making several stable contacts with the wall. However, in the case of the DC motor, the system becomes unstable as contact is made, and the user loses control. This is evident in the position of the handle in bottom image of Fig. 2.6(c). This result exhibits the better performance of the MRF-based clutch for use in haptic devices.

In fact, the clutch remained stable for $K_w < 1700 \frac{\text{Nm}}{\text{rad}}$. The comparison between the transparency of the two systems in the tests performed are given Table 2.1.

In another experiment, the maximum achievable stiffness with either of the haptic interfaces were obtained for several values of virtual damping B_w . Fig. 2.7 presents the results. The maximum achievable virtual stiffness using DC motor is limited due to constant physical damping of the motor. In the case of MRF-based clutch higher *Z-width* can be achieved. This shows the suitability of MRF-based actuators for use in haptic devices.

2.5 Concluding Remarks

MRF-based actuators exhibit promising characteristics for applications in haptic devices. Low output inertia, low mass-torque ratio, superior performance and bandwidth, precision controllability of output torque, and intrinsic passivity of MRF-based actuators are important characteristics for haptic interfaces. The results of the virtual wall experiment conducted in this paper on a large-scale prototype of an MRF-based clutch support these

Table 2.1: Transparency of the MRF-based clutch and DC Motor for different stiffness

$K_w [\frac{\text{Nm}}{\text{rad}}]$	RMS of error in Torque Display [Nm]	
	MRF-based clutch	DC Motor
200	0.105	0.803
400	0.137	0.940
600	0.185	Unstable
1000	0.185	Unstable
1700	Unstable	Unstable

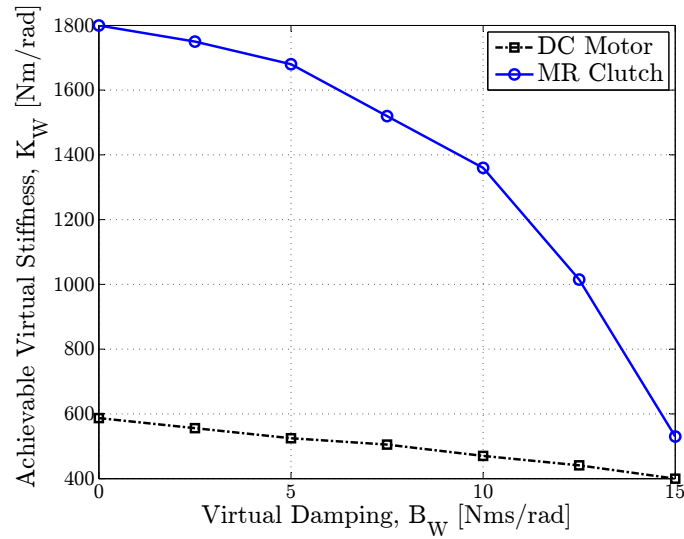


Figure 2.7: Maximum achievable virtual stiffness K_w [$\frac{\text{Nm}}{\text{rad}}$] for different virtual damping B_w [$\frac{\text{Nms}}{\text{rad}}$] at 500 Hz for the MRF-based clutch and DC motor

claims and demonstrate the desirable performance of such actuators when used in a haptic device. This provides a strong motivation for developing small-scale MRF-based actuators as a lightweight and compact actuating systems, which will be discussed in Chapter 3. Specifically, such actuators are well suited for haptic devices which are required to provide high-torque capacity, while having better stability and transparency.

Bibliography

- [1] A. Bicchi, M. Raugi, R. Rizzo, and N. Sgambelluri, "Analysis and design of an electromagnetic system for the characterization of Magneto-Rheological fluids for haptic interfaces," *IEEE Transactions on Magnetics*, vol. 41, pp. 1876 – 1879, may 2005.
- [2] R. Rizzo, N. Sgambelluri, E. Scilingo, M. Raugi, and A. Bicchi, "Electromagnetic modeling and design of haptic interface prototypes based on Magneto-Rheological fluids," *IEEE Transactions on Magnetics*, vol. 43, pp. 3586 –3600, Sep 2007.
- [3] Y. Nam, M. Park, and R. Yamane, "Smart Glove: Hand master using Magneto-Rheological fluid actuators," in *Proceedings of SPIE*, vol. 6794, pp. 679434–679434–6, 2007.
- [4] K. Kuchenbecker and G. Niemeyer, "Induced master motion in force-reflecting teleoperation," *Journal of Dynamic Systems, Measurement, and Control*, vol. 128, no. 4, pp. 800–810, 2006.
- [5] D. Senkal and H. Gurocak, "Haptic joystick with hybrid actuator using air muscles and spherical MR-brake," *Mechatronics*, vol. 21-6, pp. 951–60, 2011.
- [6] M. Reed and W. Book, "Modeling and control of an improved dissipative passive haptic display," in *IEEE International Conference on Robotics and Automation*, vol. 1, pp. 311 – 318, Apr 2004.
- [7] R. Lozano, N. Chopra, and M. Spong, "Passivation of Force Reflecting Bilateral Teleoperation with Time Varying Delay," *Journal of Mechatronics*, vol. 12, pp. 215–223, 2002.
- [8] I. Polushin, X. Liu, and C. Lung, "Stability of bilateral teleoperators with generalized projection-based force reflection algorithms," *Automatica*, vol. 48-6, pp. 1005–1016, 2012.
- [9] A. Shafer and M. Kermani, "On the feasibility and suitability of MR fluid clutches in human-friendly manipulators," *IEEE/ASME Transactions on Mechatronics*, vol. 16-6, pp. 1073 – 82, Dec 2010.
- [10] A. Shafer and M. Kermani, "On the feasibility and suitability of MR and ER based actuators in human friendly manipulators," in *IEEE/RSJ International Conference on Intelligent Robots and Systems*, pp. 2904 –2909, 2009.
- [11] J. Carlson, D. Catanzarite, and K. Clair, "Commercial Magneto-Rheological fluid devices," in *5th International Conference on Electro-Rheological, Magneto-Rheological Suspensions and Associated Technology*, 1995.

- [12] W. Wen, H. Huang, S. Yang, K. Lu, and P. Sheng, "The giant Electro-Rheological effect in suspensions of nanoparticles," *Natural Materials*, vol. 2, pp. 727–730, 2003.
- [13] M. Zinn, B. Roth, O. Khatib, and J. Salisbury, "A new actuation approach for human friendly robot," *The International Journal of Robotics Research*, vol. 23-4, p. 379, Apr 2004.
- [14] F. Ahmadkhanlou, G. Washington, and S. Bechtel, "Modeling and control of single and two degree of freedom Magneto-Rheological fluid-based haptic systems for telerobotic surgery," *Journal of Intelligent Material Systems and Structures*, vol. 20, pp. 1171–86, May 2009.
- [15] Y. Bar-Cohen, C. Mavroidis, M. Bouzit, B. Dolgin, D. Harm, and W. R. Kopchok, G.E., "Virtual reality robotic telesurgery simulations using MEMICA haptic system," in *SPIE Smart Structures Conference*, 2001.
- [16] P. Rankin, J. Ginder, and D. Klingenberg, "Electro- and Magneto-Rheology," *Current opinion in colloid and interface science*, vol. 3, pp. 373–381, Jul 1998.
- [17] A. Shafer and M. Kermani, "Design and validation of a MR clutch for practical control applications in human-friendly manipulation," in *International Conference on Robotics and Automation*, 2011.
- [18] N. Takesue, J. Furusho, and K. Kiyota, "Fast response MR-fluid actuator," *Journal of Society of Mechanical Engineering*, vol. 47, pp. 783–791, 2004.
- [19] P. Yadmellat and M. Kermani, "Adaptive modeling of a fully hysteretic Magneto-Rheological clutch," in *IEEE International Conference on Robotics and Automation*, 2012.
- [20] P. Yadmellat and M. Kermani, "Adaptive modeling of a Magneto-Rheological clutch," *IEEE/ASME Transactions on Mechatronics*, vol. 19, pp. 1716–1723, Oct 2014.
- [21] M. Seong, K. Sung, and S. Choic, "Damping force control of MR damper for a passenger vehicle considering hysteretic compensator," *Advanced Materials Research*, vol. 47, pp. 145–148, Jun 2008.
- [22] A. Olabi and A. Grunwald, "Design and application of Magneto-Rheological fluid," *Materials and Design*, vol. 28, pp. 2658–64, Nov 2007.
- [23] C. Pfeiffer, C. Mavroidis, Y. Bar-Cohen, and B. Dolgin, "Electro-Rheological fluid based force feedback device," in *SPIE International Society for Optical Engineering*, 1999.
- [24] E. Sontag, *Nonlinear and Optimal Control Theory*, ch. Input-to-state stability: Basic concepts and results, pp. 163–200. Springer-Verlag, 2006.

- [25] S. Sandberg, "Some results on the theory of physical systems governed by nonlinear functional equations," *Journal of Bell System Technology*, vol. 44, no. 1, pp. 871–98, 1965.
- [26] G. Zames, "On the input-output stability of time-varying nonlinear feedback systems. Part I: Conditions derived using concepts of loop gain, conicity, and positivity," *IEEE Transaction on Automatic Control*, vol. 11, no. 4, pp. 228–38, 1966.
- [27] Z. Jiang, A. Teel, and L. Praly, "Small-gain theorem for ISS systems and applications," *Mathematics, Control, Signals, Systems*, vol. 7, no. 1, pp. 95–120, 1994.
- [28] A. Teel, "A nonlinear small gain theorem for the analysis of control systems with saturation," *IEEE Transaction on Automatic Control*, vol. 41, no. 9, pp. 1256–70, 1996.
- [29] Z. Jiang, *Optimal Control, Stabilization, and Nonsmooth Analysis*, ch. Control of interconnected nonlinear systems: A small gain viewpoint, pp. 183–195. Springer-Verlag, 2004.
- [30] R. Oboe, "Force-reflecting teleoperation over the internet: the JBIT project," *Proceedings of the IEEE*, vol. 91, no. 3, pp. 449–462, 2003.
- [31] D. Liberzon, "Quantization, time delays, and nonlinear stabilization," *IEEE Transactions on Automatic Control*, vol. 51, no. 7, pp. 1190–1195, 2006.
- [32] I. Polushin, H. Marquez, A. Tayebi, and P. Liu, "A multichannel IOS small gain theorem for systems with multiple time-varying communication delays," *IEEE Transactions on Automatic Control*, vol. 54, pp. 404–409, Feb 2009.
- [33] I. Polushin, A. Tayebi, and H. Marquez, "Control schemes for stable teleoperation with communication delay based on IOS small gain theorem," *Automatica*, vol. 42, no. 6, pp. 905–915, 2006.
- [34] H. Khalil, *Nonlinear Systems*. Prentice Hall, 2002.
- [35] J. Abbott and A. Okamura, "Effects of position quantization and sampling rate on virtual-wall passivity," *IEEE Transactions on Robotics*, vol. 21-5, pp. 952–64, 2005.
- [36] M. Lin and M. Otaduy, *Haptic Rendering: Foundations, Algorithms and Applications*. A K Peters, 2008.
- [37] K. Kawashima, K. Tadano, G. Sankaranarayanan, and B. Hannaford, "Bilateral teleoperation with time delay using modified wave variables," in *IEEE/RSJ International Conference on Intelligent Robots and Systems*, pp. 424–429, Sep 2008.

- [38] J. Huang, Y. Shi, and J. Wu, "Transparent virtual coupler design for networked haptic systems with a mixed virtual wall," *IEEE/ASME Transactions on Mechatronics*, vol. 17, pp. 480–487, Jun 2012.
- [39] J. Colgate and J. Brown, "Factors affecting the Z-Width of a haptic display," in *IEEE International Conference on Robotics and Automation*, vol. 4, pp. 3205–10, 1999.
- [40] J. An and D. Kwon, "Stability and performance of haptic interfaces with active/passive actuators," *International Journal of Robotics Research*, vol. 25, pp. 1121–36, Nov 2006.
- [41] J. An and D. Kwon, "In haptics, the influence of the controllable physical damping on stability and performance," in *IEEE/RSJ International Conference on Intelligent Robots and Systems*, 2004.
- [42] D. Lee, Y. Nam, M. Park, and R. Yamane, "Transparency improvement of a 1-DOF hybrid haptic device with wide-ranged torque reflection," *International Journal of Applied Electromagnetics and Mechanics*, vol. 33, pp. 47–53, 2010.
- [43] A. Shafer and M. Kermani, *MR Clutch with Sensors Measuring Electromagnetic Field Strength*. US Patent 20130047772, Feb 2013.
- [44] M. Jolly, J. Bender, and J. Carlson, "Properties and applications of commercial Magneto-Rheological fluids," in *SPIE International Symposium on Smart Structures and Materials*, 1998.
- [45] W. Li, P. Yadmellat, and M. Kermani, "Linearized torque actuation using FPGA-controlled Magneto-Rheological actuators," *IEEE/ASME Transactions on Mechatronics*, vol. PP, pp. 1–9, May 2014.
- [46] M. Yu, S. Wang, J. Fu, and Y. Peng, "Unsteady analysis for oscillatory flow of Magneto-Rheological fluid dampers based on Bingham plastic and Herschel-Bulkley models," *Intelligent Material Systems and Structures*, vol. 24, pp. 1067–78, 2013.
- [47] P. Yadmellat and M. Kermani, "Output torque modeling of a MR based actuator," in *18th IFAC World Congress*, 2011.

Chapter 3

Design of a Small-Scale MRF-Based Clutch Suitable for a Haptic Interface

The promising results obtained in Chapter 2 led to the design and construction of a small-scale MRF-based actuator for a haptic interface. In this chapter, the design of such a small-scale MRF-based clutch, suitable for a multi-DoF haptic interface with a medical application, is discussed and its torque capacity, inertia, and mass are compared with conventional servo systems. Conclusions drawn from this chapter demonstrates the great potential of the new design to be used in haptic applications.

This chapter contains material published in (1) "Application of Magneto-Rheological Fluid Based Clutches for Improved Performance in Haptic Interfaces", presented at the IEEE Int Conf on Robotics and Automation, Hong Kong, June 1-4, 2014. and (2) "Suitability of Small-Scale Magneto-Rheological Fluid Based Clutches in Haptic Interfaces for Improved Performance", accepted for publication in the IEEE/ASME Transactions on Mechatronics, August 2014.

3.1 Introduction

In Chapter 2, actuators based on Magneto-Rheological Fluid (MRF) have been proposed as an alternative for electrical motors to be used in haptic devices. Such systems exhibit remarkable characteristics, including high yield stress, low mass-torque and inertia-torque ratios, compact size, intrinsic passivity, and precision controllability [1, 2]. It is expected that the superior characteristics of MRF-based actuators in comparison to active actuators will enable the design of a more transparent and stable haptic interface [3]. An investigation into this idea was performed in the previous chapter, and the tests on a large-scale MRF-based clutch, used as an haptic interface, supported these claims. However, as the work moves from the large-scale systems (not suitable for haptic applications) toward smaller scale ones (suitable for haptic interfaces), the main factors effective in the performance of such systems will be reduced significantly which might result in degraded superiority of MRF-based systems over electrical motors. The two main factors affecting the performance are the contact area between the two surfaces containing MRF and the strength of magnetic field which is a function of the magnetic reluctance and number of magnetic coil turns. In order to address this concern, a new design for small-scale MRF-based clutch, called "Armature-Based" design, which is suitable for a multi-DoF haptic interface is given in Section 3.2. In designing this new actuator the main focus is on higher contact area as well as stronger and more efficient use of magnetic field in comparison to conventional MRF-based clutch designs. By providing the analysis of such small-scale MRF-based system in Section 3.6, *i.e.*, its torque capacity, inertia, and mass, it is shown that in fact the proposed MRF-based actuator still exhibits desirable characteristics in comparison to the small-scale conventional actuators. This can contribute to the performance of a haptic interface. The current study lays the ground work for developing a multi-DoF haptic interface to be integrated in a surgical training environment, which will be presented in Chapters 4 and 5.

3.2 Preliminary Design of a Small-Scale MRF-Based Clutch

This section provides the results of a preliminary study on the design of such an actuator. The proposed actuator in this section is developed and the results are given in Chapter 4. The end goal of this project is to implement such actuators into a multi-DoF haptic interface which will be integrated in a surgical training environment. This is discussed in Chapter 5.

3.3 Proposed Clutch Structure

There are two main approaches to the design of MRF-based clutches reported in the literature, namely multiple-disk and drum-based designs [4]. The prototype discussed in Section 2.4 is an example of multiple-disk clutch where MRF fills the gap between the disks. Fig. 3.1(a) depicts the structure of such a design. In a disk-based design, the input shaft breaks out into a set of input disks, which are aligned in parallel to a set of output disks attached to the output shaft. MR fluid fills the space between input and output disks. A driver motor applies a constant torque to the input shaft. By energizing the electromagnetic coil, the viscosity of MR fluids, thereby the compliancy of the clutch is controlled [5]. In a drum-based design, the MRF fills the gap between two concentric cylinders, depicted in Fig. 3.1(b) [6]. Using a cylindrical coil inside the inner cylinder the shear stress between the two surfaces can be controlled [7].

Modified and hybrid versions of these two designs also exist [8]. The drum-based design is known to exhibit higher torque-volume ratio [4]. Thus, this approach is suitable when a compact and high-torque capacity actuator is desirable. On the other hand, the drum based design exhibits higher friction and inertia as the size of the actuator increases [5].

One major drawback of this design is the limited volume of the MRF that is energized between the two cylinders. Since the axis of the coil is collinear to the axis of the inner cylinder in this design, the magnetic field is applied to the MRF only at the two ends of the coil [9]. Hence the majority of the MRF gap is not activated during operation. In addition, an important tradeoff exist in designing drum-based clutches. By increasing the area that is needed for wiring the coil, the strength of the generated magnetic field will be increased. However, by doing so the area of contact between the inner and outer cylinder decreases which results in lower torque. In addition, since the field is only generated by one coil the magnetic circuit can become saturated which can significantly limit the torque capacity of the system. In this study, a new design – called armature-based – is proposed to improve the performance of the drum-based approach by increasing the effective MRF volume and the

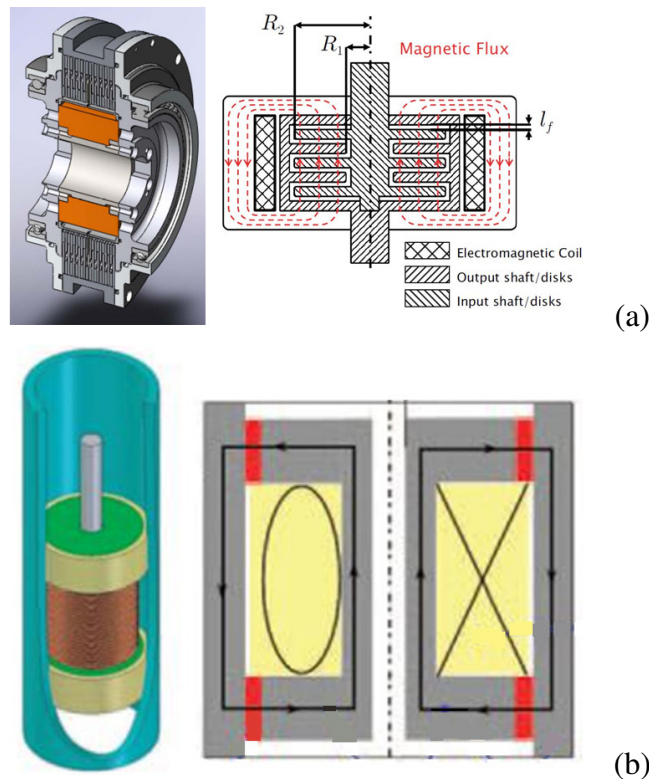


Figure 3.1: The structure of (a) disk- [1] and (b) drum-based clutches [6].

area of contact, as well as, improving the efficiency of magnetic field usage. The structure of the armature-based actuator is similar to that of a DC motor, as shown in Figs. 3.2(a,b).

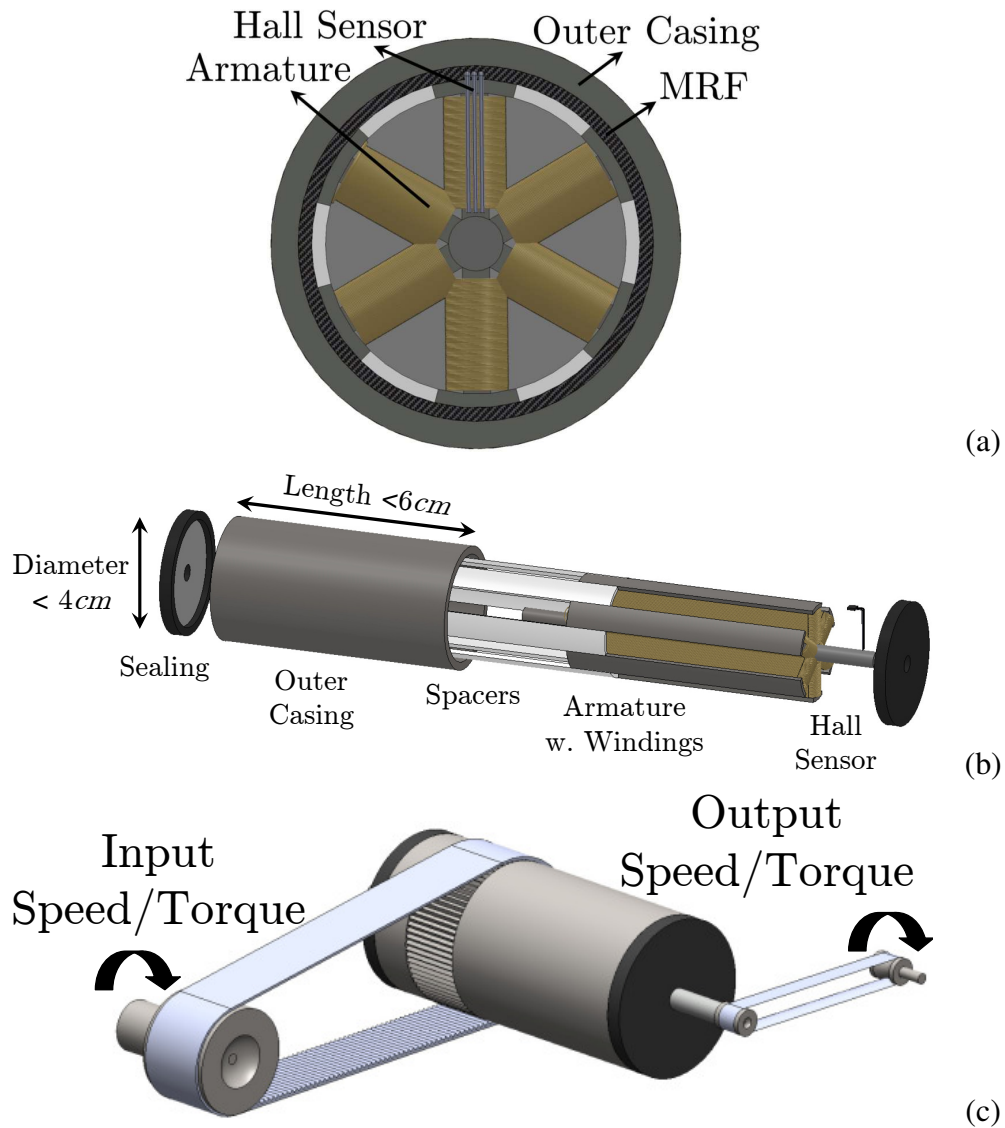


Figure 3.2: (a) Cross-sectional and (b) exploded view of the proposed small-scale MRF-based clutch. (c) Depiction of the proposed clutch operation.

In this design, the MRF fills the gap between a cylindrical casing and an armature, both made of ferromagnetic materials. The wire windings on the armature creates a magnetic field in the axial direction. Spacers, made out of light and nonmagnetic materials, separate the armature stack slots to avoid drag forces created by the fluid accumulated between the armature poles. Two Hall sensors will be used at the top of two of the poles (symmetrically) to measure magnetic field strength. As opposed to DC motors, commutation is not required in this design since there is no need for alternating poles.

Fig. 3.2(c) describe the overall configuration of this actuator. A constant input speed/torque is applied to the outer casing of the clutch, *e.g.*, using a motor. The output speed/torque controlled by the clutch is delivered to the output link using cables/belts. It should be noted that the clutch is only capable of providing unidirectional motion. In Chapter 5, the expansion of the proposed design into a multi-DoF system is discussed.

3.4 Figures of Merit

In this section, the derivation and analysis of the torque capacity, mass, and reflected inertia of the armature-based clutch is given. The symbolic dimensions of the outer casing and a single pole of the armature-based clutch is shown in Fig. 3.3. R_{c1} and R_{c2} , are the outer and inner casing radii, respectively. R_{a1} and R_{a2} are the outer and inner radii of armature tooth, respectively. θ_p is the angle of the arc of the armature tooth. R_{sh} is the radius of the armature shaft. W_p , W_{MR} , and W_c are the thicknesses of the armature pole, MRF gap, and the outer casing, respectively. In addition to these parameters, L_c is the length of clutch. Also, N_p , N_w , and i are the numbers of poles, number of wire turns at each pole, and the armature coil current, respectively.

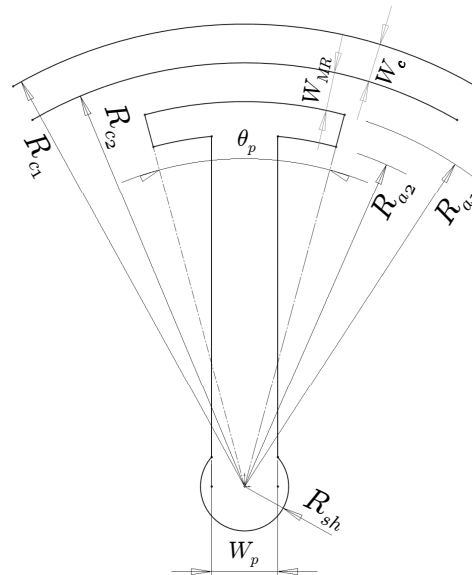


Figure 3.3: Dimension of the outer casing and a single pole of the clutch

3.4.1 Magnetic Reluctance and Flux

In order to obtain the torque capacity of the proposed design, first the magnetic reluctance of different parts of the magnetic circuit are obtained. A simplified model of the magnetic circuit is depicted in Fig. 3.4.

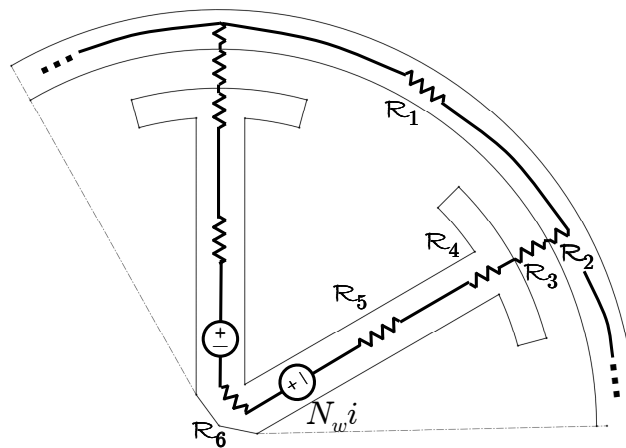


Figure 3.4: Magnetic circuit model of the armature-based clutch

Based on the dimensions of the clutch, the length l_k and area \mathcal{A}_k and subsequently, the magnetic reluctance \mathcal{R}_k of each armature part is obtained as follows ($k = 1, \dots, 6$),

$$\begin{aligned}
 l_1 &= \theta_p(R_{c1} + R_{c2}) & \mathcal{A}_1 &= W_c L_c & \mathcal{R}_1 &= \frac{l_1}{\mu_{st} \mathcal{A}_1} \\
 l_2 &= \frac{W_c}{2} & \mathcal{A}_2 &= \theta_p R_{c2} L_c & \mathcal{R}_2 &= \frac{l_2}{\mu_{st} \mathcal{A}_2} \\
 l_3 &= W_{MR} & \mathcal{A}_3 &= \theta_p R_{a1} L_c & \mathcal{R}_3 &= \frac{l_3}{\mu_{MR} \mathcal{A}_3} \\
 l_4 &= R_{a1} - R_{a2} & \mathcal{A}_4 &= \theta_p R_{a2} L_c & \mathcal{R}_4 &= \frac{l_4}{\mu_{st} \mathcal{A}_4} \\
 l_5 &= R_{a2} - R_{sh} & \mathcal{A}_5 &= W_p L_c & \mathcal{R}_5 &= \frac{l_5}{\mu_{st} \mathcal{A}_5} \\
 l_6 &= 2\theta_p R_{sh} & \mathcal{A}_6 &= R_{sh} L_c & \mathcal{R}_6 &= \frac{l_6}{\mu_{st} \mathcal{A}_6}
 \end{aligned} \tag{3.1}$$

where μ_{st} and μ_{MR} are the magnetic permeability of the steel and the MRF, respectively. The magnetic flux ϕ and the magnetic flux density B at the MRF gap perpendicular to the armature surface can now be obtained as,

$$\phi = \frac{4N_w i}{\mathcal{R}_1 + 4\mathcal{R}_2 + 4\mathcal{R}_3 + 4\mathcal{R}_4 + 4\mathcal{R}_5 + \mathcal{R}_6} \tag{3.2}$$

$$B = \frac{\phi}{\mathcal{A}_{MR}} = \frac{\phi}{\mathcal{A}_3} \tag{3.3}$$

where $\mathcal{A}_{MR} = \mathcal{A}_3$ is the activated area of MRF at each pole. The magnetic saturation should be considered in the above equations. Bingham-Visco plastic model [10–12] can be used to calculate the shear stress τ at the gap,

$$\tau(B, \omega) = \tau_y(B) + \eta\omega R_{a1} W_{MR}^{-1} \quad (3.4)$$

where τ_y is the field-dependant yield stress, η is the newtonian viscosity, and ω is angular velocity between the casing and armature. Data relating to the yield stress τ_y of a fluid are generally published by the manufacturer. Typical values of this parameter are 50 to 100 kPa. The viscosity η of the carrier fluid is typically in the range of 0.1-0.3 Pa.s. Hence, in this study, we consider the torque transmitted solely by the field dependant yield stress of the MRF. Calculating the value of τ_y , the magnitude of the generated braking torque T will be obtained as,

$$T_{arm} = N_p \tau_y(B) \mathcal{A}_{MR} R_{a1} \quad (3.5)$$

REMARK 4. This method of calculation of the output torque is based on the direct application of the physical laws as well as measurement of the applied magnetic field. This method has been previously used in other studies to calculate the output torque [6, 10, 13–15].

From (3.5), it is clear that the amount of torque a clutch can produce highly depends on the strength of the magnetic field. In order to create a stronger magnetic field, a larger number of wire turns in the winding and higher electrical current are required. The number of wire turns and the wire gauge (maximum safe current) are limited by the available space in the armature stack slots, as well as, the limit on the mass and inertia of the armature. On the other hand, the dimensions of the armature poles and shaft can limit the created magnetic field due to magnetic saturation. If the smallest area $\mathcal{A}_{min} = \min(\mathcal{A}_1, \dots, \mathcal{A}_6)$ of the armature magnetic circuit is designed to be much smaller than the MRF gap area, *i.e.*, $\mathcal{A}_{min} \ll \mathcal{A}_{MR}$, then that area can become saturated (*i.e.*, $\frac{\phi}{\mathcal{A}_{min}} \gg \frac{\phi}{\mathcal{A}_{MR}}$), and significantly reduce the magnetic field at the MRF gap.

An important factor affecting the transparency of a haptic interface is the off-state friction forces and torques. In order to calculate the value of zero-field friction torque for the proposed clutch, first the value of magnetic field density is set to zero in (3.4). Then for any given rotational speed the zero-field shear stress $\tau(0, \omega)$ is obtained. This value is substituted with $\tau_y(B)$ in equations (3.5) to calculate the zero-field torque T_0 ,

$$T_0(\omega) = N_p \mathcal{A}_{MR} (\tau_y(0) R_{a1} + \eta \omega R_{a1}^2 W_{MR}^{-1}) \quad (3.6)$$

Note that the sealing friction is not included in this calculation.

3.4.2 Actuator Mass and Reflected Inertia

As mentioned, the effective inertia of the armature and the weight of the clutch are also important factors with regards to the transparency of a haptic interface. The weight of the clutch M_{cl} can be obtained as,

$$M_{cl} = \rho_{st} (V_{sh} + N_p V_p + V_c) + \rho_{MR} V_{MR} + M_w \quad (3.7)$$

where ρ_{st} and ρ_{MR} are the density of steel and MRF, respectively, V_{sh} , V_p , V_c , V_{MR} are the volume of the armature shaft, pole, outer case, and MRF gap, respectively, and M_w is the mass of wire windings. These values are derived as,

$$V_{sh} = \pi R_{sh}^2 L_c \quad (3.8)$$

$$V_p = L_c (W_p (R_{a2} - R_{sh}) + \frac{\theta_p}{2} (R_{a1}^2 - R_{a2}^2)) \quad (3.9)$$

$$V_c = \pi L_c (R_{c1}^2 - R_{c2}^2) \quad (3.10)$$

$$V_{MR} = \pi L_c (R_{c2}^2 - R_{a1}^2) \quad (3.11)$$

$$M_w = 2N_p N_w (L_c + W_p) m_w \quad (3.12)$$

where m_w is value of the mass per unit of the wire used in the coil. The reflected inertia of the armature J_{arm} can also be obtained as,

$$J_{arm} = J_{sh} + N_p J_p + J_w \quad (3.13)$$

where J_{sh} , J_p , and J_w are the moment of inertia of the armature shaft, pole, and wire winding, respectively. These values are derived as,

$$J_{sh} = \frac{\pi}{2} \rho_{st} L_c R_{sh}^4 \quad (3.14)$$

$$J_p = N_p \rho_{st} L_c \left[\frac{\theta_p}{4} (R_{a1}^4 - R_{a2}^4) + \dots \right. \\ \left. \frac{W_p^3}{12} (R_{a2} - R_{sh}) + \frac{W_p}{3} (R_{a2}^3 - R_{sh}^3) \right] \quad (3.15)$$

$$J_w = \frac{1}{2} M_w (R_{sh}^2 + R_{a2}^2) \quad (3.16)$$

3.5 Optimization

An optimization problem is defined and solved to calculate the proper dimensions which result in the optimal characteristics of the MR clutch. Three main factors are considered in this optimization, namely the maximum torque, inertia, and zero-field friction torque of the clutch. Each factor is a function of MR clutch dimensions, represented with the vector \mathbf{D} , plus the number of wire turns N_w . Hence, The objective function is defined as,

$$E(\mathbf{D}, N_w) = \frac{T_0(0)J_{arm}}{T_{arm}J_{critical}} \quad (3.17)$$

where $J_{critical}$ is the maximum allowable value for the inertia of the armature (defined based on system minimum requirements). A set of constraints $\mathbf{f}(\mathbf{D}, N_w)$, in the forms of equalities and inequalities, are also defined. These constraints limits the minimum or/and maximum allowable range for the dimensions and wire turns and they include, but not limited to,

- the desired diameter and length of the clutch
- trivial relations between dimensions (*e.g.*, $R_{c2} < R_{c1}$, $R_{a1} < R_{c2}$, etc.)
- constraints due to magnetic saturation (*e.g.*, $\frac{\phi}{A_{min}} \leq B_{sat}$, B_{sat} is the saturation field)
- constraints due to machining and structural limitations (*e.g.*, minimum thickness of the casing wall, poles, etc.)
- minimum acceptable dimensions (*e.g.*, the optimization tends to make the MRF gap as small as possible to increase magnetic field, hence, this should be avoided by setting a lower bound on its dimensions)
- limitation on the number of wire turns due to the available space between the armature stack slots and the magnetic saturation

Thus, the optimization problem is defined as,

$$\begin{aligned} \min \quad & E(\mathbf{D}, N_w) \\ \text{subject to} \quad & \\ \mathbf{f}(\mathbf{D}, N_w) \quad & \end{aligned} \quad (3.18)$$

Several trade-offs exist in this problem. One such trade-off is the effect of the number of wire turns on the torque capacity and armature inertia. By increasing N_w the magnetic flux density in the MRF gap becomes larger which in turn can result in higher generated torque. However, this degrades the transparency of the system by adding more weight and inertia to the armature. In addition, the increase in number of turns becomes redundant after a certain level due to the magnetic saturation in narrower parts of the magnetic circuit. The thickness of MRF gap (*i.e.*, W_{MR}) also plays an important role in this optimization. The smaller the MRF gap, the greater the maximum produced torque will be. However, the small gap size results in higher value of zero-field torque. In the rest of the chapter, the results obtained based on the above optimization will be used in subsequent calculations. Since, the problem defined in (3.18) is nonlinear, a numerical approach from the family of Quasi-Newton optimization techniques, specifically, Davidson-Fletcher-Powell is used for obtaining a solution [16, 17]. This algorithm exhibits quadratic convergence.

3.6 Comparison with MRF and Conventional Actuators

In this section, the characteristics of the armature-based clutch are compared with that of counterpart MRF-based clutches and DC motors.

3.6.1 Comparison with Drum- and Disk-Based Clutches

To study the magnetic field inside the MRF-based actuators, the Finite Element Modeling (FEM) method was used. This work took advantage of FEMM Software [18] to perform the FEM. Fig. 3.5(a) depicts the magnetic field paths inside an armature-based clutch and Fig. 3.5(b) shows the magnitude of the flux density within the MRF gap, perpendicular to the armature surface. Figs. 3.5(b) and (c) present the same information for a drum-based and a disk-based clutch, respectively. Note that the volume of all three actuators are considered to be the same.

As seen, the armature-based design creates a more homogenous and stronger magnetic field at the MRF gap. On the other hand, the magnetic field in a drum-based design is stronger closer to the coil. In this design, the MRF gap is not uniformly activated and a large portion of the MRF is not activated. These shortcomings limit the maximum achievable torque in a drum-based clutch. As will be discussed later in this section, disk-based actuators exhibit the lowest magnetic field magnitude due to their large MRF gap. However, disk-based design takes advantage of a large overlapping area between the input and output disks which significantly increases the torque capacity of a disk-based clutch. In addition, there is no trade off between area of contact and the number of wire turns in this design, as opposed to drum-based systems. As the size of the clutch becomes smaller, it is anticipated that the torque capacity of the disk-based clutch decreases drastically due to the decrease in the area of MRF gap.

The torque of a drum-based clutches can be obtained as [7],

$$T_{drum} = 4\pi\tau_y(B)L_pR_{dr}^2 \quad (3.19)$$

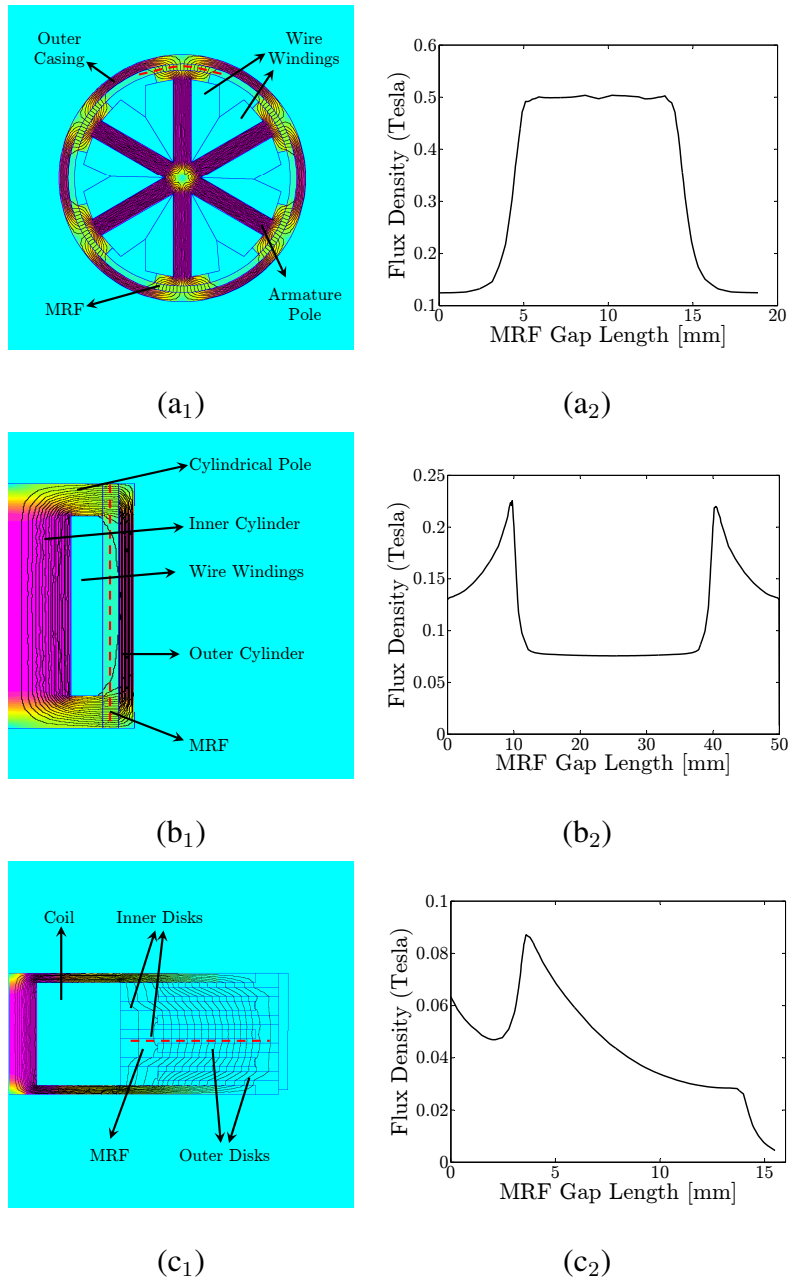


Figure 3.5: Figures in the left column show the magnetic field distribution in (a₁) cross-sectional view of armature-based, and axisymmetric views of (b₁) drum-based, and (c₁) disk-based designs, with same volume. Figures in the right column depict the magnitude of the magnetic density in the MRF gap (shown by red dashed lines) perpendicular to the (a₂) armature surface, (b₂) cylindrical pole surface, and (c₂) disk surface.

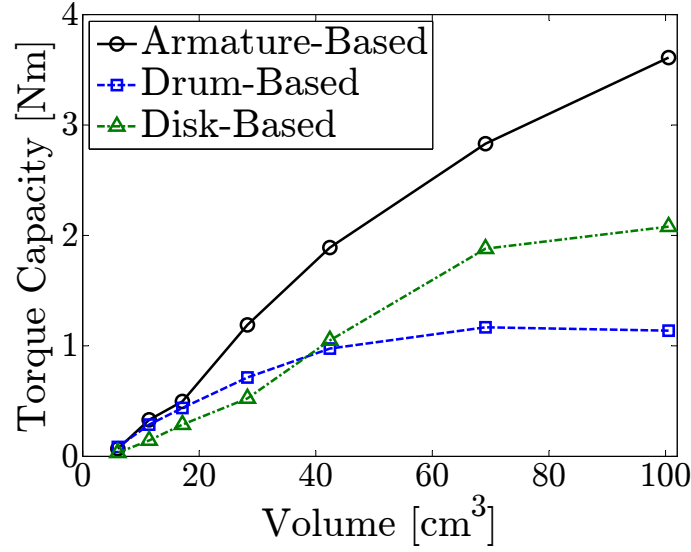


Figure 3.6: Comparison between the torque capacity of armature-, drum-, and disk-based designs with comparable volume

where L_p and R_{dr} are the length of cylindrical pole and the radius of the inner drum, respectively. In the case of a disk-based clutch this value is derived as [5],

$$T_{disk} = \frac{4}{3}\pi N_d \tau_y (B) (R_{d1}^3 - R_{d2}^3) \quad (3.20)$$

where N_d , R_{d1} , and R_{d2} are the number, outer radius, and inner radius of the disks, respectively. In order to compare the torque capacity of the three designs, clutches with identical volume were considered and their maximum torque capacities were obtained based on equations (3.5), (3.19), and (3.20). The results are depicted in Fig. 3.6. For the armature- and drum-based clutches the dimensions were identical with the dimensions of Maxon EC-Max series (included in Table 3.1). For the disk-based design, equal volume were considered. The number of disks in the latter case was calculated based on the corresponding dimensions and it ranged between two to four pairs of disks.

As seen, our proposed armature-based design exhibits a higher torque capacity in comparison to its counterparts. This can be attributed to several factors in this design; (1) The strength and homogeneity of the magnetic field at the MRF gap is an important factor as can be seen in equation 3.5. (2) Another important factor is the larger area of activated MRF between the armature and the outer casing in this structure. The poles cover the whole length of the clutch, which is not the case for the drum-based clutch. This results in a larger overlapping area (*i.e.*, $N_p \theta_p R_{a1} L_c > 2\pi L_p R_{dr}^2$). The disk-based torque capacity decreases as the size of the disk overlap becomes smaller. (3) The placement and concentration of the coil in one place in the drum- and disk-based designs also limits the output torque due to the problem of magnetic saturation. In fact, the increase in the number of wire turns becomes redundant after a certain level in this design since some parts of the actuator become saturated due to the highly concentrated generated magnetic field. This problem is alleviated in the armature-based design by sharing the responsibility of magnetic field generation between multiple poles.

The inertia- and mass-torque ratios of the three designs were also compared. Figs. 3.7(a) and (b) present the result of such comparisons. It can be concluded from these results that the armature-based clutch exhibits better inertia-torque and mass-torque ratios, which makes it suitable for application in haptic interfaces.

Next, the zero-field friction torque of the three designs are compared. This is done for an armature- and drum-based clutch with diameters of 3 cm and lengths of 6 cm, as well as, a disk-based actuator with thickness of 3 cm, diameter of 4.25 cm, and 4 sets of disks. Note that the friction caused by sealing is not considered in this section. The result is presented in Fig. 3.8. The drum-based design exhibits the lowest friction torque among the three. However, when considering the percentage of such a force (*i.e.*, $\frac{T_0}{T_{max}}$), the armature-based design is the most optimized. This percentage ranges between 3.4 to 6.2%. This value is

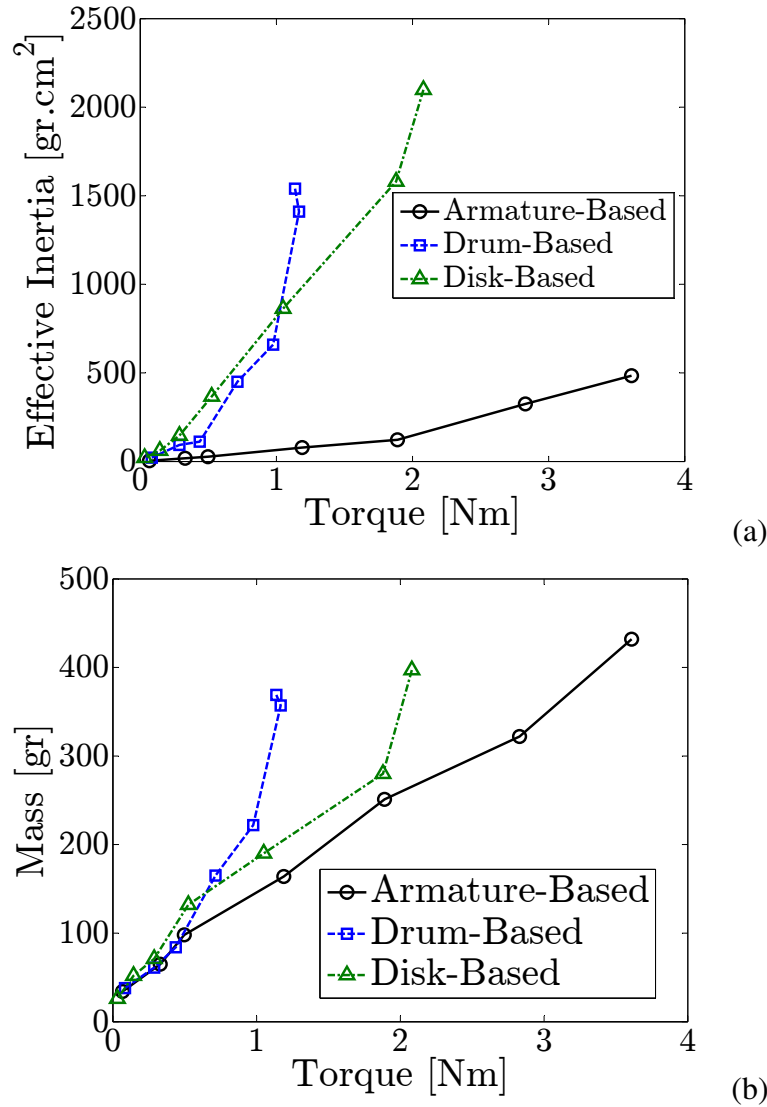


Figure 3.7: Comparison of (a) inertia-torque and (b) mass-torque ratios between armature-, drum-, and disk-based designs with comparable volume

4.5 – 8.5% for the drum-based and 15 – 39% for the disk-based designs. One possible solution for further decreasing the zero-field torque might be the use of MRF foam as reported in [6]. However, such a solution and its possible effects on the clutch torque capacity will be tested in the manufacturing stage of the study. As discussed in this section, the armature-based design exhibits better characteristics comparing to drum- and disk-based clutches. This can contribute to the stability and transparency when used in a haptic interface. The

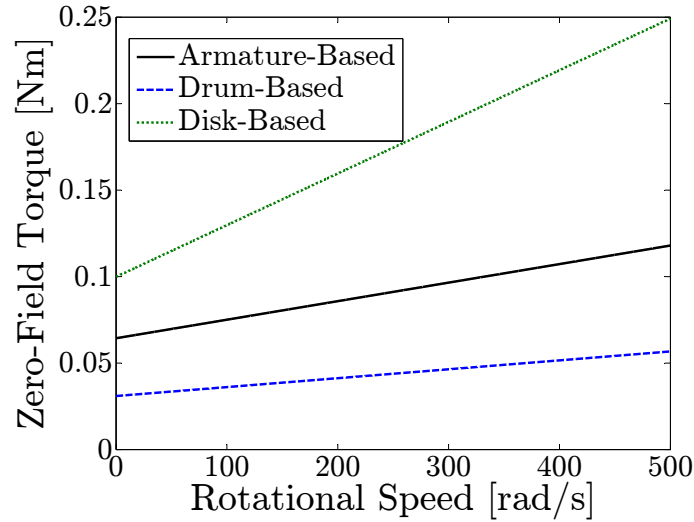


Figure 3.8: Comparison of zero-field friction torque between armature-, drum-, and disk-based designs with comparable volume

main disadvantage of this design is its complex structure relative to drum- and disk-base designs. Nevertheless, the structure is simple enough for manufacturing at a low price.

3.6.2 Comparison with Conventional DC Motors

In order to further assess the suitability of the proposed armature-based design, a comparison with Maxon EC-max DC motors [19] is performed in this section. This series of motors includes some of the most powerful and versatile small-scale DC motors. To perform the comparison, the armature-based MRF-based clutches with the exact dimensions of the Maxon motors and with six poles ($N_p = 6$) are considered. Then, their torque capacity, reflected inertia, and weight are compared with those of the Maxon motors. Table 3.1 presents the torque capacity of the motor and the clutch with similar dimensions. The results show the superiority of the clutch in comparison to the Maxon motors.

Table 3.1: Comparison between torque capacity of Maxon EC-max and MRF-based clutch with same dimensions *Note: ECXX YYW = EC-Max XX, YY Watt*

Motor Model	EC40 120W	EC40 70W	EC30 60W	EC30 40W	EC22 25W	EC22 12W	EC16 8W
Diameter [cm]	4	4	3	3	2.2	2.2	1.6
Length [cm]	8	5.5	6	4	4.5	3	3
Nominal Torque [Nm]	0.168	0.094	0.063	0.034	0.023	0.010	0.008
Stall Torque [Nm]	2.090	0.636	0.519	0.160	0.127	0.035	0.022
Clutch Torque [Nm]	3.610	2.830	1.890	1.190	0.497	0.330	0.068

Next the mass and effective inertia are compared. Fig. 3.9 presents a comparison of the inertia-torque and mass-torque ratios. MRF-based clutches exhibit lower ratios, which demonstrates their suitability for use in a haptic interface.

It should be noted that to have a fair comparison between the inertia of the actuators, the reflected inertia of the DC motors is calculated as $J_{eq} = G_r^2 J_{rot}$. J_{rot} is the rotor inertia of the DC motor [19]. G_r is the gear ratio required to create an output motor torque comparable to that of the clutch, *i.e.*, $T_{eq} = G_r T_{stall}$. However, the gear reduction is not considered when comparing the actuator's mass. The stall torque (and not the nominal torques) of the motors are considered in these results.

3.7 Challenges and Shortcomings

A few challenges are expected in developing the armature-based clutch and the multi-DoF haptic interface. In what follows some of the main challenges and shortcomings of the designed actuators are presented and the planned solutions to avoid or remedy these problems are discussed.

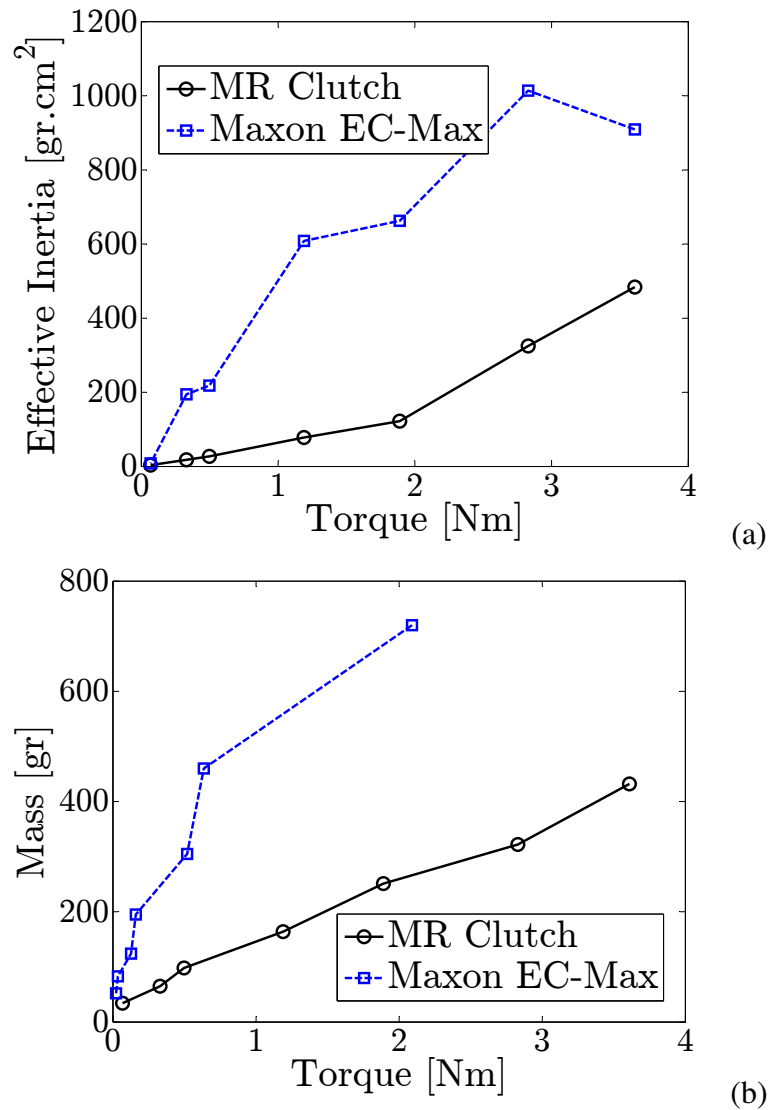


Figure 3.9: (a) Inertia to torque (with gear reduction) and (b) mass to torque (without gear reduction) ratios for Maxon EC-max and MRF-based clutch

3.7.1 Heat Generation

The electrical current in the wound armature can generate thermal energy in the clutch. MR fluids have a typical operable temperature range of -40 to 150°C , however their behavior might change as a result of temperature variation. The outer casing of the clutch (made of

steel), which has a large area of contact with air can act as a heat sink. This can moderate the temperature deviations. Fins can be added to the surface of the casing to increase the area of thermal exchange. Temperature sensors should be integrated in the clutch to account for any temperature deviations in the system model. Since temperature-dependant model variation in MRF characteristics is very moderate [13], the integration of the temperature sensors in the system will be postponed for the second generation of the device.

3.7.2 Leakage

The proper sealing of the clutch to avoid any fluid leakage is an important issue. The heating effect of the wires, which can increase the fluid pressure, adds to the importance of proper sealing in the clutch. O-rings are considered to seal the gap between the outer casing and the caps. This method has been proved effective in previous designs in our group. The main challenge is in sealing the bearing that is placed between the armature shaft and the casing caps. If any particles leak into the balls of the bearing, it can cause friction and even jamming in the bearing. Shielded bearings can be implemented to decrease the chance of leakage, however, based on the existing experience, this solution helps but is not sufficient. Stretch-fit rotary-shaft oil seals, placed on the armature shaft, should be used to protect the bearing. But this adds to the friction of the system.

3.7.3 Friction

Any friction in the system can degrade the transparency of the system. The zero-field friction torque (Section 3.6) is caused as a result of the viscosity of the fluid. Any residual magnetic field in the system can result in a biased shear stress and the user will feel added friction as a result. Also the aforementioned oil seals can create large frictions. Although

this is a serious concern, the antagonistic configuration, presented in Chapter 5, will solve this problem to a great extent (if not completely). This is due to the fact that the created friction forces in a pair of clutches antagonistically connected to a single joint will have similar magnitude, but in opposite directions. Hence, the friction forces will cancel out each other.

3.7.4 Thickening

MRF are consisted of an oil-like carrier fluid and suspended ferrous particles. If the fluid is left stationary for a long time, the particles will precipitate and the thickening of the fluid will occur. The MRF manufacturers alleviated this problem by using stabilizer additives to the fluid. This will slow down the precipitation and elongates the fluid life. Even if as the result of immobility the fluid is thickened, it is believed that the particles will mix very quickly by creating a few jerky motion. The facts that these fluids have been used in automotive industry for more than a decade shows the durability of such devices. Nevertheless, a device might require maintenance as a result of severe thickening, which will add to the effective cost of the system.

3.7.5 Nonlinearity and Hysteresis

As mentioned in Chapter 2, MRF-based actuators suffer from nonlinear hysteretic relationships between the input current and output torque. The overall hysteresis in MRF-based actuators can be as small as 5%, and is comparable to the hysteresis present in most commercial dampers and pneumatic actuators with respectively 50% and 40% of hysteresis. Nevertheless, this nonlinearity causes inaccuracy in the output response of the actuator, as well as, instability of the closed loop system [20]. Therefore, it is essential to study

and model the current-torque relationship in MRF-based actuators for a reliable control and actuation and delivering high-fidelity force/torque control in haptic interfaces utilizing MRF-based actuators. This issue is addressed in Chapter 4.

3.8 Concluding Remarks

MRF-based actuators exhibit promising characteristics for applications in haptic devices. Low output inertia, low mass-torque ratio, superior performance and bandwidth, precision controllability of output torque, and intrinsic passivity of MRF-based actuators are important characteristics for haptic interfaces. This provides a strong motivation for developing small-scale MRF-based actuators as lightweight and compact actuating systems. Specifically, such actuators are well suited for haptic devices which are required to provide high-torque capacity, while having better stability and transparency. Our preliminary studies on a small-scale armature-based clutch supported this claim. In the next chapter, the development and validation of the prototype small-scale high-torque MRF-based clutch is reported. This actuator will then be used in a lightweight multi-DoF haptic interface with a PA-DASA configuration for a specific medical application, as will be discussed in Chapter 5.

Bibliography

- [1] A. Shafer and M. Kermani, "On the feasibility and suitability of MR fluid clutches in human-friendly manipulators," *IEEE/ASME Transactions on Mechatronics*, vol. 16-6, pp. 1073 – 82, Dec 2010.
- [2] A. Grunwald and A. Olabi, "Design of Magneto-Rheological (MR) valve," *Journal of Sensors and Actuators*, vol. 148, no. 1, pp. 211 – 223, 2008.
- [3] A. Bicchi, M. Raugi, R. Rizzo, and N. Sgambelluri, "Analysis and design of an electromagnetic system for the characterization of Magneto-Rheological fluids for haptic interfaces," *IEEE Transactions on Magnetics*, vol. 41, pp. 1876 – 1879, May 2005.
- [4] P. Nguyen and B. Choi, "Selection of Magneto-Rheological brake types via optimal design considering maximum torque and constrained volume," *Smart Materials and Structures*, vol. 21-1, pp. 1–12, Dec 2012.
- [5] A. Shafer and M. Kermani, "Design and validation of a MR clutch for practical control applications in human-friendly manipulation," in *International Conference on Robotics and Automation*, 2011.
- [6] F. Ahmadkhanlou, G. Washington, and S. Bechtel, "Modeling and control of single and two degree of freedom Magneto-Rheological fluid-based haptic systems for telerobotic surgery," *Journal of Intelligent Material Systems and Structures*, vol. 20, pp. 1171–86, May 2009.
- [7] P. Nguyen and B. Choi, "Accurate torque control of a bi-directional Magneto-Rheological actuator considering hysteresis and friction effects," *Smart Materials and Structures*, vol. 22-25, pp. 1–12, Mar 2013.
- [8] M. Avraam, *MR-fluid brake design and application to a portable rehabilitation device*. PhD thesis, Univ Libre de Bruxelles, 2009.
- [9] D. Case, B. Taheri, and E. Richer, "Dynamical modeling and experimental study of a small-scale Magneto-Rheological damper," *IEEE/ASME Transactions on Mechatronics*, vol. 19, pp. 1015–1024, Jun 2014.
- [10] P. Yadmellat and M. Kermani, "Adaptive modeling of a fully hysteretic Magneto-Rheological clutch," in *IEEE International Conference on Robotics and Automation*, 2012.
- [11] M. Jolly, J. Bender, and J. Carlson, "Properties and applications of commercial Magneto-Rheological fluids," in *SPIE International Symposium on Smart Structures and Materials*, 1998.

- [12] W. Li, P. Yadmellat, and M. Kermani, "Linearized torque actuation using FPGA-controlled Magneto-Rheological actuators," *IEEE/ASME Transactions on Mechatronics*, vol. PP, pp. 1–9, May 2014.
- [13] A. Shafer and M. Kermani, "On the feasibility and suitability of MR and ER based actuators in human friendly manipulators," in *IEEE/RSJ International Conference on Intelligent Robots and Systems*, pp. 2904–2909, 2009.
- [14] P. Yadmellat and M. Kermani, "Output torque modeling of a MR based actuator," in *18th IFAC World Congress*, 2011.
- [15] F. Ahmadkhanlou, G. N. Washington, S. E. Bechtel, and Y. Wang, "Magneto-Rheological fluid based automotive steer-by-wire systems," in *Proceedings of SPIE*, vol. 6171, p. 61710I, SPIE, 2006.
- [16] L. Foulds, *Optimization Techniques*. Springer-Verlag New York Inc., 1981.
- [17] R. Schoenberg, "Optimization with Quasi-Newton methods," tech. rep., Aptech Systems Inc., Maple Valley, WA, 2001.
- [18] D. Meeker, "Finite Element Method Magnetics Software, Version 4.0.1, <http://www.femm.info/>." 2006.
- [19] Maxon Motor, *High Precision Drives and Systems*, 2013.
- [20] H. Khalil, *Nonlinear Systems*. Prentice Hall, 2002.

Chapter 4

Development, Modeling, Control, and Validation of the Prototype Clutch

In previous chapters, the potential benefits of Magneto-Rheological Fluid (MRF) based actuators to the field of haptics were studied. A novel design of a small-scale MRF-based clutch, suitable for haptic applications, was proposed in Chapter 3. This chapter reports on the development and experimental validation of the proposed MRF-based clutch. In addition, a closed-loop torque control strategy is presented. The feedback signal used in this control scheme comes from the magnetic field acquired from Hall sensors within the MRF-based clutch. The controller uses this feedback signal to compensate for the nonlinear behavior of the clutch using an estimated model, based on Artificial Neural Networks (ANNs). The performance of the developed design and the effectiveness of the proposed modeling and control techniques are experimentally validated. The results clearly demonstrate that the clutch shows great potential for use in a multiple degrees-of-freedom (DoF) haptic interface for a class of medical applications requiring accurate, highly transparent, and stable force representation in a teleoperation procedure.

This chapter contains material included in the paper "Magneto-Rheological Actuators for Haptic Devices: Design, Modeling, Control, and Validation of a Prototype Clutch", submitted to the IEEE International Conference on Robotics and Automation, Seattle WA, May 26-30, 2015.

4.1 Introduction

Force and tactile feedback can be used to simulate interaction with remote or virtual environments during a teleoperation procedure. Such feedback enables the user to adjust the force control actions to ensure accuracy and safety of the operation. The actuators and instruments used in designing a haptic interface play an important role with regard to the quality of force feedback (known as system transparency), as well as stability of the system [1]. This adds to the complexity of haptic interface design. Actuators based on Magneto-Rheological Fluids (MRFs) have been proposed as an alternative to electrical motors for use in haptic devices [2]. It has been demonstrated that the superior characteristics of MRF-based actuators in comparison with active actuators enables the design of a more transparent and stable haptic interface, as shown in our previous chapters. This claim was experimentally validated on a large-scale prototype MRF-based haptic system, by taking advantage of the virtual wall benchmark [3, 4]. The results of these experiments demonstrated the desirable performance of such actuators when used in a haptic device. Subsequently, a new design for a small-scale MRF-based clutch, called an armature-based design, which is suitable for a multi-DoF medical haptic interface was proposed in the previous chapter. Our preliminary studies on the small-scale armature-based clutch supported the claim that such actuators are well suited for haptic devices.

This chapter reports on the development and construction of four prototype MRF-based clutches based on the proposed design. The dimensions and electromechanical specifications of the developed clutches are provided. The contribution of the current work to the state of the art is discussed by comparing the performance factors with both conventional electrical motors and MRF-based actuators reported for haptic applications. It is shown that the proposed design provides a feasible alternative for use in a haptic interface for medical applications, especially in terms of torque-to-size ratio. In order to efficiently and accu-

rately control the torque of the system, which is essential for transparent haptic feedback, a control scheme based on an new nonlinear model is proposed. This model takes advantage of an ANN, which is trained by a set of pre-recorded experiments, to predict the hysteretic nonlinear behavior of the system. This model is then used to provide an estimated value of the output torque as the controller feedback, with no need for any external force/torque sensor. The performance of the MRF-based clutch, as well as, the efficiency of the proposed modeling and control techniques are experimentally validated. The results demonstrates the potential of the proposed design for use in haptic devices for a class of medical applications. The medical applications considered include needle-based interventions, soft-tissue palpation, and surgical training and skills assessment.

4.2 Development of Four Prototype Small-Scale Clutches

4.2.1 Design Concept: Review

There are two main approaches to the design of MRF-based clutches reported in the literature, namely multiple-disk and drum-based designs [5]. These designs takes advantage of a large area of contact and strong magnetic field, respectively, which contribute to their torque generation range. However, when made in small-scale, the decrease in these factors drastically degrades the performance of the system and makes them unsuitable for haptic applications. In the previous chapter, a new design – called armature-based – was proposed to improve the performance of the disk-based and drum-based approach by increasing the effective MRF volume and the area of contact as well as improving the efficiency of magnetic field usage. Numerical analysis of the proposed design, given in Chapter 3, demonstrated the superiority of this design over disk- and drum-based systems, as well as conventional servo systems.

4.2.2 Final Design

Fig. 4.1(a) shows the final version of a single unit of an armature-based clutch. Belt pulleys are mounted on the casing cap to deliver the motor driving motion to the outer casing. A capstan pulley is also implemented at the armature, which enables the transmission of the generated torque to a haptic interface joint. Four precision ball bearings are used inside the caps, which enable disengaged and free motion of belt pulleys and outer casing on the armature. The design takes advantage of a slip ring to provide current to the armature coil, as well as readings from the Hall sensors.

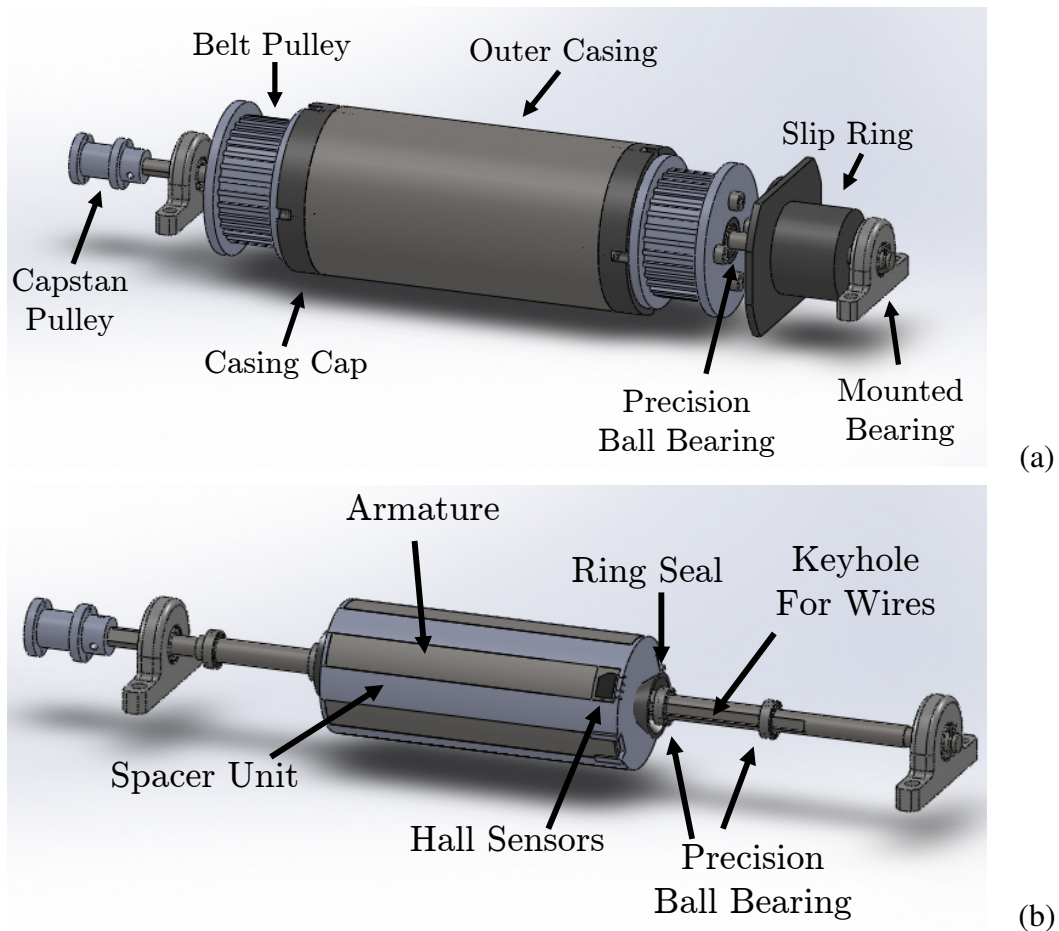


Figure 4.1: (a) Final version of the armature-based clutch and (b) the internal view

Fig. 4.1(b) depicts the internal view of the same unit. A keyhole is placed on the armature shaft for routing the wires from the coils and Hall sensors to the slip ring. The proper sealing of the clutch to avoid any fluid leakage is an important issue. The heating effect of the wires, which can increase the fluid pressure, adds to the importance of proper sealing in the clutch. O-rings are used to seal the gap between the outer casing and the caps. This method has proven effective in previous designs. The main challenge is in sealing the bearing that is placed between the armature shaft and the casing caps. If any particle leaks into the balls of the bearing, it can cause friction and even jamming in the bearing. Shielded bearings can be implemented to decrease the chance of leakage; however, based on previous experience, this solution was found to help but is not sufficient. To this end, stretch-fit rotary-shaft oil seals, placed on the armature shaft, should be used to protect the bearing. However, this adds to the friction of the system.

4.2.3 Development and Construction

A wire Electrical Discharge Machining (EDM) system was used to construct the armature of the clutch (Fig. 4.2(a)). Since the gap between the armature and the outer casing is very small, the machining tolerance plays a crucial role in the outcome. As a result, the highest tolerance on EDM was used to construct the armature.

The armature was then coiled with a AWG (American Wire Gauge) 28 wire (Fig. 4.2(b)). Insulating sheets were used to insulate the surface of the armature from the wires. In addition, it is crucial that the armature coil be insulated from the MRF. This is due to the fact that, in case of exposure, the particles inside the fluid will mostly accumulate inside the gaps between the wires, where the magnetic field is very large. This will reduce the concentration of the particles over the poles which contributes to the torque capacity of

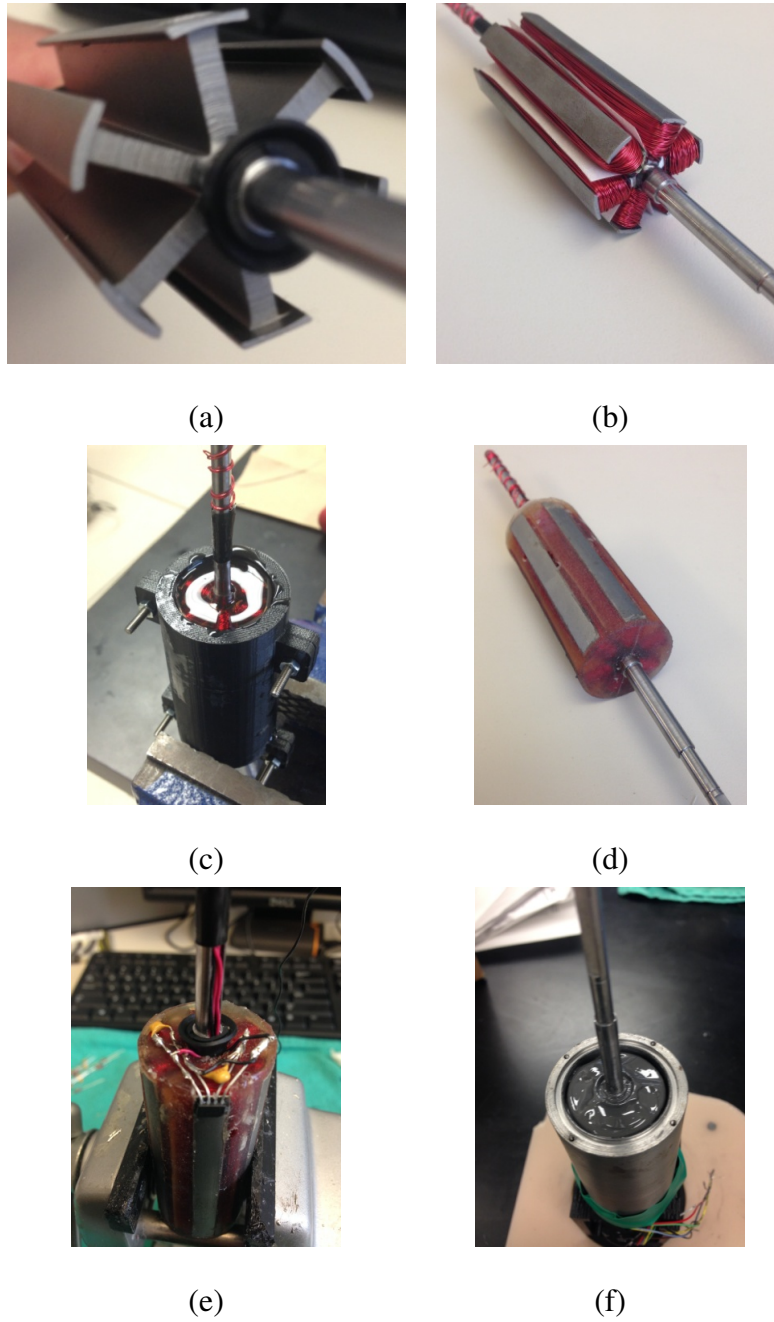


Figure 4.2: (a) Machined and (b) coiled armature of the system. (c) Silicon molding method used for (d) insulating the coil of the armature. (e) Location of one of the Hall sensors on the pole and routing of the wires through the keyhole. (f) Filling the gap between armature and outer casing with MRF.

the system. To this end, urethane rubber polymer [6] was used to insulate the wire. This material consists of a liquid adhesive and liquid rubber, which when mixed, after a certain period of time (called pot time), starts to harden and eventually turns into solid rubber. A customized 3-Dimensional (3D) printed mold, with an inner diameter equal to the outer diameter of the armature was used for this purpose. The polymer mixture was poured inside the mold (Fig. 4.2(c)) and after a cure time of 20 hours, the coils were insulated by the created polymer cover as shown in Fig. 4.2(d). This cover is removable and provides adequate sealing of the wires from the MRF. The Hall sensors and the required filtering circuits were also attached to the pole of the armature, and an epoxy adhesive material was used to insulate the wires (Fig. 4.2(e)). Next, the finished armature was placed inside the outer casing and MRF was inserted in the gap between the two surfaces (Fig. 4.2(f)). Air vacuum was used to remove any air from inside the fluid. The end result, after attaching the caps, pulleys, and slip rings is shown in Fig. 4.3. Four prototypes of the proposed design were constructed in our lab with the goal of developing a multi-DoF haptic interface for medical application, as will be discussed in the next chapter.

REMARK 5. It should be noted that the proposed clutch is only capable of providing uni-



Figure 4.3: The developed armature-based MRF clutch

directional motion. The expansion of the proposed design into a multi-DoF haptic system, for medical applications, which can create bi-directional forces will be performed through a distributed antagonistic configuration in Chapter 5. In addition, the antagonistic use of MRF-based clutches can alleviate the problem of friction, due to the sealing of the clutch, to a great extent. The results of this study will be reported in Chapter 5.

REMARK 6. The electrical current in the wound armature can generate thermal energy in the clutch. MR fluids have a typical operating temperature range of -40 to 150°C . However their behavior might change as a result of temperature variation. The outer casing of the clutch (made of steel), which has a large area of contact with air, can act as a heat sink. This can moderate the temperature deviations. Fins can be added to the surface of the casing to increase the area for thermal exchange. Since temperature-dependent model variation in MRF characteristics is very moderate [7], the integration of temperature sensors in the system will be postponed to the second generation of the device.

4.3 Figures of Merit

In the following sections, the dimensions and mechanical characteristics of the designed clutches are provided. In addition, an evaluation of the torque capacity and bandwidth of the system are also given. In order to determine the required outer diameter and length of the clutch, a desired torque range of 0 - 1.5Nm was considered and simulations were used. This torque range is suitable for the medical applications of interest to our group. Knowing these values, by taking advantage of the constrained optimization method reported in the previous chapter, the rest of the dimensions were obtained. These dimensions are shown in Table 4.1. The symbolic dimensions of the outer casing and a single pole of the armature-based clutch were shown in Fig. 3.3 in the previous chapter. The masses of all parts in

the clutch are also given in Table 4.2. As can be seen, a major part of the total mass is contributed by the outer casing. The large thickness of this part was due to the machining restrictions in making the O-ring groove and holes for the cap screws, and not due to limitations in the magnetic field strength. Hence, by using better machining tools, the thickness of the outer casing, and subsequently its mass, can be reduced. Nevertheless, since the outer casing and armature are decoupled through bearings, the user interaction is mostly with the armature of the clutch, which is very light. This fact helps to improve the transparency of the haptic sensation.

Table 4.1: MR Clutch Dimensions and Specifications

Parameter	Symbol	Value
Length of the Clutch	L_c	60.0 mm
Outer Radius of Outer Casing	R_{c_1}	18.0 mm
Inner Radius of Outer Casing	R_{c_2}	14.0 mm
Outer Radius of Armature	R_{a_1}	13.0 mm
Inner Radius of Armature	R_{a_2}	12.0 mm
Radius of Armature Shaft	R_{sh}	5.0 mm
Thickness of Armature Pole	W_p	2.5 mm
Thickness of MRF Gap	W_{MR}	1.0 mm
Current Rating of Coil	i_{max}	1.4 A
Arc of the Armature Tooth	θ_p	30.0°
Number of Coil Turns on Each pole	N_w	110
Number of Armature Poles	N_p	6

Table 4.2: MR Clutch Mass Specifications

Part (Quantity)	Mass
Armature without coil and Rubber (1)	115 gr
Armature with coil and Rubber (1)	128 gr
Outer Casing (1)	253 gr
Casing Caps (2)	27 gr
Belt Pulley (2)	63 gr
MR Fluid (12 ml)	32 gr
Seals, Screws, etc.	5 gr
Total Mass of Clutch	598 gr

4.4 Comparison with Conventional Electrical Motors

Other important factors in the stability and transparency of a haptic system are torque capacity, output inertia, and bandwidth of the system. Table 4.3 provides the values of these parameters for the designed system. The experiments used to obtain these values are discussed in Section 4.7. In addition to the information on the MRF-based clutch, the values of the parameters for three well-known electrical motors of commensurate size are also given. One should note that the values mentioned for the electrical motors are only true when they are used with no gear reduction. In fact, the inertia, bandwidth, and mass of these systems will degrade when used with a gearbox, which is essential for achieving the desirable torque range. The developed MRF-based clutch requires no gear reduction, which is one of its main advantages. Nevertheless, the results show that, even without gear reduction, the designed MRF-based actuator have comparable and in many cases better characteristics in comparison to electrical motors. By considering this in addition to the effect of MRF-based

Table 4.3: MR Clutch Electromechanical Specifications and Comparison

Parameter	MRF Clutch	Maxon EC-M40	Parker BE164Z	Anaheim BDR-44
Nominal Torque [Nm]	1.1	0.21	0.38	0.09
Stall Torque [Nm]	1.5	0.83	1.15	0.73
Output Inertia [gr.cm ²]	427	404	448	-
Mechanical Bandwidth [Hz]	30	34	32	40
Mass [gr]	598	720	570	340

actuators on the stability of the system, a conclusion can be drawn that this system has great potential to be used in a haptic interface, as an alternative to electrical motors.

4.5 Comparison with Conventional Rheological Actuators

There have been several Magneto- and Electro-Rheological based actuators developed specifically for haptic applications. Table 4.4 summarizes the size and torque capacity of some of these. As can be seen, the developed armature-based design has one of the best torque-to-size ratios. The proposed system not only has an acceptable range of torque suitable for medical applications, but is also small enough to be employed in a medium-sized haptic interface. The other information for these clutches, such as inertia and mass, were mainly missing, and hence was not considered in this comparison. Nevertheless, a thorough review on this subject was given in the previous chapter. In addition, one should not that MRF-based linear dampers have also been used in haptic application. However, due to the large zero-current force of such systems, they are not suitable for medical applications and are not reviewed in this section.

Table 4.4: Clutch Electromechanical Specifications and Comparison (\varnothing = diameter size)

Research	Type	Dimensions	Torque
Current Work	Armature	$\varnothing 3.6 \times 6\text{cm}$	1.5 Nm
Liu et al. [8]	Disk	$\varnothing 15\text{cm}$	0.9 Nm
Melli-Huber et al. [9]	Disk	$\varnothing 4.3 \times 2\text{cm}$	0.7 Nm
Furusho et al [10]	Disk	$\varnothing 20\text{cm}$	2.0 Nm
Yamaguchi et al. [11]	Disk	$\varnothing 17\text{cm}$	10 Nm
Blake et al [12]	Disk	$\varnothing 2.5 \times 1.4\text{cm}$	0.2 Nm
Nguyen et al. [5, 13]	Disk	$\varnothing 10\text{cm}$	10 Nm
Ahmadkhanlou et al. [14]	Drum	$\varnothing 8 \times 10\text{cm}$	1.5 Nm

4.6 Modeling And Control

MRF-based actuators suffer from nonlinear hysteretic relationships between the input current and output torque. For a single-input single-output system, hysteresis is the presence of a non-degenerate input-output closed curve as the frequency of excitation tends toward a DC signal [15]. Although this nonlinearity is less serious than in the case of pneumatic or hydraulic systems, it causes inaccuracy in the output response of the actuator, as well as, instability in the closed-loop system [16]. Therefore, it is essential to study and model the current-torque relationship for MRF-based actuators for reliable control and actuation and for delivering high-fidelity force/torque control in haptic interfaces utilizing MRF-based actuators.

Two main approaches to modeling of hysteretic systems are reported, namely a) physics-based modeling, and (b) phenomenological modeling. The first category is structured around the physical principles of magnetics. Jiles model [17] and Hodgdonas model [18]

are two such models used for MRF-based actuators. However the application of such models has been mainly restricted to off-line simulation and actuator design and rarely has been used for control purposes. Preisach [19, 20], Prandtl-Ishlinskii [21], and Krasnoselskii-Pokrovskii [22] models are among the second category of modeling methods. These models are mainly successful in predicting magnetic hysteresis. However, implementation problems associated with such methods limit their use in closed-loop controllers [23]. The implementation of non-model based controllers for MRF-based system have also been reported in the literature [24]. However, their poor results demonstrate the crucial need for model-based controllers for MRF-based actuators. To this end, several efforts were made by our group to develop an efficient model-based control scheme. A novel non-linear adaptive observer that relates the internal magnetic field to the applied current was introduced in [25]. This model facilitates accurate control of the actuator using its input current. In another study [26], a simple PID controller was used for controlling an MRF-based clutch. As its feedback signal, the controller took advantage of an estimated value of the output torque obtained using an efficient model, which was a combination of Bingham Visco-Plastic model [23, 27] (relating magnetic field to shear stress), a geometric model (relating shear stress to static torque), and a dynamic model (relating static torque to dynamic torque). In this way, the input-output relationship of the MRF-based clutch was linearized which allowed an efficient closed-loop control of the system. In both previous works, since they were large-scale systems, the overall hysteresis in MRF-based actuators could be as small as 5% of the total torque range. However, in the current work, due to the small range of torque capacity, the hysteresis can result in more serious issues in terms of accuracy. In what follows, the design of a closed-loop control for the designed actuator is given. In this method, an ANN is used to model the hysteretic behavior of the system. As mentioned, Hall sensors are used to measure the magnetic field inside the fluid. This measurement is then used as the input of the ANN to estimate the output torque of the

clutch. This estimated value is then used as feedback in the control loop. The main advantage of the proposed controller is that it eliminates the need for any additional force/torque sensors, which results in significant advantages in terms of cost reduction and performance improvement, thanks to the unique properties of MR fluids.

4.6.1 ANN-Based Modeling Method

Universal function approximators (*e.g.*, ANNs and fuzzy logic systems) have been extensively used in robust control of nonlinear systems [28–31]. This interest is due to their high capability in learning and adaptation [28]. The proposed solution for modeling the nonlinear behavior of the clutch is based on training of an ANN based on a set pre-recorded measurement of a torque sensor and Hall sensors, when known current signals are applied to the system. By learning different patterns, the ANN can then predict the output torque in a real-time fashion, only based on the embedded Hall sensors' feedback. The architecture of the ANN can play an important role in the results of the prediction. Fig. 4.4 shows an empirical architecture of a feed-forward ANN that comprises 5 input neurons, 6 hidden neurons, and 1 output neuron. This topology was obtained through trial and error. The hidden layer has a tan-sigmoid transfer function, while the output layer uses a linear transfer function. The inputs of the network consist of the last four sample of the magnetic field reading from the Hall sensor (*i.e.*, $B(t - nT_s)$, $n = 0, \dots, 3$, and T_s is the sampling time), as well as, the last estimated output torque $T_e(t - T_s)$. The output is the estimated value of the output torque $T_e(t)$. The number of Hall sensor reading samples (*i.e.*, n in $B(t - nT_s)$) used in ANN can have a significant effect on the accuracy of the prediction. While a large number of samples (*i.e.*, $n > 3$) may result in more accurate prediction, it places the prediction process at the disadvantage of computational complexity and difficulty in predicting sudden changes. Through trial and error, we came to the conclusion that $n = 3$ is a good

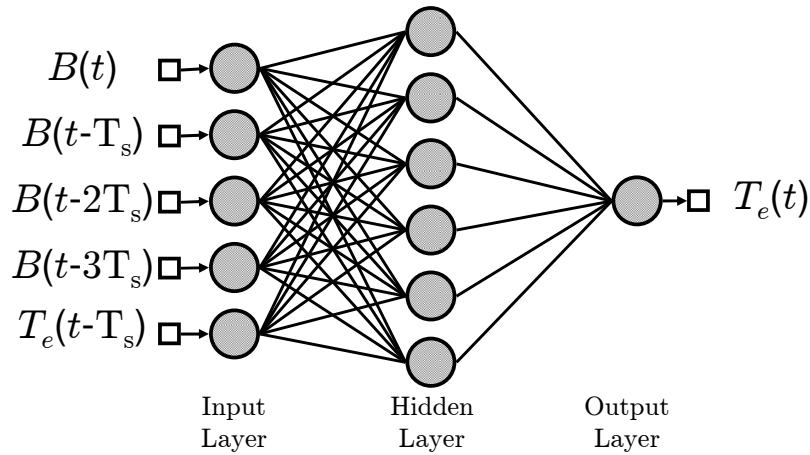


Figure 4.4: The architecture of the ANN used for estimating output torque based on Hall sensor readings.

choice for this application. Another point to note is the use of torque estimation history (*i.e.*, $T_e(t - T_s)$) as an input. During training of the network, more samples of torque estimation history considerably decreased the prediction error, particularly in cases that involved sudden torque changes. However, during evaluation, the accumulative error in the system, caused by the large number of samples, resulted in failure of prediction. In our study, it was decided to use just one sample of the torque estimation history. In order to obtain a training data set for the network, the MRF-based clutch was connected to a torque sensor (more details on the experimental setup can be found in Section 4.7). Next, several current inputs were applied to the clutch and the output of the Hall (magnetic field sensing) and torque sensors were recorded. In order to enable the network to predict the output torque in any scenario, several different current patterns were applied, which included the following signals; chirp, step, sinusoidal (with different magnitudes and frequencies), damped sinusoidal, multi-sinusoidal, etc. This set of data was then used to train the ANN using the Levenberg-Marquardt algorithm [32]. In this algorithm, the energy function of the error was used as an indicator of the performance. The effectiveness of the proposed modeling method is shown in Section 4.7.

4.6.2 Torque Control Scheme

The control scheme used in this chapter is the same as the one developed in our research group and reported in [25, 33, 34]. This method has been examined rigorously and its effectiveness has been validated. Fig. 4.5 depicts this closed-loop control configuration. In this structure, a simple PID controller provides the control current for a desired torque value. The PID controller uses the error between the estimated value of the output torque with its desired value as the input signal. The main difference between this work and our previous work, is that the ANN, proposed in Section 4.6.1, is used to estimate the output torque. The effectiveness of the overall control method is shown in Section 4.7.

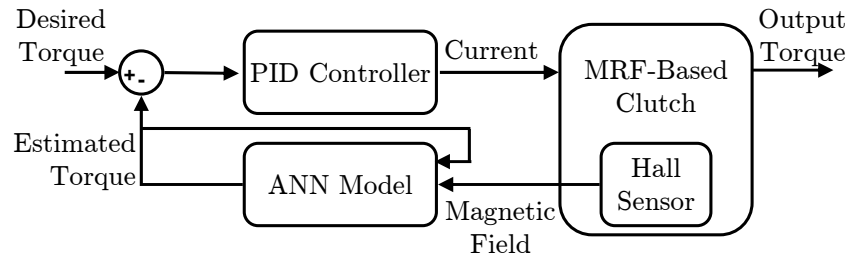


Figure 4.5: Closed-loop control configuration using embedded Hall sensors and the proposed ANN model

4.7 Results

This section presents the result of experimental validation of the designed MRF-based clutch, the modeling method, and the control scheme discussed in the previous sections.

4.7.1 Experimental Setup

Fig. 4.6 depicts the experimental setup used for validating the performance of the developed MRF-based clutches. A driver motor (Maxon Brush-less EC-60) provides a constant

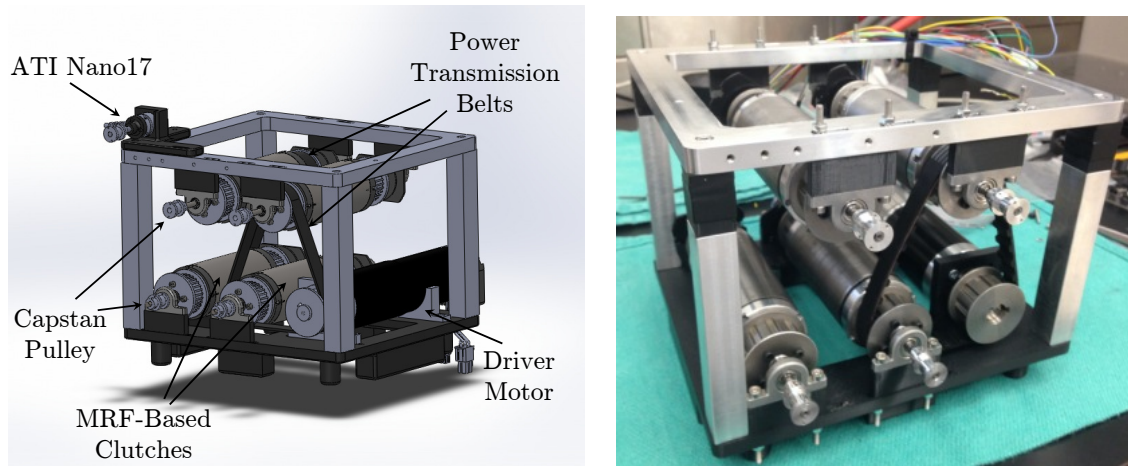


Figure 4.6: Experimental Setup

input torque to the outer casing of all clutches through power transmission belts. The armature shafts are equipped with capstan pulleys which can transmit power to an ATI Nano17 Force/Torque Sensor through a system of cables. Each clutch is connected to an individual current driver which controls the current of the coil, and subsequently the magnetic field inside the clutch, at 1KHz. A data acquisition card is employed to provide the current drivers with the reference current, as well as, to read the output of the ATI and Hall sensors.

Note that this setup is designed to be used as a prototype multi-DoF haptic interface for medical applications (Chapter 5). However, at this stage of the work, each clutch was tested individually. To this end, the ATI sensor was connected to one clutch at a time while the tests were performed.

4.7.2 Frequency Response

The frequency response is examined by measuring the torque response to a sinusoidal chirp current signal, which sweeps from 0.5Hz to 60Hz. Although this system is nonlinear, a sinusoidal input does result in a sinusoidal output. Fig. 4.7 demonstrates the frequency

response of the system. The bandwidth is measured to be approximately 30 Hz.

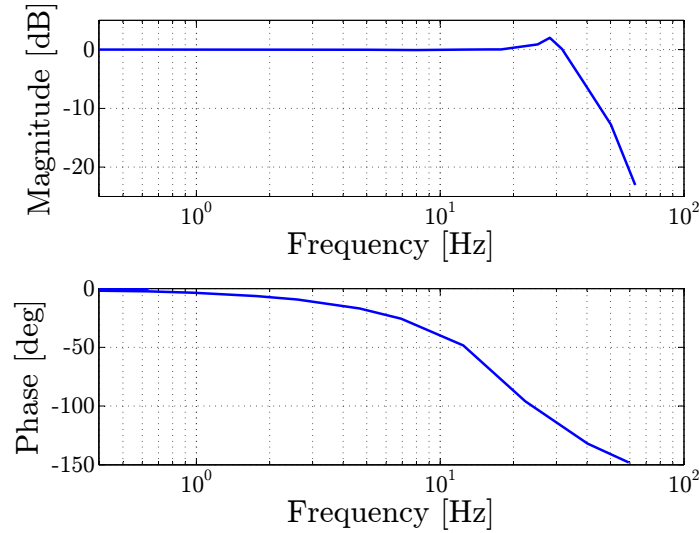


Figure 4.7: Frequency response of the system.

4.7.3 Validation of the Modeling Method

In order to validate the modeling method introduced in Section 4.6.1, a set of different current patterns were applied to the MRF-based clutch. The actual output torque was measured using the ATI Nano17 sensor. In addition, the ANN-based model was used to estimate the output torque. These two values were then compared. Furthermore, to study the improvement of the modeling technique over the conventional geometric modeling method [14, 19, 26], the estimated torque using this model has also been included in the comparison of the results. This model is a combination of the Bingham-Visco plastic model (which relates the magnetic field to the shear stress), and the geometrical and physical relationships in the system (which relates the shear stress to output torque).

In order to study the accuracy of the ANN-based model in predicting the nonlinear behavior of the system, two sinusoidal signals with frequencies of 1Hz and 4Hz were applied to the

system. Fig. 4.8 presents the magnetic-field-to-torque and current-to-torque relationships in the system. As can be seen, the proposed model is highly capable of predicting the hysteretic behavior of the system, while the geometric method is less successful due to the assumed linear relationship between the magnetic field and torque. Next, to evaluate the model in predicting the inner loops of the hysteretic behavior, a damped sinusoidal signal was applied. Fig. 4.9 presents the result. Once more, there is strong agreement between the actual measurement and the ANN-based prediction which demonstrates the efficiency of the ANN-based model.

In order to further validate the modeling method, a set of different current patterns were applied to the MRF-based clutch. Fig. 4.10 shows the results of several of these tests. As can be seen, the ANN-based model is very successful in predicting the output torque. However, the geometric model has larger error, specifically in case of high frequency changes in the

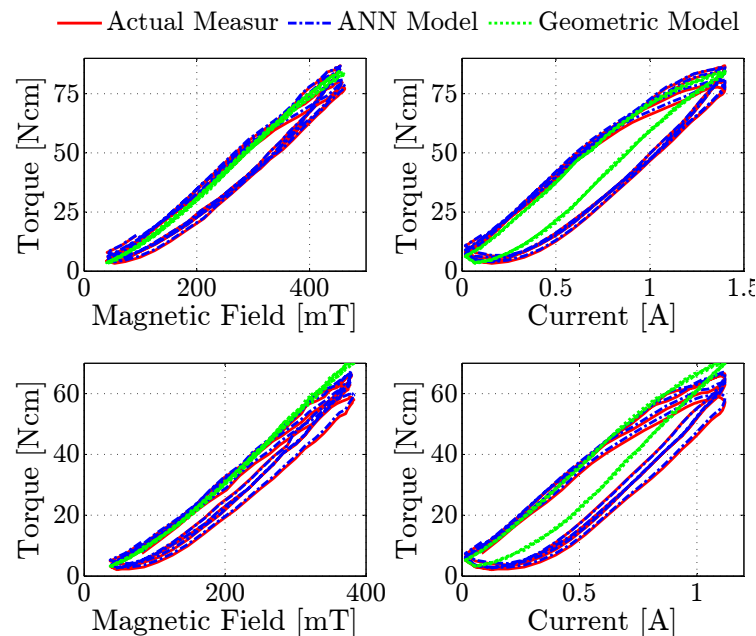


Figure 4.8: Modeling of hysteretic behavior of the system in response to sinusoidal currents of 1Hz (top row) and 4Hz (bottom row).

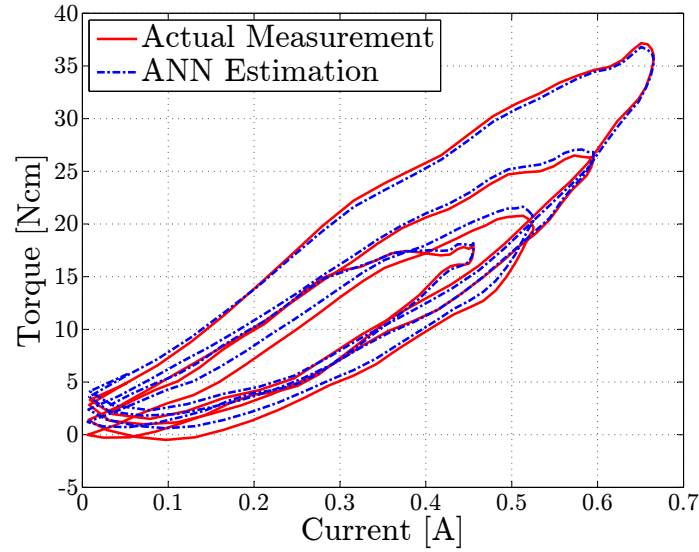


Figure 4.9: Modeling of the inner loops of the hysteresis

signal, which is usually more important for control purposes. This is due to the fact that in this method, a one-to-one relationship is considered between the magnetic field and the torque of the system. This assumption is acceptable in case of systems with a large range of torque; however, in the current application, hysteresis comprises a large portion of the signal and this assumption does not hold. Hence, based on the results, the proposed ANN-model demonstrates great potential for use in a control scheme in small-scale applications.

4.7.4 Evaluation of the Control Technique

Next the performance of the control scheme introduced in Section 4.6.2 was evaluated. In these experiments, a PI controller was used to control the output torque of the clutch ($P=9$ and $I=0.1$, obtained manually). The Hall sensor measurements in addition to the ANN-based torque estimator were used as the feedback signal for the PID controller (Fig. 4.5). The ATI sensor was also used to evaluate the performance of the combination of the modeling and control techniques. It should be noted that this sensor was only used for validation of the results, and it was not used to provide feedback signal. Fig. 4.11 shows the results

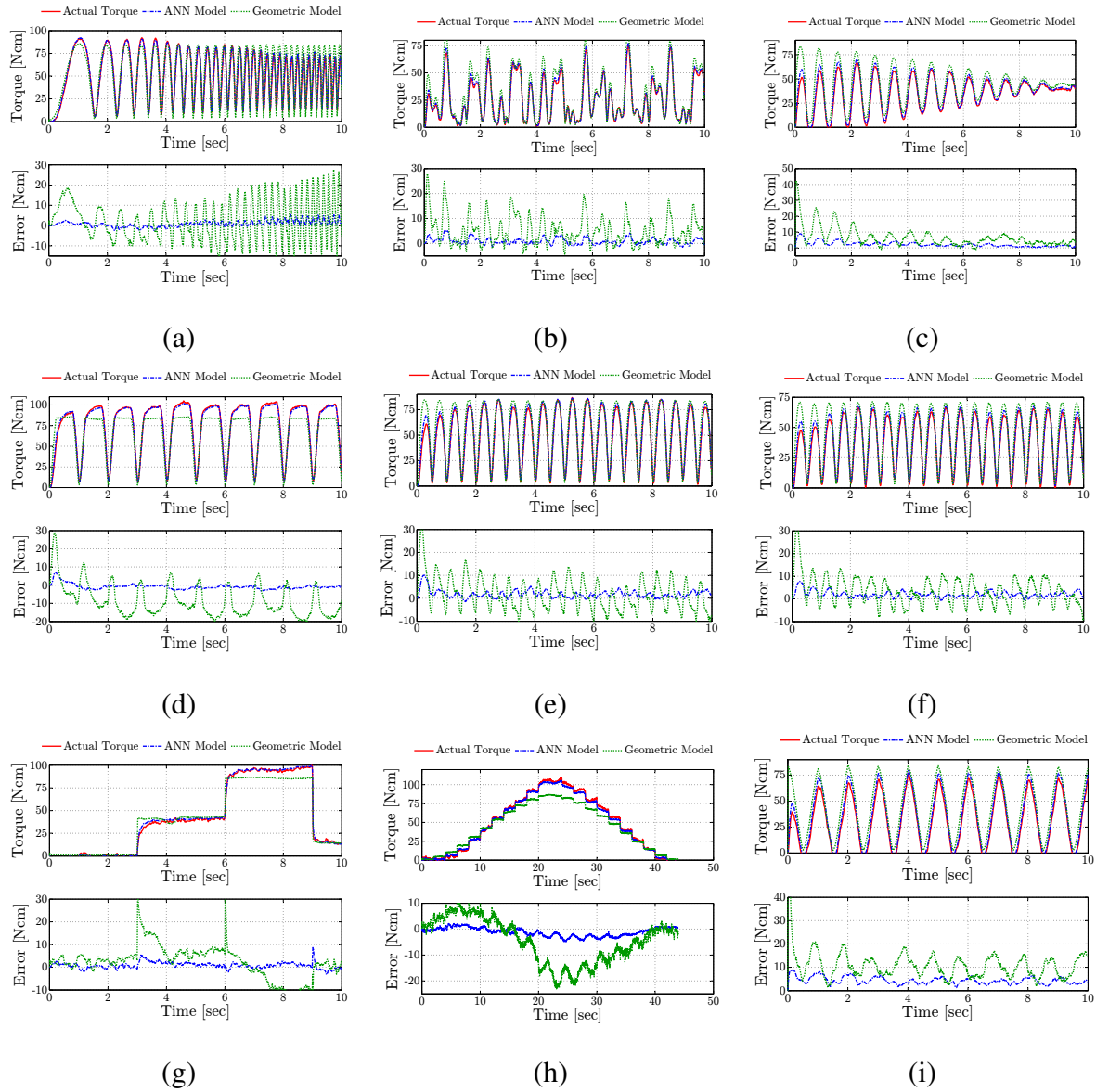


Figure 4.10: Results for the validation of the modeling technique by applying (a) chirp, (b) multi-sinusoidal, (c) damped sinusoidal, (d) cropped sinusoidal, (e) sinusoidal (1Hz), (f) sinusoidal (4Hz), (g and h) step-sequence current, and (i) sawtooth signals.

of several experiments. As can be seen, the controller has an acceptable performance in tracking these desired torque signals. The major advantage of this control approach is that there is no need for an external force/torque sensor, which is a significant improvement in the state of the art. While our proposed technique does not outperform conventional force/torque control schemes (at least by a significant margin) in terms of the accuracy of the delivered torque, it provides a much more viable alternative to these schemes [26].

4.8 Concluding Remarks

The design and development of a novel small-scale MRF-based clutch was reported in this chapter. This actuator is designed for use in a haptic device for medical applications. Electromechanical specifications of the system were given and compared to conventional small-scale electrical motors and existing MRF-based actuators designed for haptic applications. It was demonstrated that the proposed system shows a significant improvement over the state of the art, especially in terms of torque-to-size ratio. A modeling and control scheme based on artificial neural networks and embedded Hall sensors were proposed and it was shown through experimental results that they present a very accurate and efficient means of providing accurate and high fidelity torque delivery which is essential for haptic devices in certain medical applications. In addition, the control scheme does not require any external force/torque sensor which contributes to lower cost and greater simplicity for the system. The extension of the developed clutches into a multi-DoF haptic interface will be discussed in the next chapter.

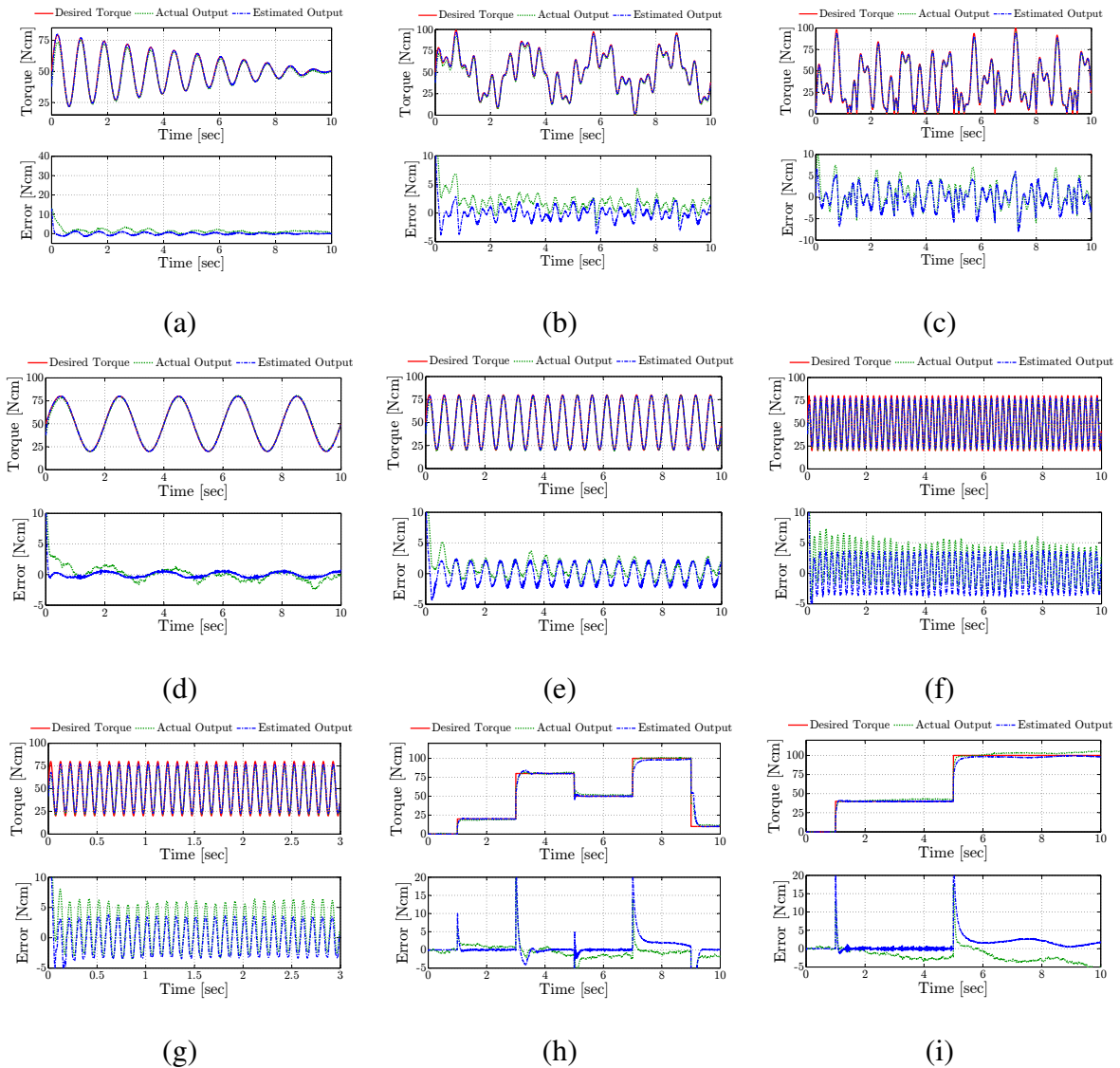


Figure 4.11: Results for the validation of the control method by applying (a) damped sinusoidal, (b and c) multi-sinusoidal, sinusoidal of (d) 0.5Hz, (e) 2Hz, (f) 5Hz, (g) 10Hz, and (h and i) step-sequence reference signals.

Bibliography

- [1] D. Lawrence, "Stability and transparency in bilateral teleoperation," *IEEE Transactions on Robotics and Automation*, vol. 9, pp. 624–637, Oct 1993.
- [2] A. Bicchi, M. Raugi, R. Rizzo, and N. Sgambelluri, "Analysis and design of an electromagnetic system for the characterization of Magneto-Rheological fluids for haptic interfaces," *IEEE Transactions on Magnetics*, vol. 41, pp. 1876–1879, may 2005.
- [3] J. Abbott and A. Okamura, "Effects of position quantization and sampling rate on virtual-wall passivity," *IEEE Transactions on Robotics*, vol. 21-5, pp. 952–64, 2005.
- [4] M. Lin and M. Otaduy, *Haptic Rendering: Foundations, Algorithms and Applications*. A K Peters, 2008.
- [5] P. Nguyen and B. Choi, "Selection of Magneto-Rheological brake types via optimal design considering maximum torque and constrained volume," *Smart Materials and Structures*, vol. 21-1, pp. 1–12, Dec 2012.
- [6] Smooth-On Co., Easton PA, *VytaFlex Series - Liquid Urethane Rubbers*, 011011-JR ed., 2011.
- [7] A. Shafer and M. Kermani, "On the feasibility and suitability of MR fluid clutches in human-friendly manipulators," *IEEE/ASME Transactions on Mechatronics*, vol. 16-6, pp. 1073–82, Dec 2010.
- [8] B. Liu, W. Li, P. Kosasih, and X. Zhang, "Development of an MR-brake-based haptic device," *Smart Materials and Structures*, vol. 15, pp. 1960–1966, 2006.
- [9] J. Melli-Huber, B. Weinberg, A. Fisch, J. Nikitzuk, C. Mavroidis, and C. Wampler, "Electro-Rheological fluidic actuators for haptic vehicular instrument controls," in *Symposium on Haptic Interfaces for Virtual Environment and Teleoperator Systems*, 2003.
- [10] J. Furusho, M. Sakaguchi, N. Takesue, and K. Koyanagi, "Development of ER brake and its application to passive force display," *Journal of Intelligent Material Systems and Structures*, vol. 13, pp. 425–429, 2002.
- [11] Y. Yamaguchi, S. Furusho, S. Kimura, and K. Koyanagi, "Development of high-performance MR actuator and its application to 2D force display," *International Journal of Modern Physics B*, vol. 19, pp. 1485–1491, 2005.
- [12] J. Blake and H. Gurocak, "Haptic glove with MR brakes for virtual reality," *IEEE/ASME Transactions on Mechatronics*, vol. 14, pp. 606–615, oct. 2009.

- [13] P. Nguyen, V. Lang, N. Nguyen, and B. Choi, "Geometric optimal design of a Magneto-Rheological brake considering different shapes for the brake envelope," *Smart Materials and Structures*, vol. 23, pp. 1–11, Jan 2013.
- [14] F. Ahmadvanlou, G. Washington, and S. Bechtel, "Modeling and control of single and two degree of freedom Magneto-Rheological fluid-based haptic systems for telerobotic surgery," *Journal of Intelligent Material Systems and Structures*, vol. 20, pp. 1171–86, May 2009.
- [15] J. Oh, B. Drincic, and D. Bernstein, "Nonlinear feedback models of hysteresis," *IEEE Control Systems Magazine*, vol. 29, pp. 100–119, 2009.
- [16] H. Khalil, *Nonlinear Systems*. Prentice Hall, 2002.
- [17] C. Jedryczka, P. Sujka, and W. Szlag, "The influence of magnetic hysteresis on Magneto-Rheological fluid clutch operation," *The International Journal for Computation and Mathematics in Electrical and Electronic Engineering*, vol. 28, pp. 711–21, Oct 2009.
- [18] J. An and D. Kwon, "Modeling of a Magneto-Rheological actuator including magnetic hysteresis," *Journal of Intelligent Materials System Structures*, vol. 14, pp. 541–550, 2003.
- [19] P. Yadmellat and M. Kermani, "Output torque modeling of a MR based actuator," in *18th IFAC World Congress*, 2011.
- [20] J. Jayender, R. Patel, S. Nikumb, and M. Ostojic, "Modeling and control of shape memory alloy actuators," *IEEE Transactions on Control Systems Technology*, vol. 16, pp. 279–287, March 2008.
- [21] A. Vinstin, *Differential models of hysteresis*. Springer Verlag, 1994.
- [22] M. Krasnoselskii and A. Pokrovskii, *Systems with hysteresis*. Springer, 1989.
- [23] P. Yadmellat and M. Kermani, "Adaptive modeling of a fully hysteretic Magneto-Rheological clutch," in *IEEE International Conference on Robotics and Automation*, 2012.
- [24] J. Deur, Z. Herold, and M. Kostelac, "Modeling of electromagnetic circuit of a Magneto-Rheological fluid clutch," in *IEEE Control Applications*, pp. 113–118, July 2009.
- [25] P. Yadmellat and M. Kermani, "Adaptive modeling of a Magneto-Rheological clutch," *IEEE/ASME Transactions on Mechatronics*, vol. 19, pp. 1716–1723, Oct 2014.

- [26] W. Li, P. Yadmellat, and M. Kermani, "Linearized torque actuation using FPGA-controlled Magneto-Rheological actuators," *IEEE/ASME Transactions on Mechatronics*, vol. PP, pp. 1–9, May 2014.
- [27] M. Jolly, J. Bender, and J. Carlson, "Properties and applications of commercial Magneto-Rheological fluids," in *SPIE International Symposium on Smart Structures and Materials*, 1998.
- [28] M. Chen, S. Ge, and B. Voon Ee How, "Robust adaptive neural network control for a class of uncertain MIMO nonlinear systems with input nonlinearities," *IEEE Transactions on Neural Networks*, vol. 21, pp. 796–812, May 2010.
- [29] Y. Liu, C. L. P. Chen, G.-X. Wen, and S. Tong, "Adaptive neural output feedback tracking control for a class of uncertain discrete-time nonlinear systems," *IEEE Transactions on Neural Networks*, vol. 22, pp. 1162–1167, July 2011.
- [30] B. Subudhi and D. Jena, "A differential evolution based neural network approach to nonlinear system identification," *Applied Soft Computing*, vol. 11, no. 1, pp. 861 – 871, 2011.
- [31] C. Lin, A. Ting, C. Hsu, and C. Chung, "Adaptive control for MIMO uncertain nonlinear systems using recurrent wavelet neural network," *International Journal of Neural Systems*, vol. 22, no. 01, pp. 37–50, 2012.
- [32] S. Haykin, *Neural Networks and Learning Machines*. Pearson Education Inc., 3rd ed., 2009.
- [33] P. Yadmellat, A. Shafer, and M. Kermani, "Design and development of a single-motor, two-dof, safe manipulator," *IEEE/ASME Transactions on Mechatronics*, Accepted 2013.
- [34] W. Li, P. Yadmellat, and M. Kermani, "Linear torque actuation using FPGA-controlled Magneto-Rheological actuators," in *International Conference on Robotics and Automation*, 2014.

Chapter 5

Development and Evaluation of the Prototype Haptic Interface

This chapter reports on the design, construction, and evaluation of a prototype two degree-of-freedom (DoF) haptic interface, which takes advantage of Magneto-Rheological Fluid (MRF), based clutches for actuation. The design of small-scale clutches were discussed in Chapter 3, and their development and evaluation was reported in Chapter 4. A distributed antagonistic configuration is used to develop the 2-DoF haptic interface based on these actuators, for a class of medical applications. This device is incorporated in a master-slave teleoperation setup that is used for medical percutaneous and palpation interventions. Evaluation of the performance of the haptic interface in this setup show a great potential of MRF-based actuators to for integration in haptic devices for medical interventions that require reliable, safe, accurate, transparent, and stable force representation.

This chapter contains material included in the papers (1) "Design and Evaluation of a Prototype Two-DoF Haptic Interface for Medical Applications based on Magneto-Rheological Actuation", submitted to the IEEE International Conference on Robotics and Automation, Seattle WA, May 26-30, 2015, and (2) "Design of a Haptic Interface for Medical Applications using MRF-based Actuators", submitted to IEEE/ASME Transactions on Mechatronics, 2014.

5.1 Introduction

Since its inception, haptics has attracted a great amount of interest from different sectors of the robotics industry. The force and tactile feedback provided by haptic devices can enable the user to adjust the force control actions to ensure accuracy and safety of the operation. This significantly improved the quality of telerobotic tasks. In recent years, with the rapid growth in applications of minimally invasive medical interventions, the integration of haptics into such applications has been identified as a high-priority objective in major medical robotics roadmaps [1, 2]. Motivated by in-depth research, it is not difficult to imagine the benefits of providing a clinician using robotics-based systems with the feeling of being directly in contact with tissues and organs. Such sensation can improve the intuitiveness of minimally invasive interventions. In addition, it enables the clinicians to control the quality of tasks during procedures (*e.g.*, proper suture knot tying, achieving adequate contact during cardiac ablation) and to avoid causing any damage to tissue by exerting too much force [3]. However, the introduction of haptics in minimally invasive applications brings to light a number of safety concerns particularly among standardization bodies, robotic manufacturers, and researchers [4, 5]. This is to be expected since the fundamental premise behind existing safety norms is complete reliability and safety of medical devices. However, the issue of stability of haptics-enabled telerobotic systems hampered the introduction of haptics into medical environments [2]. Due to the susceptibility of bi-lateral teleoperation systems to time delays, there is a possibility that such systems can become unstable as a result of the reflected slave force and induced master motion mechanism [6]. Thus, much research has focused on developing reliable control techniques for haptic applications. To this end, the use of passivity-based and small-gain approaches have been reported in [7, 8]. However, the conservative nature of such methods results in degraded transparency, which calls for a long and costly amount of training for the staff to be able to efficiently use the system.

Another body of work has focused on addressing this issue through redesigning the actuation mechanisms in haptic interfaces. The use of electrical motors in haptic devices, especially for medical applications, has proved to be challenging for several reasons. The poor dynamics of electrical motors, imposed by the need for gear reduction, can significantly reduce the transparency of the system by increasing the damping, inertia, and friction of the haptic device [9]. This is highly problematic in medical applications that require high-fidelity and accurate force reflection. Moreover, their active nature (which may be exhibited in the form of oscillations and jerks) can result in degradation of stability, which is unacceptable in medical applications [6, 10]. Actuators based on Magneto-Rheological fluids have been proposed as an alternative for use in haptic devices [11]. As discussed in the virtual wall benchmark [12] and use of the small-gain theorem [8], such a characteristic contributes to the stability of a bilateral teleoperation system. These claims were experimentally studied and validated in the previous chapters. While the application of MRF-based actuators *does not* fully address the issue of safety in haptic devices for medical applications, our promising results motivated us to further investigate their application in this field. To this end, a small-scale design of an MRF-based clutch, suitable for haptic applications, was proposed in Chapter 3. Based on this design, four prototype clutches were developed and validated and the results are provided in Chapter 4. This chapter reports on the design and development of a prototype two degree-of-freedom (DoF) haptic interface based on the developed MRF-based clutches. First an overview of existing technologies in the field of MRF-based haptic interfaces is provided (Section 5.2). A distributed antagonistic configuration is introduced which enables the construction of a 2-DoF haptic interface based on the actuators (Section 5.3). This device is incorporated in a master-slave teleoperation setup that is used for a needle-based percutaneous application (Section 5.5). This setup takes advantage of a state-of-the-art needle insertion robot developed in our group for prostate brachytherapy. Our studies on the performance of the prototype haptic interface

show their significant potential for haptic devices for use in soft-tissue medical applications that require reliable, accurate, and stable force representation.

5.2 State of the Art

Several haptic devices have been developed based on Magneto-Rheological and Electro-Rheological Fluids (ERF). In this section some of these studies are reviewed. Only devices that provide force reflection are considered.

There has been some work on designing MRF-based haptic joysticks. In one such study, a 2-DoF ERF-based joystick was developed [13]. This device takes advantage of 2 ERF-based disk-type brakes and a 2-DoF joint, on which the joystick handle is mounted. This device is capable of generating passive torques in the range Nm. In another design, a 2-DoF MRF-based joystick was developed for virtual reality applications [14]. This joystick was constructed of two disc-shaped MRF-based brakes positioned perpendicularly with a gimbal structure. The joystick provides wide resistive torque in the range 0.5-10 Nm. The device was used in 2D and pseudo-3D virtual experiments and was shown successful.

Force displays have also been designed based on MRF-based actuation. Furusho et al. [15] developed a low inertia cylindrical type ERF-based actuator and used these actuators within a 2-DoF force display in the form of a parallel-link manipulator. This force display is capable of generating about 2.0 Nm passive torque. Experimental results on a virtual wall demonstrated the effectiveness and stability of such display in providing passive force feedback. Reed et al. [16], proposed a 2-DoF dissipative force display. This device was in the form of a parallel five-bar linkage actuated by commercial MRF-based brakes. This force display was tested by using a virtual environment. Preliminary results were promising with potential benefits for the area of obstacle avoidance. Yamaguchi et al. [17] developed a

semi-active high-performance 2-DoF MRF-based force display. In this design, 2 DC motors and four MRF clutches were used. The maximum generated torque is about 10 Nm.

The useful characteristics of the smart actuators makes them suitable candidates to be used in haptic hand master devices [18, 19]. Winter et al. [20] took advantage of MRF-based dampers and developed an MRF-based actuated glove. Five MRF-based dampers (weighing only 0.035 lb) which can exert passive force up to 6 N were placed on the back of the hand. A novel exoskeleton mechanical power transmission system was designed to transmit the resistive forces of the dampers to the user's fingertips. Nam et al. [21] developed an MRF-based glove, called "Smart Glove". It took advantage of 5 MRF-based dampers placed on the wrist, each capable of applying up to 26 N of passive force. A tendon-type flexible link was designed to connect the fingertips to the MRF actuators. The main drawback of the previous two designs is that the employed dampers produce a large amount of force in the off-state, which degrades transparency of the system. Blake et al. [22], developed a haptic glove by taking advantage of six MRF-based brakes. The developed brakes are compact and can apply up to 0.899 Nm of passive torque. The glove weighs about 1.4 lb. The main advantage of this glove is that it only applies 0.005 Nm of torque in the off-state, which results in higher transparency.

Table 4.4 (in the previous chapter) summarizes the size and torque capacity of some of the MRF-based actuators developed for haptic applications. Our designed MRF-based clutch has also been included in this table. Note that only the MRF-based dampers are not considered in this comparison, due to their large off-state force, which makes them unsuitable for medical applications. As can be seen, the developed armature-based design has one of the best torque-to-size ratios. The proposed system not only has an acceptable range of torque suitable for medical applications, but also is also small enough to be employed in a medium-sized haptic interface.

5.3 Design of the Two-DoF Haptic Interface

This section describes the development of the prototype two-DoF haptic interface.

5.3.1 MRF-Based Clutch

The prototype haptic interface takes advantage of four MRF-based clutches as its actuation mechanism. These actuators have been developed based on armature-based design proposed in the previous chapters. Fig. 5.1 shows one of these actuators. In this design, the MRF fills the gap between a cylindrical outer casing and an armature, made of ferromagnetic materials. These two parts are decoupled through the use of ball bearings and both can rotate freely. To operate the clutch, a driving motor will apply a constant input torque to the outer casing of the clutch. Belt pulleys are mounted on the caps for this purpose. The armature is equipped with magnetic coils, which can create an axial magnetic field inside the MRF gap. In this way by controlling the magnetic field, the viscosity and shear stress of MRF, and subsequently the share of the input torque that is transferred to the output shaft can be controlled. Hall sensors are embedded in the system to measure the magnetic field strength. The output torque can then be delivered to the output link using cables or belts. A slip ring is used to provide current to the armature coil, as well as readings from the Hall sensors. The specification of these clutches are given in Table 5.1.

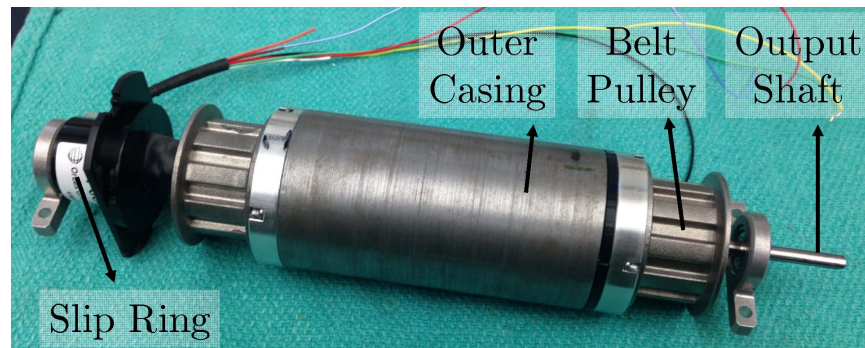


Figure 5.1: The developed MRF-based clutch used for actuation of the haptic interface.

Table 5.1: Specifications of MRF-Based Clutches

Parameter	Value
Length	60 mm
Outer Radius	18 mm
Shaft Radius	5 mm
Maximum Current	1.4 A
Mass	598 gr
Output Inertia	427 gr.cm ²
Bandwidth	30 Hz
Maximum Torque	1.5 Nm

5.3.2 Bidirectional Actuation: Antagonistic Configuration

It should be noted that the proposed clutch is only capable of providing unidirectional motion. In order to achieve bidirectional actuation, an antagonistic configuration is used, as shown in Fig. 5.2. In this configuration, clutches work in pairs to provide motions in both directions. The driver motor applies the input torque to both clutches in the same direction. However, the cable attaching the capstan pulleys is installed in an ∞ shape. In this way, the output torques of the clutches are applied in opposite directions, which enables bidirectional actuation of the link through a push-pull cable mechanism. Hence, by switching between the two clutches, the direction of operation can be changed.

The antagonistic configuration delivers a hidden blessing for the haptic device. Any friction in the system can degrade the transparency of the system. Different factors can contribute to the friction of the system. The viscosity of the fluid creates an off-state torque. Any residual magnetic field in the system can result in a biased shear stress and the user will feel added friction as a result. Also the seals that are used to avoid leakage of the fluid can create

large frictions. Although this could be a serious concern, the antagonistic configuration presented here addresses this problem to a great extent. This is due to the fact that the created friction forces in a pair of clutches antagonistically connected to a single joint will have similar magnitude, but in opposite directions. Hence, the friction forces will tend to cancel each other out. This is a useful property for haptic devices, which require minimal friction for high transparency.

5.3.3 Multi-DoF System: PA-DASA Configuration

The use of MRF-based clutches in a multi-DoF haptic device can be addressed using the concept of Pluralized Antagonistic Distributed Active Semi-Active (PA-DASA) actuation [23], which is an expansion of the antagonistic configuration described in the previous

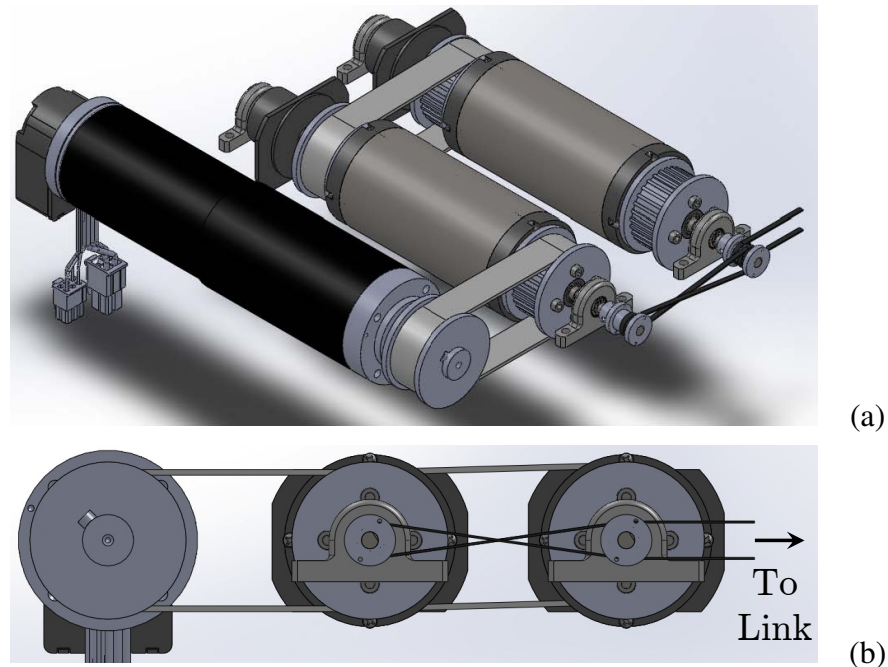


Figure 5.2: (a) Isometric and (b) front views of the antagonistic configuration for bidirectional actuation.

section, *e.g.*, Fig. 5.3. In this structure multiple MR clutches can be driven by a single motor (active actuator), which is located at the base of the haptic interface to keep the link masses low. The single motor applies a constant unidirectional torque to *all* sets of clutches through a system of cables and pulleys. A set of two clutches is employed in an antagonistic configuration to apply torques to each joint through cables and pulleys [23]. The torque direction and magnitude can then be changed by controlling the magnetic field in the MR clutch pair, without altering motor direction or torque. This has the benefit of rectifying a possible dead-zone due to motor direction change. This concept is the key strategy behind developing the multi-DoF haptic interface. The PA-DASA mechanism is intended to increase the performance of the interface, while offering reduced mass and effective inertia at all joints over using conventional servo motors [24]. In addition to these benefits, more cost-effective motors can also be used in lieu of expensive servomotors in PA-DASA configuration, since MR clutches are insensitive to momentary lack of mechanical power [24].

It should be noted that the only control required at the single motor stage is to provide constant torque. The application of PA-DASA in large-scale two- and three-DoF industrial

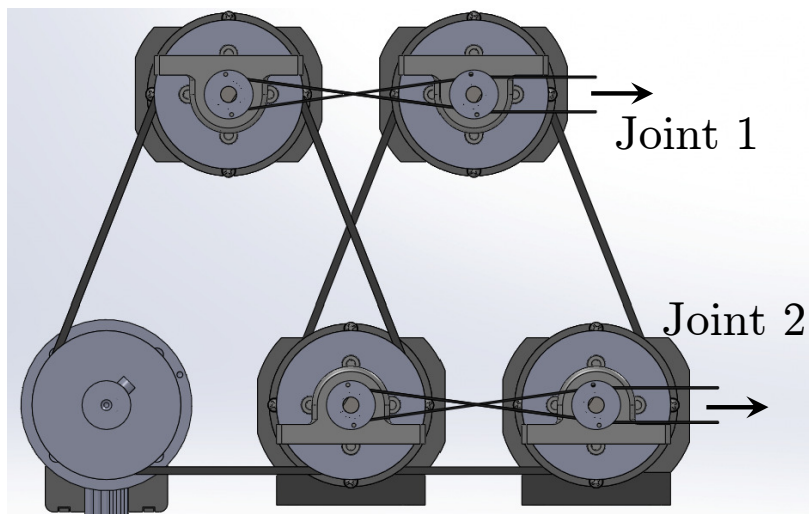


Figure 5.3: PA-DASA configuration for bidirectional multi-DoF actuation.

robots has been assessed in our group and the results has shown the suitability of such a configuration [24, 25]. Hence, by taking advantage of the small-scale MRF-based clutches in a PA-DASA configuration, a lightweight and compact multi-DoF haptic interface can be made.

5.3.4 Two-DoF Prototype Haptic Interface

Based on the PA-DASA configuration, a two-DoF prototype haptic interface has been developed. The structure of this device is shown in Fig. 5.4. A brushless Maxon EC-60 DC motor is used to drive the clutches. A 3-DoF planar haptic handle is also constructed using rapid prototyping. A system of cables and capstan pulleys are used to transmit bidirectional torques from each pair of clutches to first and second joint. The third joint is passive. Table 5.2 provides the specifications of this device and Fig. 5.5 shows the workspace of the system. A comparison between the developed prototype device and three off-the-shelf haptic interfaces are given in Section 5.4.

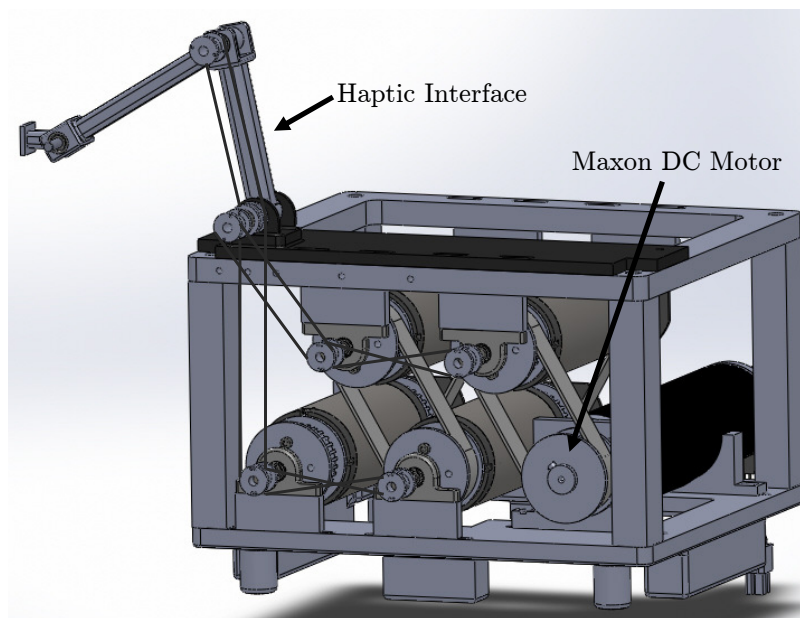


Figure 5.4: Structure of the multi-DoF haptic interface.

Table 5.2: Haptic Interface Specifications

Parameter	Value
Length of Link 1	100 mm
Length of Link 2	80 mm
Length of Link 3	50 mm
Haptic Box Length	200 mm
Haptic Box Width	170 mm
Haptic Box Height	100 mm
Joint 1 Motion Range	200 deg
Joint 2 Motion Range	190 deg
Maximum Joint Torque	1.5 Nm
Maximum Cartesian Force	10 N

5.3.5 Modeling and Control

Reliable control and actuation is a critical issue in haptic devices for delivering high-fidelity force/torque feedback, especially in case of medical applications. MRF-based actuators

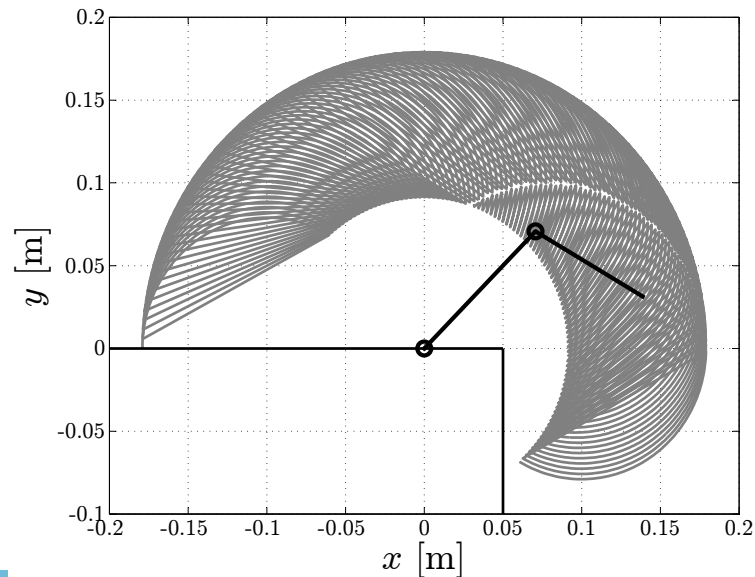


Figure 5.5: Workspace of the multi-DoF haptic interface.

suffer from nonlinear hysteretic relationships between the input current and magnetic field, as well, as the magnetic field and shear stress (output torque). This nonlinearity can cause inaccuracy in the output response of the actuator, as well as, instability in the closed-loop system, which is highly undesirable in practical applications. Therefore, it is essential to study and model the current-torque relationship for MRF-based actuators. A modeling and control scheme for such actuators has been proposed in Chapter 4. In this section, this method is briefly discussed; A simple PID controller provides the control current for a desired torque value to the coil of the clutch. This controller uses the error between an estimated value of the output torque with its desired value as the input signal. The main goal of this control technique is to avoid using any external force/torque sensor [26]. To this end, an approximator based on an artificial neural network (ANN) is used to predict and model the output torque of the system (which is used for feedback), just based on the measurement of the magnetic field strength by the embedded Hall sensors in the clutch. The ANN is trained based on a set of pre-recorded measurements. The results in Chapter 4 showed the efficient performance of this modeling and control strategy. In the next section, the performance of this method in controlling an antagonistic pair of clutches is evaluated.

5.4 Comparison to Off-the-Shelf Haptic Interfaces

In this section, specifications of the prototype MRF-based haptic device are compared with those of three well-known off-the-shelf haptic interfaces, namely Geomatic PHANTOM Omni [27], Geomatic PHANTOM Desktop [27], and Quanser Haptic Wand [28]. Based on the findings of [29], several performance measures were considered to compare these devices. These factors are listed in Table 5.3.

It is evident that, while the developed device has fewer degrees of freedom and comparable

weight and dimensions to the other devices, it is capable of producing the largest force, torque, and stiffness. As mentioned in Chapter 4, the weight and size of the device can be reduced in the next generation of the system through using more appropriate machining techniques. About 1 kg of the device weight is the weight of the Maxon EC-60 motor used in the setup for driving the clutches. This motor can be replaced with a lighter and less powerful one, since the PA-DASA configuration reduces the need for a powerful servo system (Section 5.3.3).

As will be discussed in the experimental results, the large range of achievable stiffness (impedance) for the MRF-based device in comparison with other devices, shows the potential of this system for use in a wide range of medical applications, including low force applications (*i.e.*, soft-tissue manipulation), as well as, high force ones (such as bone marrow biopsy, and some orthopedic interventions). However, at the current size, the designed

Table 5.3: Comparison to Off-the-Shelf Haptic Interfaces

Parameter	Prototype	PHANTOM	PHANTOM	Quanser
	Device	Omni	Desktop	Haptic Wand
DoF (w/ Force Feedback)	2	3	3	5
Height [mm]	100	70	120	350
Footprint [mm]	170×200	143×184	168×203	335×450
Weight [kg]	3.5	1.8	3.1	20.0
Off-state Force [N]	0.2	0.06	0.26	-
Cont. Exertable Force [N]	8.0	0.9	1.8	2.3-3.0
Max. Exertable Force [N]	12.0	3.3	7.9	7.7-9.0
Max. Joint Torques [Nm]	1.5	-	-	0.37-0.96
Stiffness [N/m]	18000	2310	2350	6000

clutches can not produce the forces required in very large force applications such as drilling in orthopedic interventions.

In order to extend the clutch to 3-DoF, 2 more clutches are required. Based on our calculation, by reducing the weight of the next generation of the MRF-based haptic device, reconfiguring the location of the clutches in the device (see Appendix A), and using a lightweight driving motor, a 3-DoF device can be made which has the dimensions of $200 \times 200 \times 100$ mm and weight of 4 kg, which shows great torque-to-size and weight ratios. Nevertheless, the developed device, as constructed, demonstrates the great potential of MRF-based actuation for use in haptic interfaces.

5.5 Experimental Setups

Fig. 5.6 shows the developed 2-DoF prototype haptic device. In this section, the experimental setups used for validating the performance of the developed MRF-based haptic

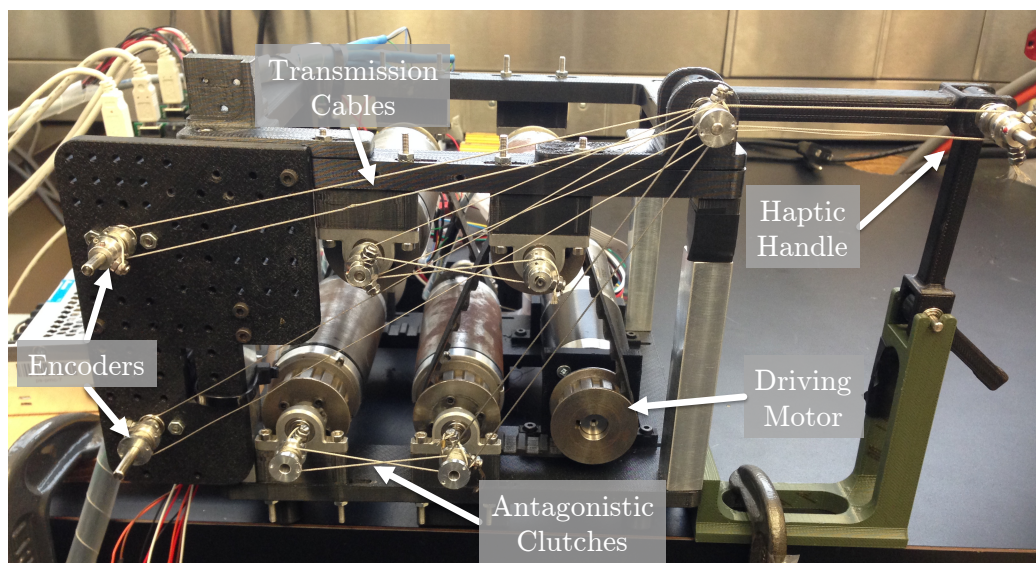


Figure 5.6: The two-DoF haptic interface.

interface are introduced. The haptic interface operates as follows; each joint of the haptic handle is connected through cables to an antagonistic pair of clutches. A switching algorithm activates the desired clutches based on the direction of the feedback force. Four PID controllers (implemented in software) are used to control the output torque of the clutches at 1KHz. As mentioned in Section 5.3.5, the ANN model is employed to provide the feedback signal of the PID controllers, based on the readings of the embedded Hall sensors. The coils of clutches are connected to individual current drivers (Maxon EPOS 50/5 controller operating in current mode), which controls the current of the coil at 1KHz. The PID controller provides the set-point for the current drivers. The joints angles of the haptic handle are measured using two optical encoders (with 1024 counts per revolution). A data acquisition card (Sensoray 626) is employed to provide the current drivers with the reference current (from PID controller), as well as, to read the output of the Hall sensors and encoders. The driving motor (Maxon EC-60) is also controlled using a Maxon EPOS 50/5 controller, operating in constant torque mode. It what follows the configurations used to evaluate the performance of the haptic device are reviewed.

5.5.1 Configuration A: Evaluation of Modeling and Control Methods

The evaluation of the modeling and control methods for a single clutch was given in Chapter 4. In this chapter, a few tests are performed to study the performance of these techniques in an antagonistic configuration. The setup is equipped with an ATI Nano17 sensor (Fig. 5.6). In order to evaluate the modeling and control method, a pair of clutches was connected to the sensor to read the output torque (*Configuration A*). Note that the sensor reading *was not* used as a feedback signal and in the normal operation of the haptic interface, this sensor is not needed (see Chapter 4).

5.5.2 Configuration B: Virtual Wall Experiments

In the next set of experiments, to evaluate the stability of the system, a virtual wall experiment was implemented. To this end, a virtual wall consisting of a linear spring with stiffness K_w and a damping B_w , was implemented on a computer (different from the one used for controlling the haptic interface). The wall is in the form of a plane at $x = 0$ in the Cartesian space. The two computers communicate through a UDP connection (*Configuration B*). The location of the haptic handle end effector is sent to the slave computer. The virtual wall applies force when the end effector passes the virtual wall (*i.e.*, $x < 0$). The reflected force information is sent to the master side and the haptic handle applies force to the operators hand. To compare the performance of the prototype device with a Geomatic PHANTOM Omni and a Quanser Haptic Wand, these devices were used in place of the MRF-based interface in the same configuration.

5.5.3 Configuration C: Needle Insertion Experiments

The performance of the haptic interface is also evaluated using a needle insertion and steering application from medical robotics. The large variations in forces experienced when a needle punctures into tissue provides us with the proper challenge for testing the designed system. Fig. 5.7 presents the block diagram of the master-slave haptic teleoperation system used for medical needle insertion (*Configuration C*).

In our experimental setup, a state-of-the-art robotic system designed in our group at CSTAR for percutaneous needle insertion [30, 31] was used as the slave robot. This 5-DoF manipulator can perform orientation, insertion, and rotation of the needle and linear motion of the stylet to drop radioactive seeds in the prostate during the brachytherapy procedure. To test the haptic device, only the 1-DoF-insertion force was feedback to the user. The force sensor (ATI Nano43 6-DoF F/T Sensor) installed at the base of the needle holder combined

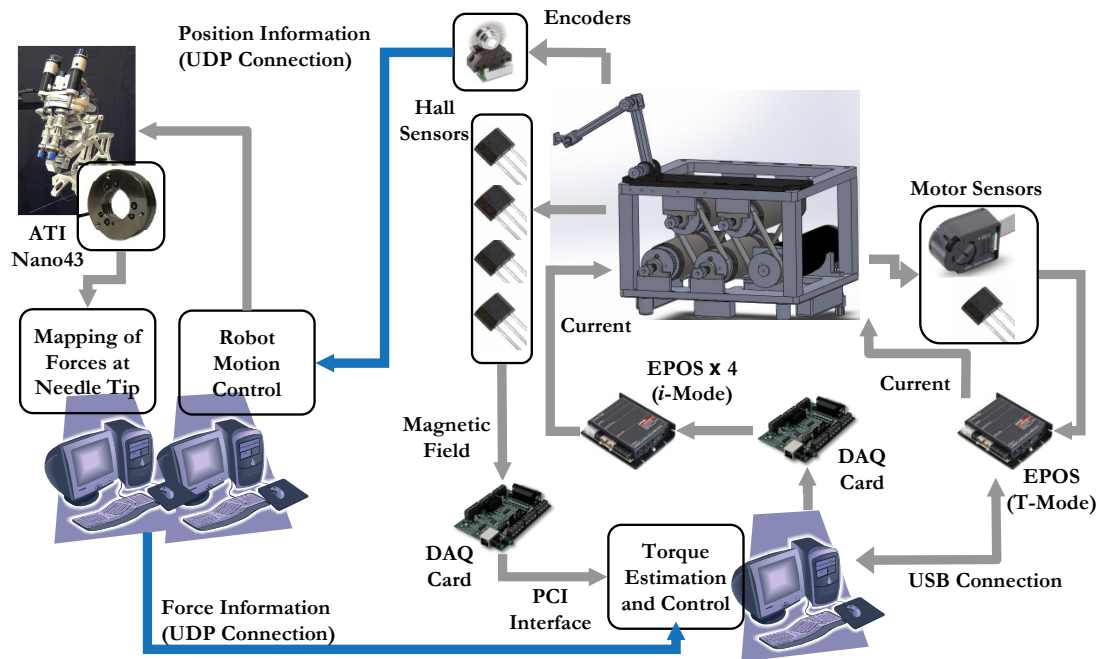


Figure 5.7: *Configuration C*: Block diagram of the master-slave haptic teleoperation.

with the force estimation technique developed in [32] was used to provide force reflection. PID controllers have been implemented to control the position of the needle at 1KHz. This system has a remote center of motion at the point of needle insertion into tissue to orient the needle about the point of insertion before it is inserted. The master and slave sides communicate with each other through internet using UDP protocol. Figs. 5.8(a) and (b) show the needle insertion robot and the needle insertion mechanism in *Configuration C*.

5.5.4 *Configuration D*: Tissue Palpation Experiments

The performance of the haptic interface is also evaluated using a tissue palpation application (Fig. 5.8(c)). The large forces experienced during palpation (*e.g.*, for tumor localization), will provide us with the proper challenge for evaluating the designed system. This configuration is basically the same as *Configuration C*; however, the needle is replaced with a palpator tool, which was made by rapid prototyping.

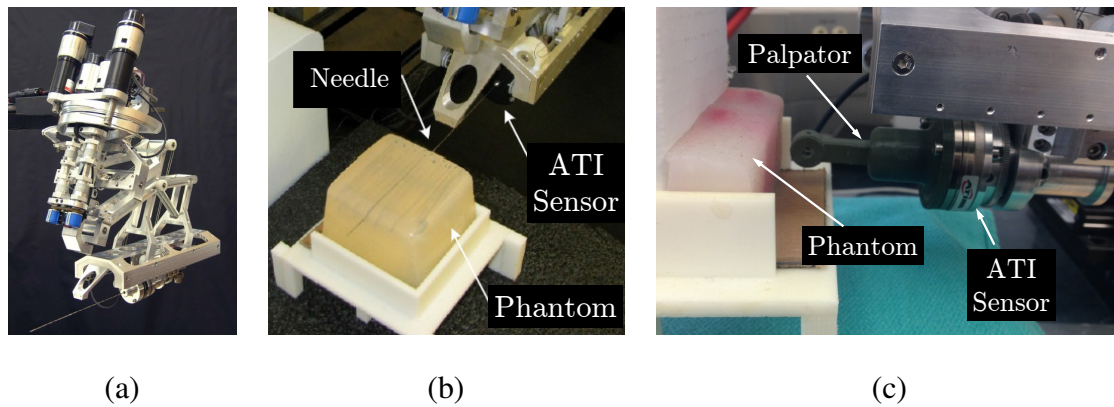


Figure 5.8: (a) The needle insertion robot [30, 31]. (b) *Configuration C*: Needle insertion setup. (c) *Configuration D*: Tissue Palpation Setup.

5.5.5 *Configurations C** and *D**: Force Feedback Transparency

To evaluate the accuracy of the device in providing accurate force feedback, *Configurations C** and *D** were considered. These are similar to *Configurations C* and *D*. However, a customized third link was constructed for the handle, which allowed the end effector to be attached to an ATI Nano43 sensor. This force sensor was mounted on a linear stage, as shown in Fig. 5.9. The linear stage was used to move the handle. The sensor measures the feedback force and provides a means for evaluating the accuracy of force feedback.

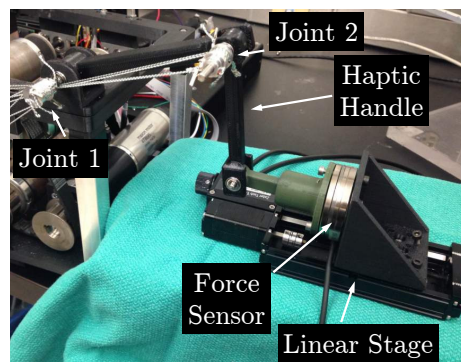


Figure 5.9: *Configurations C** and *D**: Use of a linear stage and a sensor for assessing accuracy.

5.5.6 Configurations: Summary

A summary of the configurations used in the experiments of this chapter is given in Table 5.4. Note that, for the purpose of comparison, the PHANTOM Omni or Quanser Haptic Wand can be replaced with the MRF device in any of these configuration.

Table 5.4: Summary of Configurations used in the Experiments

Configuration	Structure	Validation Goal
<i>Conf. A</i>	Antagonistic Clutches + ATI Nano 17	Antagonistic Control
<i>Conf. B</i>	MRF Device + Virtual Wall	Stability
<i>Conf. C</i>	MRF Device + Needle Insertion Setup	Stability
<i>Conf. C*</i>	<i>Conf. C</i> + Linear Stage + ATI Nano 43	Transparency
<i>Conf. D</i>	MRF Device + Palpation Setup	Stability
<i>Conf. D*</i>	<i>Conf. D</i> + Linear Stage+ ATI Nano 43	Transparency

5.6 Results: Validation of Antagonistic Control

The performance of the modeling and control method for actuating a single clutch was evaluated in Chapter 4. Furthermore, to evaluate the performance of these techniques when used in the antagonistic mode, a few additional tests were performed and the results are provided in this section. In the experiments, two PID controllers were used to control the output torque of a pair of clutches working in antagonistic configuration. The Hall sensor measurements, in addition to the ANN-based torque estimator, were used as the feedback signal for each PID controller. *Configuration A* was used in these tests. Fig. 5.10 shows the results of these experiments. Note that as the reference signal crosses 0 Nm, the responsibility of torque generation is switched between the two clutches (*i.e.*, one clutch is active at a time). As can be seen, the controller has a good performance in tracking these bidirectional desired torque signals. This test demonstrates the validity of the proposed modeling and control scheme in the antagonistic configuration.

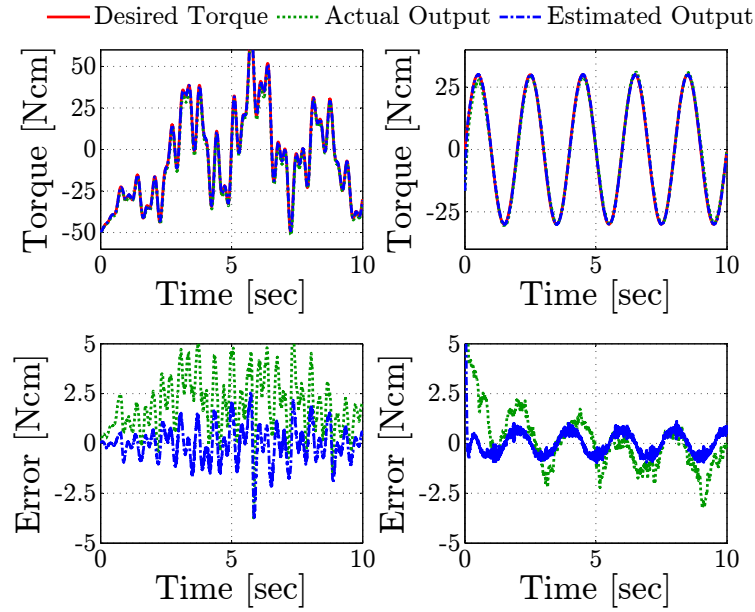


Figure 5.10: Results for validation of the antagonistic control (*Configuration A*) by applying bidirectional multi-sinusoidal (left) and sinusoidal (right) reference signals .

5.7 Results: Evaluation of Force Feedback Stability

In this section, the stability of the developed MRF-based haptic interface is compared with that of a PHANTOM Omni device and a Quanser Haptic Wand through several tests. To this end, first, the virtual wall benchmark is implemented, as described in *Configuration B*, and all devices are tested in different scenarios. Next, phantom and *in vitro* samples are used in *Configurations C* and *D* to compare the developed system's stability in real-world applications.

5.7.1 Virtual Wall Experiments

As mentioned, a virtual wall was implemented in *Configuration B*. Two sets of experiments were conducted; (1) For different values of virtual damping B_w , the maximum achievable virtual stiffness K_w by the MRF-based device, the PHANTOM Omni, and the Quanser Haptic Wand was obtained and compared, *i.e.*, by studying the *Z-Width*, as described in

Chapter 2. (2) Robustness of the stability of these devices to the variation of sampling time were evaluated and compared.

Study of Z-Width

In these experiments, *Configuration B* was used to study the *Z-width* of the system. To this end, for different values of virtual damping the maximum achievable virtual stiffness, for a stable operation of MRF-based haptic device, PHANTOM Omni, and Haptic Wand, was obtained. All the experiments in this section were performed at 1KHz. Fig. 5.11(a) shows the results. As can be seen, the MRF-based haptic interface exhibits the largest *Z-width* in comparison with the other two haptic devices. These results once more support the conclusion drawn in Chapter 2 and show the significant contribution of these type of actuators in improving the stability of a teleoperation system.

Fig. 5.12 presents the results of some of these experiments. In these tests, a virtual damping

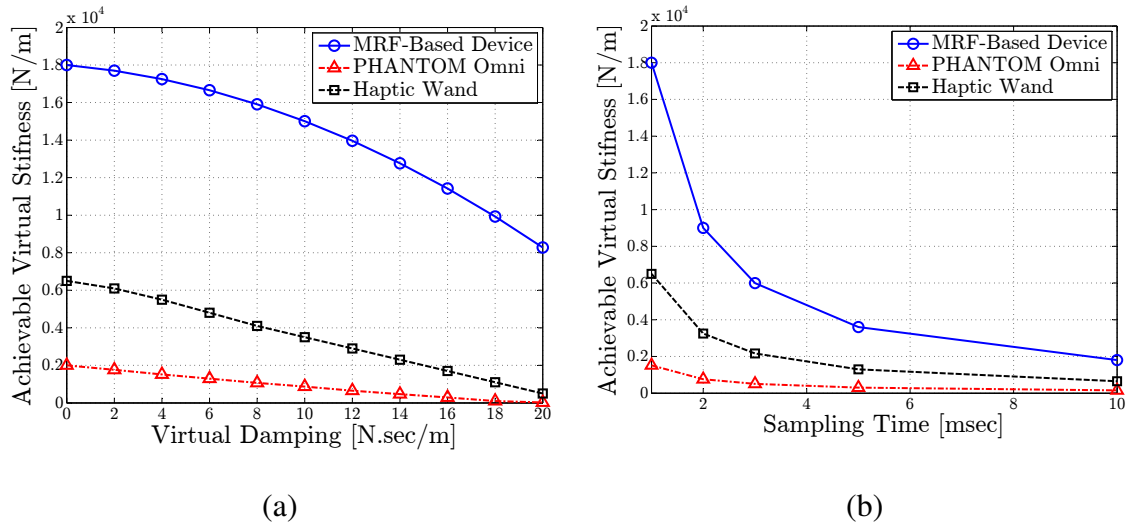


Figure 5.11: Maximum virtual stiffness that the MRF-based device, PHANTOM Omni, and Haptic Wand can render while remaining stable for (a) variable virtual damping, and (b) variable sampling time (*Configuration B*).

of $B_w = 6 \frac{N.s}{m}$ was considered. Note that the virtual slave comes into contact for positions less than or equal zero. Figures 5.12(a-c) present the stable interaction of the Omni, Haptic Wand, and MRF-based devices with a wall with stiffness of $K_w = 500, 2000,$ and $10000 \frac{N}{m}$, respectively. However, Figures 5.12(d-f) shows the result of haptic rendering of a virtual wall with stiffness just above the achievable stiffness. As seen, the MRF-based device remains stable for a very large range of virtual stiffness, which shows its high *Z-width*.

Effect of Sampling Time on Stability

Next, the robustness of the system to changes in the sampling time, T_s , of the virtual wall is examined and compared with that for the Omni and the Haptic Wand. For this purpose, a constant virtual damping ($B_w = 4 \frac{N.s}{m}$) was considered. The sampling time of the virtual wall was varied and once more the maximum achievable virtual stiffness was obtained. Note that the haptic interface still provides feedback at 1 KHz. Fig. 5.11(b) shows the results. Once more, these experiments proved that the MRF-based haptic device has larger stability margin and is more robust to the delay caused by the sampling time variation.

5.7.2 Phantom and *In Vitro* Needle Insertion and Palpation

In this section, phantom and *in vitro* samples are used in needle insertion and tissue palpation experiments to evaluate the stability of the system in real-world applications.

Needle Insertion

Configuration C was used in this section. A phantom made of agar with a concentration of 10% was used in these experiments. The user guided the needle inside the phantom using the haptic handle. Fig. 5.13(a-c) presents the result of such interaction using the three considered haptic interfaces. During operation, the PHANTOM Omni became unstable and exhibited strong oscillations as can be seen in the plot. The Haptic Wand performed

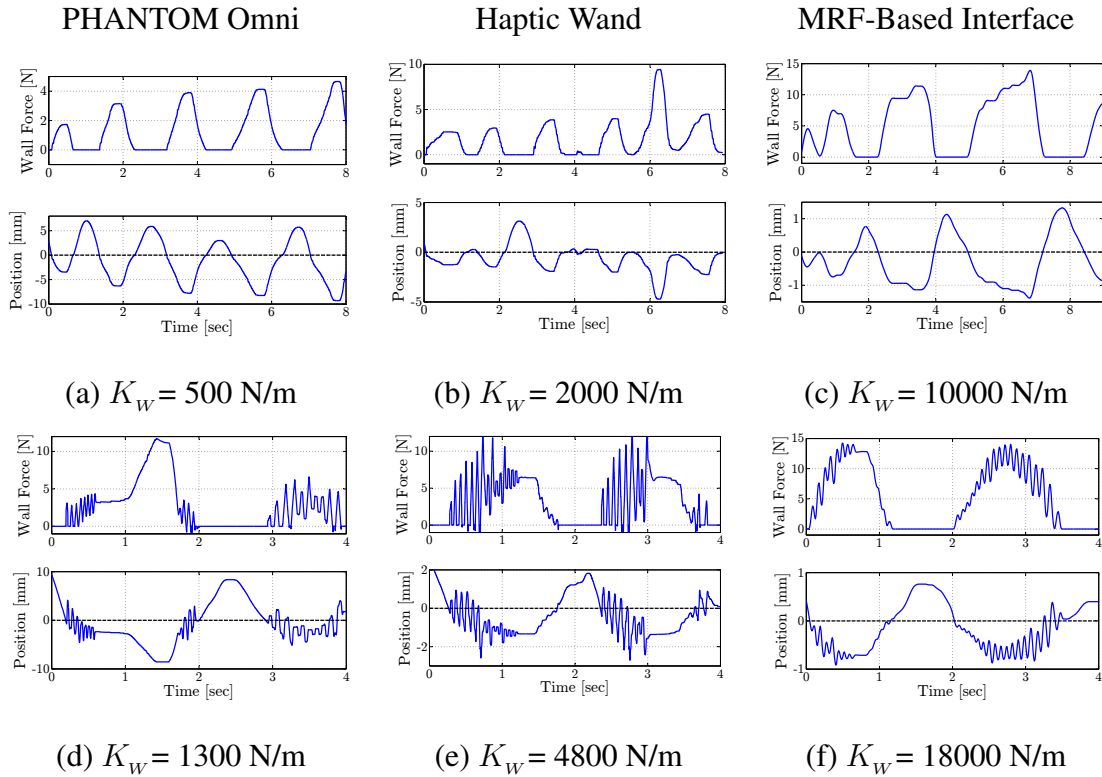


Figure 5.12: Results of interaction with the virtual wall (*Configuration B*) at 1 KHz with damping $B_w = 4 \frac{Ns}{m}$ and different stiffness for PHANTOM Omni, Haptic Wand, and the prototype system. (a-c) Stable interaction and (d-f) unstable interaction.

relatively better, however the ripples in the created force are highly undesirable for medical applications. As seen, the MRF-based haptic interface provided the most stable and desirable haptic feedback to the user. The user was able to make a very smooth insertion and retraction of the needle. In another set of experiments, the same test was performed on an *in vitro* kidney sample (beef). This organ consists one of the stiffest tissues in the body due to its thick renal cortex. Fig. 5.13(d-f) show the results. Once more both the Omni and the Haptic Wand exhibit strong ripples and oscillations. On the other hand, the MRF-based haptic interface provided very stable interaction.

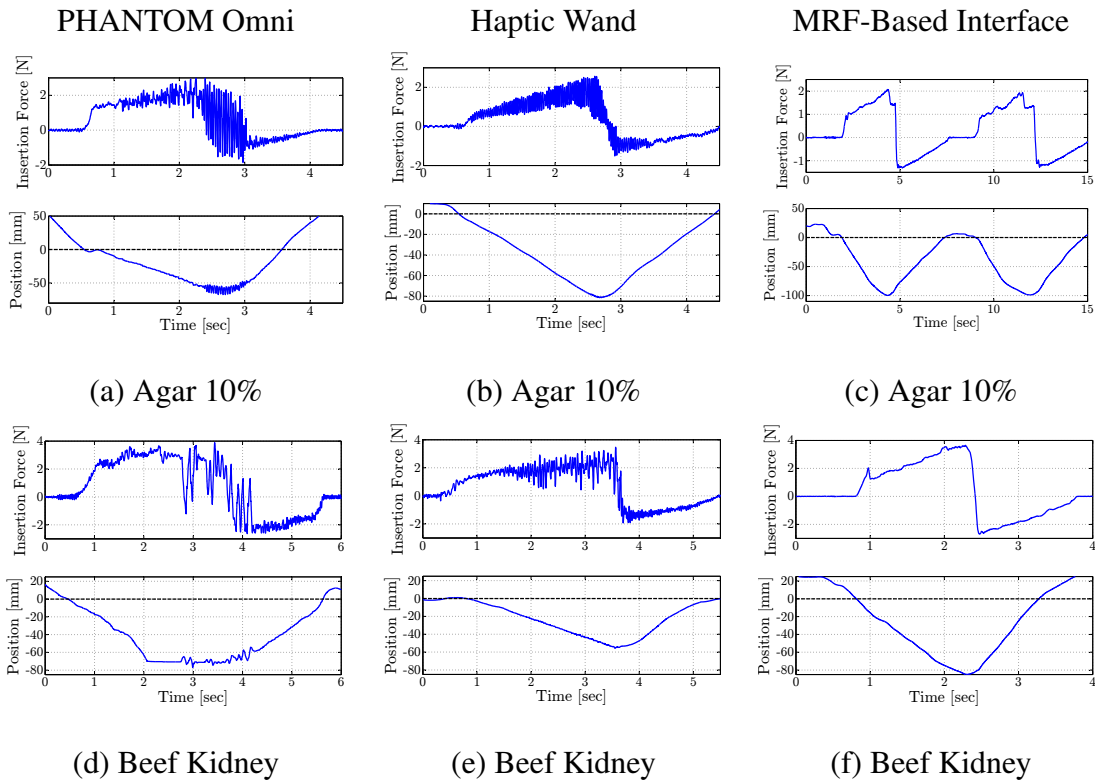


Figure 5.13: Results of needle insertion and retraction (*Configuration C*) on (a-c) an agar sample (10% concentration); and (d-f) an *in vitro* beef kidney.

Tissue Palpation

In order to further study the performance of the developed haptic interface in medical applications, *Configuration D* was used and several experiments on tissue palpation were performed. This section shows the results of the palpation of a phantom made out of agar (10%) and of an *in vitro* kidney (beef). The user tried to make several contacts with the samples using the haptic device. The results are shown in Fig. 5.14. Once more, the significant improvement in stability of teleoperation through the use of MRF-based system is visible. The other devices become unstable as the contact is made, which is exhibited as uncontrolled motions of the handle. In case of MRF-based system, the interaction remains very stable. Note that the effectiveness of the MRF-based haptic interface in distinguishing

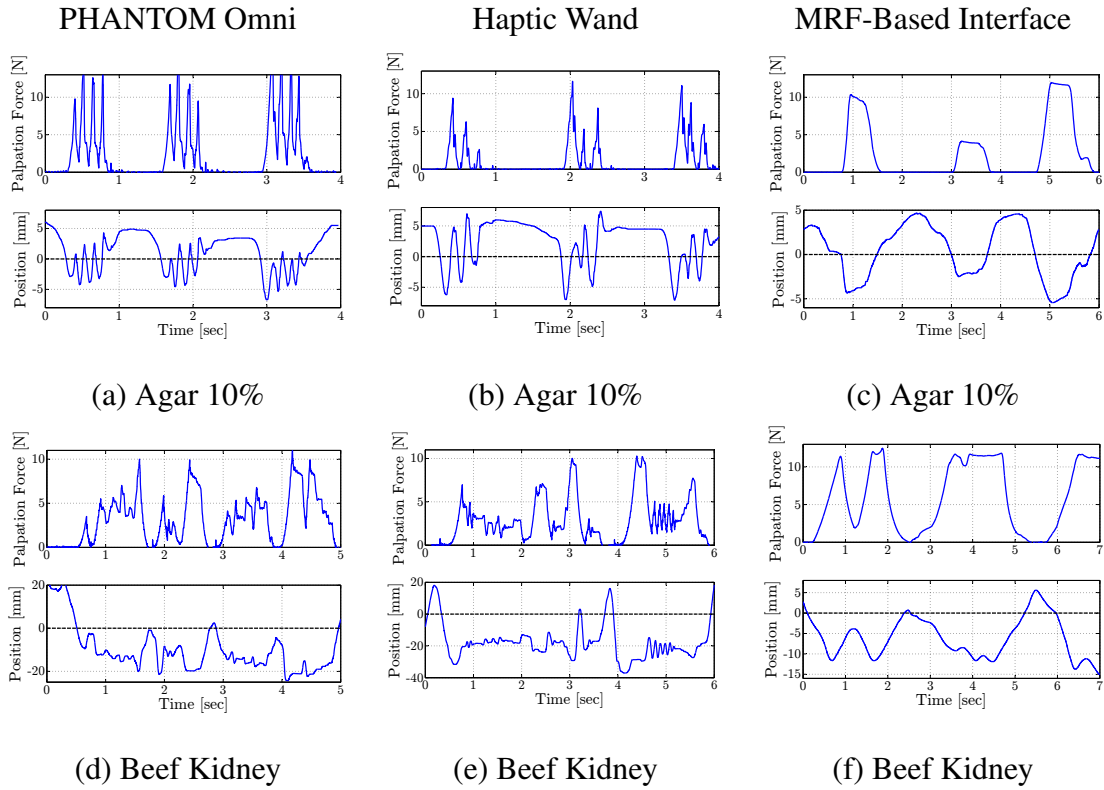


Figure 5.14: Results of tissue palpation (*Configuration D*) on (a-c) an agar sample (10% concentration) and (d-f) an *in vitro* beef kidney.

between high stiffness tissues (tumor) and lower ones is showed in next section.

5.8 Results: Evaluation of Force Feedback Transparency

The stability of the system was studied in the previous section and was compared with that of two other off-the-shelf haptic interfaces. In this section, the accuracy of force feedback provided by the MRF-based haptic interface is analyzed by taking advantage of *Configurations C** and *D**. These tests were designed for (1) validating the accuracy and transparency of the feedback and (2) studying the ability of the haptic device to provide a differentiable feel to the user of different tissues with diverse stiffnesses.

REMARK 7. In this section, the term "slave force/stiffness" is used to show the force/stiffness measured by the force sensor mounted at the based of the needle or palpator. In other words,

this is the interaction force or the sensed stiffness during needle insertion or palpation, respectively. The term "desired torques" refers to the torques that are required to create the slave force or the sensed stiffness, based on the dynamics of the system. The term "estimated torque" or "estimated force/stiffness" corresponds to the estimated output torque of the clutch and the output forces of the haptic handle which are obtained by the ANN model, discussed in Chapter 4. The term "feedback force/stiffness" refers to the force/stiffness felt by the force sensor attached to the haptic handle (*i.e.*, the actual force as opposed to the estimated one).

5.8.1 Needle Insertion

To evaluate the performance of the haptic interface in providing accurate force feedback, first the needle insertion application was considered, and a few experiments were performed. The results are given in this section. These experiments were carried out on a variety of phantom and *in vitro* samples using *Configuration C**, as shown in Fig. 5.15.

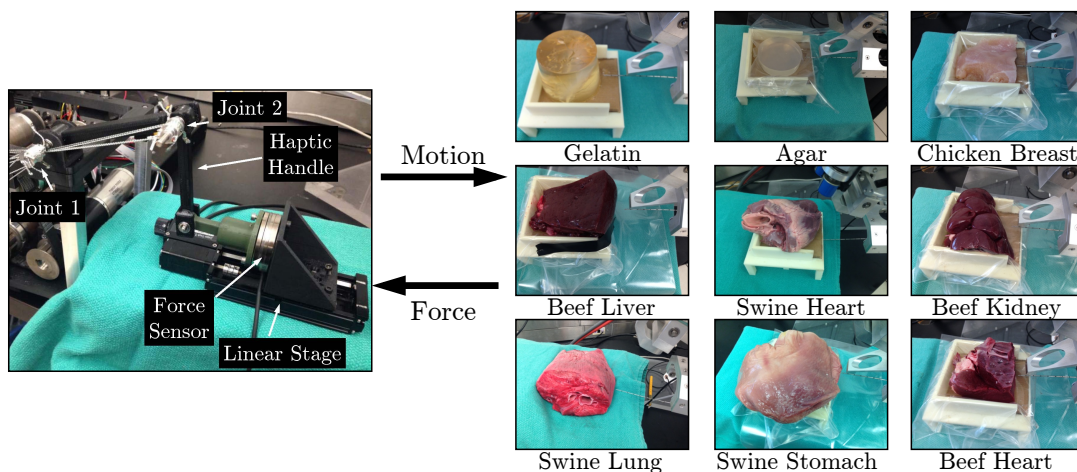


Figure 5.15: *Configuration C**, used for validating haptic feedback transparency using a large variety of samples.

The torque control is performed at the clutch level, and consequently the joint torque and end effector force are controlled. To clearly show this, first an experiment on an agar sample with a concentration of 3% was performed. As mentioned, in these experiments, the linear stage was used to command the needle insertion robot and guide the needle inside the sample. After the needle was inserted in the phantom to a depth of 5cm, the needle was stopped. The needle was then retracted from the phantom. Fig. 5.16(a) presents the desired torque and the estimated output torque of the clutches during this operation. Note that clutches 1 and 2 were antagonistically connected to joint 1 of the handle, and clutches 3 and 4 provided torque to joint 2. The direction of the generated torques in all the clutches was the same. But due to their antagonistic connection, the paired actuators created torques in opposite directions.

Fig. 5.16(b) presents the desired joint torque and the created torques at each joint by a

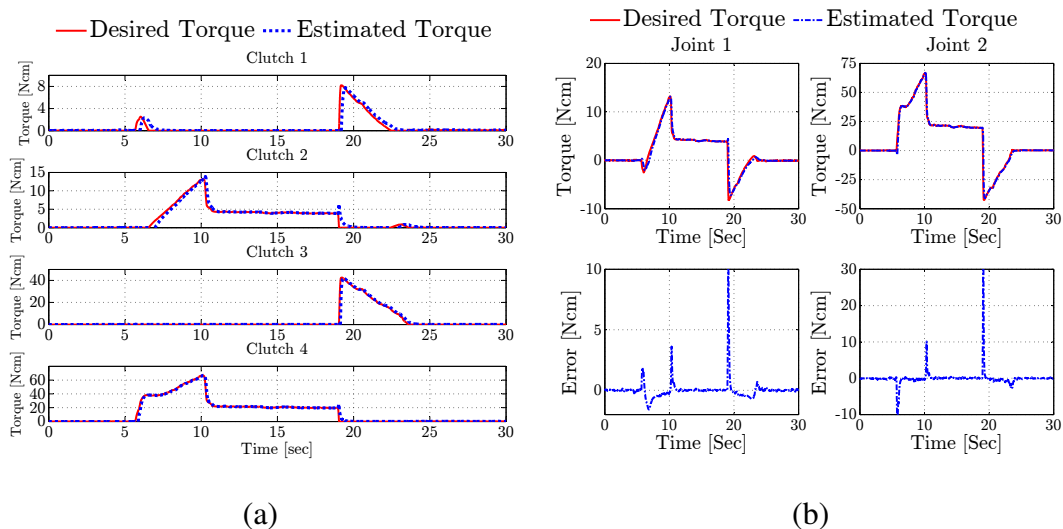


Figure 5.16: (a) Desired and estimated torques in the clutches during insertion and retraction of a needle inside a homogeneous phantom. (b) Top row: desired and approximated torques of joints. Bottom row: the error between the two variables.

pair of clutches. These torques provide force feedback at the end effector of the handle, which is measured by the force sensor. The results are shown in Fig. 5.17(a). The measured force from the slave side, the feedback force measured by the force sensor, and the estimated output force approximated by the ANN model is shown in this figure. As can be seen, the haptic interface can provide a fairly accurate force feedback on the master side. The slow response of the torque feedback during sudden changes is mainly due to the tension propagation in the cables used for transmitting the torque from the clutches to the joint. Nevertheless, these results show the potential of the MRF-based haptic interface in providing accurate force feedback.

The same experiment was performed for a large variety of phantom samples. The results are shown in Fig. 5.17. Three different concentrations of agar were used in the first three samples (Fig. 5.17 (a), (b), and (c) which have 3%, 6%, and 10% concentration rate respectively). As can be seen, the device provides accurate feedback to the user, which enables him/her to differentiate between the stiffnesses of the tissues. A gelatin sample (4%; less stiff than the agar samples used previously) was also used for comparison (Fig. 5.17(d)). Next two combinations of gelatin and agar were used to simulate puncturing through different layers of tissue. The first one was a gelatin sample, which contained two spherical tumors made out of agar (6%). The second sample consisted of layers of gelatin (4%) and agar (3% and 6%). The needle was inserted into the gelatin and was guided through these layers. Figs. 5.17(e,f) show the results. The ripples in the feedback force are caused during puncturing through these layers and as can be seen, the haptic device was able to recreate all these small deviations. Note that, the error between the ATI sensor reading (actual force feedback) and the needle (slave) force became large when the direction of the motion was changed. This is due to the delay that the cable tensions create in the system and is one of the main drawbacks of the first prototype, and will be addressed in the second generation of the device.

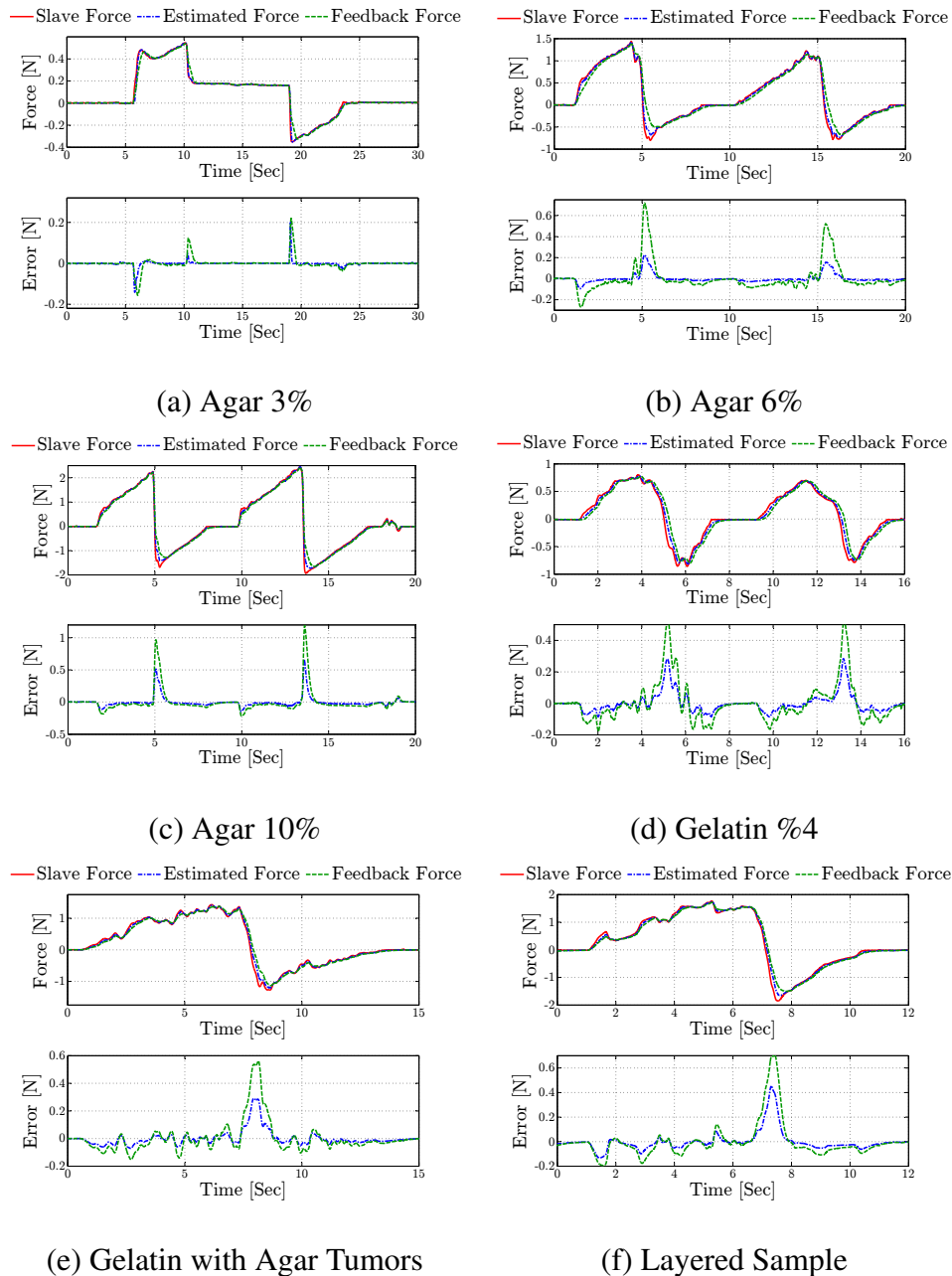


Figure 5.17: Desired, estimated, and actual force feedback at the end effector during insertion and retraction of a needle (*Configuration C^f*) inside phantoms.

Next, *in vitro* animal samples were used to test the accuracy of the device during needle insertion into animal tissue. For this purpose, several animal organs were used. Fig. 5.18 shows the results. Every tissue exhibits a different pattern of forces based on its stiffness,

stickiness, and layers. In all cases, the MRF haptic device provided fairly accurate feedback, which enabled the differentiation between tissue properties.

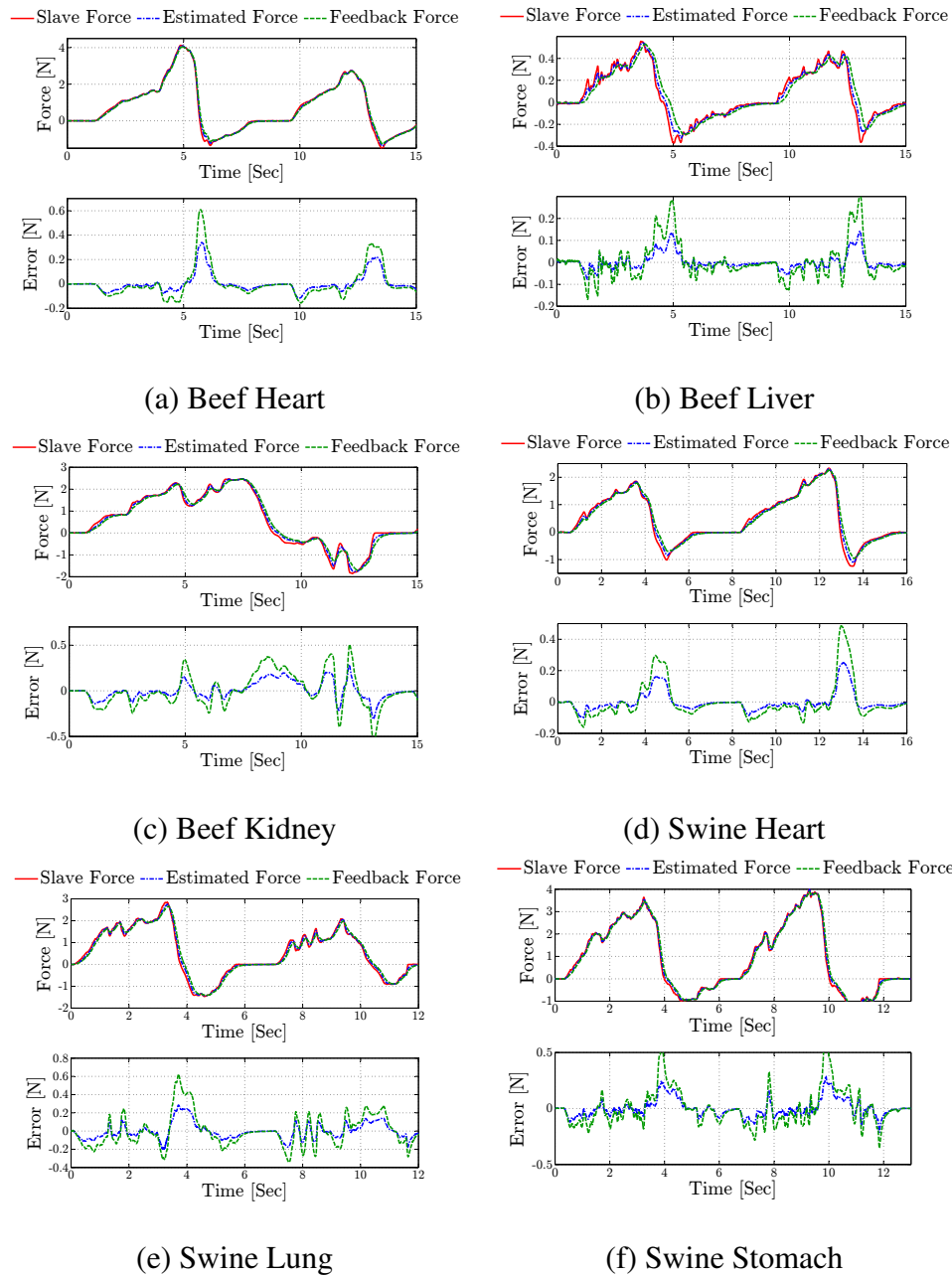


Figure 5.18: Desired, estimated, and actual force feedback at the end effector during insertion and retraction of a needle (*Configuration C**) inside *in vitro* samples.

5.8.2 Tissue Palpation

By taking advantage of *Configuration D** for tissue palpation, further experiments were performed to assess the accuracy and capabilities of the device. In the results of this section, to evaluate the transparency of the system, the stiffness (impedance or ratio of force to displacement) of the sample was compared to the reflected stiffness of the haptic handle. First palpation of phantom samples was performed. Three phantoms with different stiffnesses (*i.e.*, gelatin sample (4%), Agar samples (6% and 10%)) were used. Figs. 5.19(a-c) show the results. It is evident that the haptic interface was capable of producing the different stiffnesses felt of the samples.

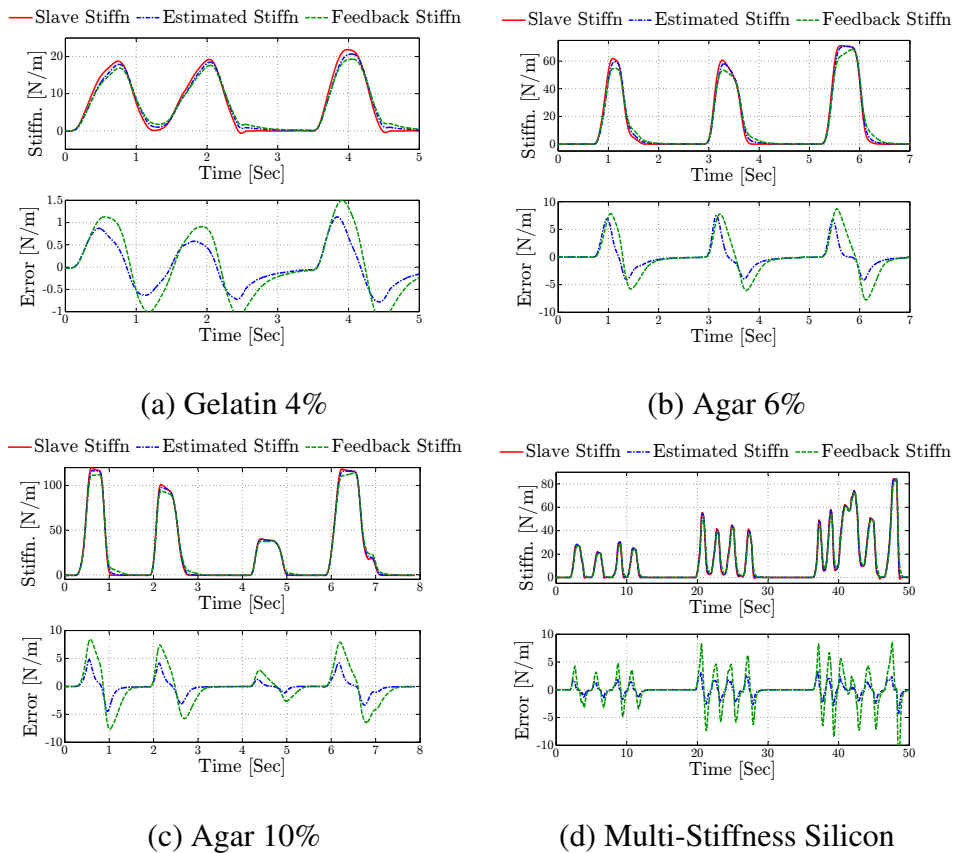


Figure 5.19: Desired, estimated, and actual stiffness at the end effector during palpation (*Configuration D**) of phantoms samples.

Tumor localization is one of the main applications of palpation in medical interventions. For open procedures, the clinician can palpate using their hands but for robotics-assisted minimally invasive procedures, a haptic interface is needed [33]. To evaluate the performance of the haptic device in providing accurate and reliable force feedback for tumor localization during a minimally invasive intervention, a silicon model that contained two embedded silicon tumors (stiffer than the surrounding material) were used. These tumor-like samples were located at different depths - at 1cm and 2cm. Three separate contacts were made with the sample, (i) several palpations of the surrounding silicon (no tumor) between 0s-12s; (ii) multiple contacts of the tissue which included the deep tumor 20s-30s; and (iii) final palpation of the tumor located at the depth of 1cm in the period of 35s-50s. Fig 5.19 shows the results of the palpation. As can be seen, the MRF-based haptic device is capable of recreating the stiffness in all three cases, which enables the localization of the two tumors.

The performance of the haptic device in simulating stiffness of *in vitro* animal organs was also studied. The results of the palpation experiments on several tissues are shown in Fig. 5.20. The outcomes in this section show the great potential of MRF-based actuators in haptic applications that require stable, high fidelity, and accurate force display. The cable-driven design of the system is one of its drawbacks due to the delay resulting from the transmission of torque to the user's hand. This issue will be addressed in the next generation of the system.

5.9 Concluding Remarks

The design and evaluation of a prototype 2-DoF haptic interface based on MRF clutches were reported in this chapter. The device was integrated and evaluated in a master-slave system for use in medical interventions consisting of needle insertion and steering, as well as, soft-tissue palpation. The stability and transparency of the system were rigorously

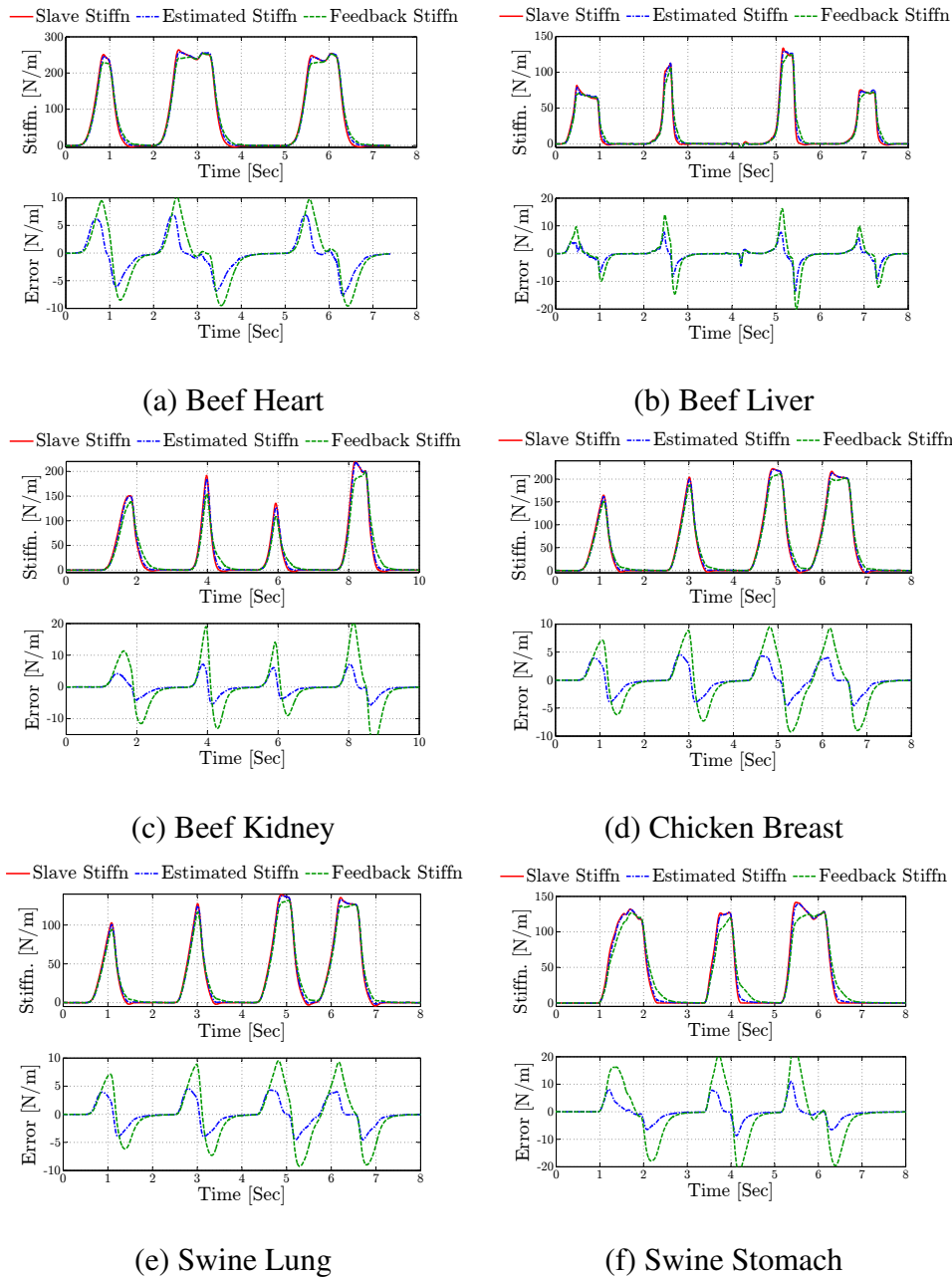


Figure 5.20: Desired, estimated, and actual stiffness at the end effector during palpation (*Configuration D**) of *in vitro* organs.

tested using a wide range of phantom and *in vitro* samples. In addition, the stability of the MRF-based haptic device was compared with that of two well-known off-the-shelf haptic interfaces. While further subject-based investigations are required to study the effect of the

device in specific medical applications, the promising results show the great potential of the MRF-based device for use in applications that require accurate and reliable performance. In the next chapter, we will summarize the contributions of this work and discuss possible future work to be conducted in this project.

Bibliography

- [1] T. Coles, D. Meglan, and N. John, "The role of haptics in medical training simulators: A survey of the state of the art," *IEEE Transactions on Haptics*, vol. 4, pp. 51–66, Jan 2011.
- [2] A. Okamura, C. Basdogan, S. Baillie, and W. Harwin, "Haptics in medicine and clinical skill acquisition [special section intro.]," *Haptics, IEEE Transactions on*, vol. 4, pp. 153–154, May 2011.
- [3] R. Robison, C. Liu, and M. Apuzzo, "Man, mind, and machine: The past and future of virtual reality simulation in neurologic surgery," *World Neurosurgery*, vol. 76(5), pp. 1750–78, 2011.
- [4] A. Hamed, S. Tang, and H. Ran, "Advances in haptics, tactile sensing, and manipulation for robot-assisted minimally invasive surgery, noninvasive surgery, and diagnosis," *Journal of Robotics*, vol. 12, pp. 1–14, 2012.
- [5] K. Ohnishi, "Real world haptics and telehaptics for medical applications," in *Industrial Electronics (ISIE), 2010 IEEE International Symposium on*, pp. 11–14, July 2010.
- [6] K. Kuchenbecker and G. Niemeyer, "Induced master motion in force-reflecting teleoperation," *Journal of Dynamic Systems, Measurement, and Control*, vol. 128, no. 4, pp. 800–810, 2006.
- [7] R. Lozano, N. Chopra, and M. Spong, "Passivation of Force Reflecting Bilateral Teleoperation with Time Varying Delay," *Journal of Mechatronics*, vol. 12, pp. 215–223, 2002.
- [8] I. Polushin, X. Liu, and C. Lung, "Stability of bilateral teleoperators with generalized projection-based force reflection algorithms," *Automatica*, vol. 48-6, pp. 1005–1016, 2012.
- [9] A. Shafer and M. Kermani, "Design and validation of a MR clutch for practical control applications in human-friendly manipulation," in *International Conference on Robotics and Automation*, 2011.
- [10] D. Senkal and H. Gurocak, "Haptic joystick with hybrid actuator using air muscles and spherical MR-brake," *Mechatronics*, vol. 21-6, pp. 951–60, 2011.
- [11] A. Bicchi, M. Raugi, R. Rizzo, and N. Sgambelluri, "Analysis and design of an electromagnetic system for the characterization of Magneto-Rheological fluids for haptic interfaces," *IEEE Transactions on Magnetics*, vol. 41, pp. 1876 – 1879, may 2005.

- [12] J. An and D. Kwon, "In haptics, the influence of the controllable physical damping on stability and performance," in *IEEE/RSJ International Conference on Intelligent Robots and Systems*, 2004.
- [13] J. Melli-Huber, B. Weinberg, A. Fisch, J. Nikitzuk, C. Mavroidis, and C. Wampler, "Electro-Rheological fluidic actuators for haptic vehicular instrument controls," in *Symposium on Haptic Interfaces for Virtual Environment and Teleoperator Systems*, 2003.
- [14] W. Li, B. Liu, P. Kosasih, and X. Zhang, "A 2-DOF MR actuator joystick for virtual reality applications," *Sensors and Actuators*, vol. 137, pp. 308–320, 2007.
- [15] J. Furusho, M. Sakaguchi, N. Takesue, and K. Koyanagi, "Development of ER brake and its application to passive force display," *Journal of Intelligent Material Systems and Structures*, vol. 13, pp. 425–429, 2002.
- [16] M. Reed and W. Book, "Modeling and control of an improved dissipative passive haptic display," in *IEEE International Conference on Robotics and Automation*, vol. 1, pp. 311 – 318, Apr 2004.
- [17] Y. Yamaguchi, S. Furusho, S. Kimura, and K. Koyanagi, "Development of high-performance MR actuator and its application to 2D force display," *International Journal of Modern Physics B*, vol. 19, pp. 1485–1491, 2005.
- [18] M. Bouzit, G. Burdea, G. Popescu, and R. Boian, "Phantom haptic interface: a device for probing virtual objects," in *International Mechanical Engineering Congress and Exposition*, 1994.
- [19] D. Cassar and M. Saliba, "A force feedback glove based on Magneto-Rheological fluid: Preliminary design issues," in *IEEE Mediterranean Electrotechnical Conference*, pp. 618–623, 26-28 2010.
- [20] S. Winter and M. Bouzit, "Use of Magneto-Rheological fluid in a force feedback glove," *IEEE Transactions on Neural Systems and Rehabilitation Engineering*, vol. 15, pp. 2 –8, Mar 2007.
- [21] Y. Nam, M. Park, and R. Yamane, "Smart Glove: Hand master using Magneto-Rheological fluid actuators," in *Proceedings of SPIE*, vol. 6794, pp. 679434–679434–6, 2007.
- [22] J. Blake and H. Gurocak, "Haptic glove with MR brakes for virtual reality," *IEEE/ASME Transactions on Mechatronics*, vol. 14, pp. 606 –615, oct. 2009.
- [23] A. Shafer and M. Kermani, "On the feasibility and suitability of MR fluid clutches in human-friendly manipulators," *IEEE/ASME Transactions on Mechatronics*, vol. 16-6, pp. 1073 – 82, Dec 2010.

- [24] P. Yadmellat, A. Shafer, and M. Kermani, "Design and development of a safe robot manipulator using a new actuation concept," in *International Conference on Robotics and Automation*, 2013.
- [25] A. Shafer and M. Kermani, *MR Clutch with Sensors Measuring Electromagnetic Field Strength*. US Patent 20130047772, Feb 2013.
- [26] W. Li, P. Yadmellat, and M. Kermani, "Linearized torque actuation using FPGA-controlled Magneto-Rheological actuators," *IEEE/ASME Transactions on Mechatronics*, vol. PP, pp. 1–9, May 2014.
- [27] Geomatic Technologies Inc., Woburn MA, *Specifications for the PHANTOM Desktop and PHANTOM Omni haptic devices*, 2009.
- [28] Quanser, Markham ON, *5-DOF Haptic Wand -Product Information Sheet S25*, C ed., 2008.
- [29] V. Hayward and O. Astley, "Performance measures for haptic interfaces," in *Robotics Research* (G. Giralt and G. Hirzinger, eds.), pp. 195–206, Springer London, 1996.
- [30] H. Bassan, *Design, construction and control of a micro manipulator for prostate brachytherapy*. PhD thesis, University of Western Ontario, 2007.
- [31] H. Bassan, R. Patel, and M. Moallem, "A novel manipulator for percutaneous needle insertion: Design and experimentation," *IEEE/ASME Trans. Mechatron.*, vol. 14(6), pp. 746–761, 2009.
- [32] A. Asadian, *Robotics-Assisted Needle Steering for Percutaneous Interventions: Modeling and Experiments*. PhD thesis, University of Western Ontario, 2013.
- [33] A. Talasaz, R. Patel, and M. Naish, "Haptics-enabled teleoperation for robot-assisted tumor localization," in *IEEE International Conference on Robotics and Automation*, pp. 5340–5345, May 2010.

Chapter 6

Concluding Remarks and Future Work

The design, development, construction, and evaluation of a two-DoF haptic interface based on the use of MRF-based actuators for medical application were reported in this work. This chapter provides concluding remarks that address the contributions, discuss the manufacturing expenses and shortcomings of the system, and outline the future steps of the work.

6.1 Summary of Research and Achievements

MRF-based actuators exhibit promising characteristics for applications in haptic devices: low output inertia, low mass-torque ratio, superior performance and bandwidth, precise controllability of output torque, and intrinsic passivity of MRF-based actuators. Theoretical studies of the properties of MRF-based actuators through the use of the small-gain theorem and virtual wall benchmark demonstrated the potential of such actuators for use in haptic devices with improved transparency and stability. The experimental results of the virtual wall test described in Chapter 2 on a large-scale prototype of an MRF-based clutch support these claims and demonstrate the desirable performance of such actuators when used in a haptic device. While the large-scale MRF-based clutch was not suitable for use in a practical haptic interface, the results provided a strong motivation for developing

small-scale MRF-based actuators as a lightweight and compact actuating system. It was discussed that the conventional designs for MRF-based actuators will lose their advantage when their size is reduced. Hence, a new design for small-scale MRF-based actuators was proposed, called armature-based design. This new model takes advantage of a strong and uniform magnetic field and a large area of contact, which contribute to its torque capacity. Our preliminary analytical studies on the proposed design support this claim in Chapter 3. It was shown that this novel design exhibits superior mechanical characteristics in comparison with both conventional small-scale electrical motors and conventional MRF-based clutches. The development of the MRF-based clutch was described in Chapter 4. It was experimentally demonstrated that the proposed system shows a significant improvement over the state of the art, especially in terms of torque-to-size ratio. A modeling and control scheme based on artificial neural networks and embedded Hall sensors was proposed and it was shown through experiments that it presents a very accurate and efficient means of providing transparent and high fidelity torque delivery which is essential for haptic devices in medical applications. In addition, the control scheme does not require any external force/torque sensors, which contributes to lower cost and greater simplicity for the system. The design and development of a prototype 2-DoF haptic interface based on the armature-based clutch were reported in Chapter 5. This system takes advantage of a distributed and antagonistic configuration. The device was integrated and evaluated in a master-slave system that can be used for medical interventions that involving needle insertion and steering, and soft-tissue palpation. The stability and transparency of the system was rigorously examined using a wide range of phantom and *in vitro* samples. In addition, its performance was compared with that of the Geomagic PHANTOM Omni and the Quanser Haptic Wand. The promising results demonstrated the great potential of this approach for use in medical applications that require accurate and reliable force feedback.

6.2 Contributions

This section lists the contributions of the thesis.

- A theoretical and experimental study of the effect of MRF-based actuators on the performance (stability and transparency) of haptic interfaces was performed.
- A new design of a small-scale MRF-based clutch, called an armature-based clutch, was proposed, which exhibits high torque capacity and low inertia and mass. Simulation and analytical study of the design was provided. Figures of merit were derived, and the suitability of the design for use in haptic interfaces was demonstrated.
- Four prototypes of the proposed design were developed and evaluated through several experiments. The results supported the findings in the design stage.
- A modeling method for predicting the nonlinear behavior of the MRF-based clutch based on the measurement of the magnetic field using Hall sensors was proposed and experimentally validated. A feedback in a torque control scheme using feedback of the output of the model was developed. This resulted in efficient and simple torque control without the need for a force/torque sensor.
- Using the developed clutches, a prototype two-DoF haptic interface was constructed for medical applications. This design takes advantage of a distributed antagonistic configuration of clutches. The structure provides a robust, efficient, and low inertia of operation which contributes to higher transparency of the system.
- The effectiveness of MRF-based actuators in improving the stability of a teleoperation system and its efficiency in providing accurate and reliable force feedback was validated through several experiments on teleoperated needle insertion and soft-tissue palpation setups. Several phantom and *in vitro* samples were used. The results demonstrated the great potential of these actuators.

6.3 Discussion: Manufacturing Expenses

Manufacturing cost of the clutch was one of our main design criteria during the design of the system. Given the simple mechanical design of the clutch and the robustness of this design with respect to the fabrication process, we believe that MRF-based clutches can be mass produced at a relatively low cost. The clutches presented in this thesis were the first prototypes that were built in-house at Western Engineering's University Machine Services and using an EDM wire cut machining technique. As a result, the fabrication cost of each clutch was about \$2000 CAD, of which the labor cost was a major part (about 70% of the total cost). Another measure that can significantly contribute to lower cost of systems built using our actuation principle is the use of Hall sensors within the design of the clutch, as discussed in Chapter 4. Using Hall sensors, we are able to achieve accurate torque measurements and eliminate the need for external and costly force/torque sensors.

Table 6.1: List of Expenses for Manufacturing of a Single Clutch

Part	Method	Quantity	Total Cost
Armature	EDM Wire Cut	1	\$1,217.96
Outer Casing	Machining	1	\$329.19
Casing Caps	Machining	2	\$167.50
Slip Ring	Purchase	1	\$166.30
Belt Pulleys	Machining	2	\$161.26
Capstan Pulleys	Purchase	2	\$114.71
Bearings	Machining	4	\$48.64
Magneto-Rheological Fluid	Purchase	12.8 ml	\$12.71
Total			\$2,082.57

6.4 Discussion: Shortcomings and Drawbacks

The current design has some shortcomings and drawbacks. In this section, these are addressed and potential solutions are proposed.

Wire Routing: The current use of a keyhole for routing the coil and Hall sensors wires to the slip ring caused a few problems. This keyhole is vulnerable to leakage. The design will be modified in the next generation to address this issue.

Heating: Although the issue of heating did not cause significant problems at this stage, temperature sensing should be integrated in the next generation of the system. Deviations in the torque output were evident after long periods of operation which was associated with heating.

Thickening and Maintenance: As mentioned earlier, the issue of thickening is one of the main problems in MRF-based systems. Fig. 6.1 shows a case of thickening occurring during this work. It is likely that this was a result of a lower quality MRF and possibly a failure in sealing, which allowed drainage of the oil from the clutch. However, new generation of commercial MRF consists of a stabilizer additive, which prolongs its efficient life. Nevertheless, in the long term, these systems will require regular maintenance due to



Figure 6.1: The problem of thickening in MRF-based clutch.

this issue. Overall, in comparison with electrical motors, the need for regular maintenance could add to the cost of the system. In the opinion of the author, this is one of the main drawbacks of MRF-based actuators.

Cable-Driven System: The device was designed as a cable-driven system with the goal of making the haptic handle simple, compact, low inertia, and lightweight. However, the delay caused by the propagation transmission via the cables reduced the bandwidth of the system and degraded the force feedback transparency. The next generation of the device will be made with a belt and pulley configuration. Although this approach will add to the design complexity and size of the haptic handle, it should provide a low inertia and mass interface for the user.

6.5 Future Work

This section concludes this chapter by outlining some of the next steps in this study.

- The second generation of the armature-based clutch should include temperature sensing that should also be taken into account in the modeling and control. Also fins should be placed on the outer casing to help reduce heat build up. The wire routing should be modified. Two sealable holes should be incorporated on the outer casing to facilitate the process of filling and maintenance. The mass of the clutch should be reduced by decreasing the thickness of outer casing through the use of proper machining techniques.
- The cable transmission should be replaced by a belt and pulley actuation system to alleviate the problems of delay caused by cables in the current version of the device.
- The second generation of the haptic interface should include 3 DoF to evaluate the efficiency of MRF-based actuators in general purpose medical applications.

- A mathematical analysis of the effect of MRF-based actuators on transparency should be performed. In addition, comparison with other well-known haptic interfaces is required to further study the improvement in transparency.
- Further investigation regarding stable performance of the haptic device should be carried out for teleoperation systems with time delays. Also, applications, which involve larger environment forces, should be considered for verification of the system performance.
- The system should be tested in *in vivo* and active environments to study the effect of natural motions and forces (*e.g.*, breathing, heart beat, body motion) on the stability and effectiveness of the system.
- A series of subject-based experiments should be conducted to statistically study the effect of the MRF-based haptic interface in medical tasks, such as tumor localization, needle insertion and steering, *etc.* The performance measures should include, the success rate, completion time, average exerted force, accuracy in controlling interaction forces, comparison with force control based on the haptic interface and that based on force measurements, control of tool motion, and overall ease of using the device, *etc.* In addition, subject-based experiments are required for further study of stability. It is shown in the literature that different human behaviors may result in changes in the stability.
- The applicability of the system should be investigated in other medical applications, such as catheter steering and guidance of probes/catheters for tissue ablation.
- Further safety analysis should be performed to determine the potential of the system to meet all safety requirements imposed by regulatory health organizations.

Appendix A

Technical Drawings of the Parts

In this Appendix, detailed specifications of the parts that have been designed are given.

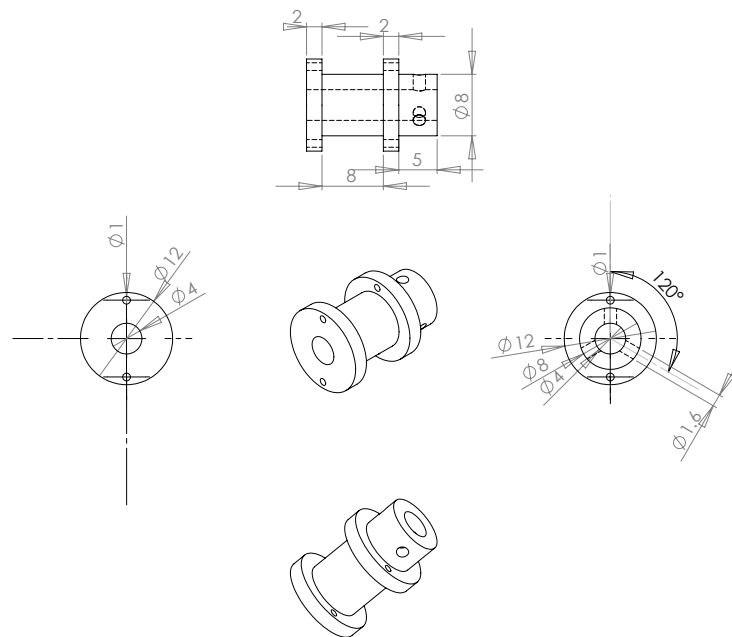


Figure A.1: Dimensions of the capstan pulley in [mm]

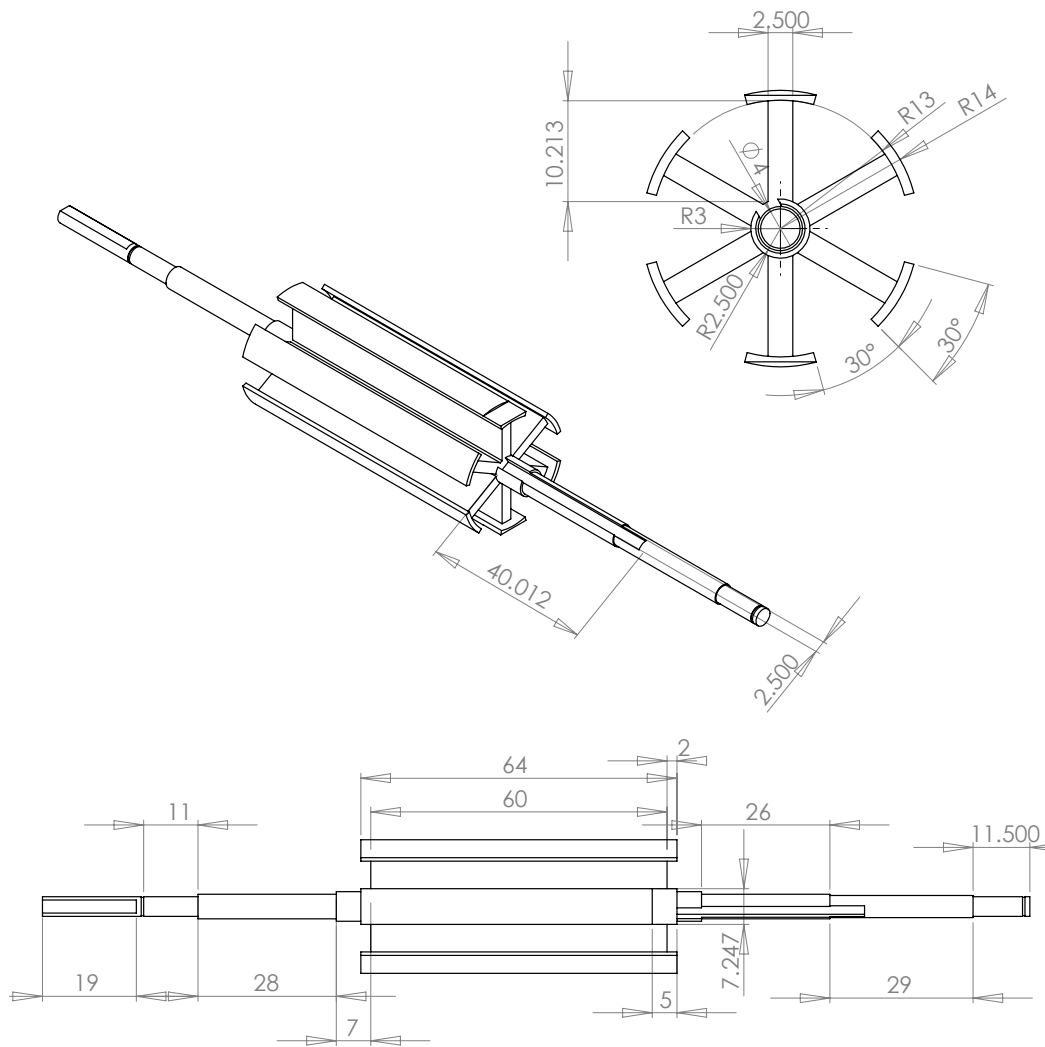


Figure A.2: Dimensions of the Armature in [mm]

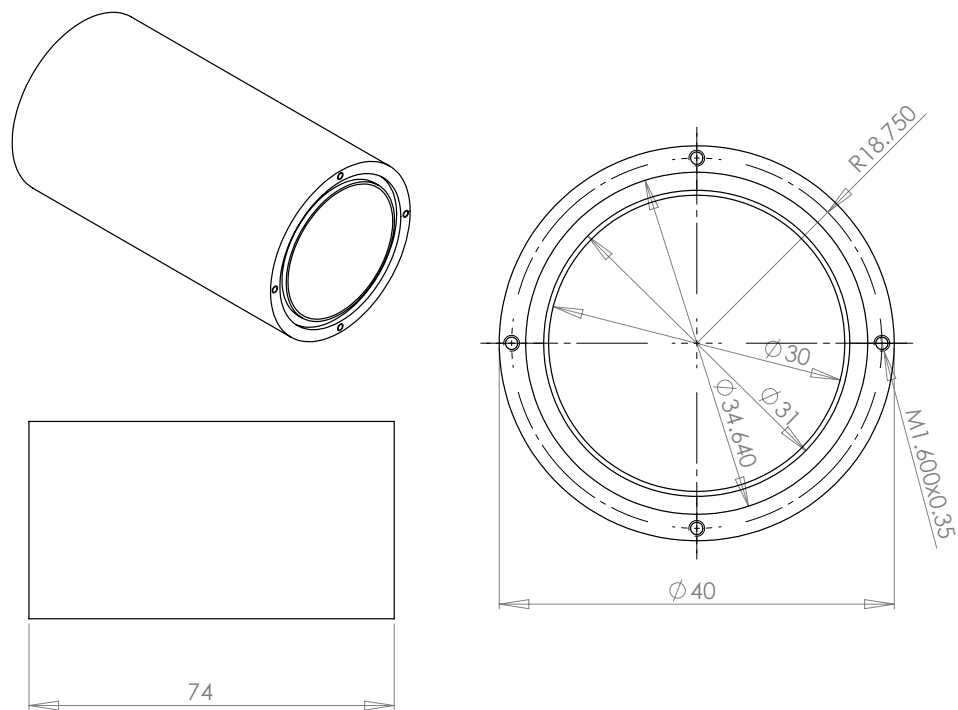


Figure A.3: Dimensions of the outer casing in [mm]

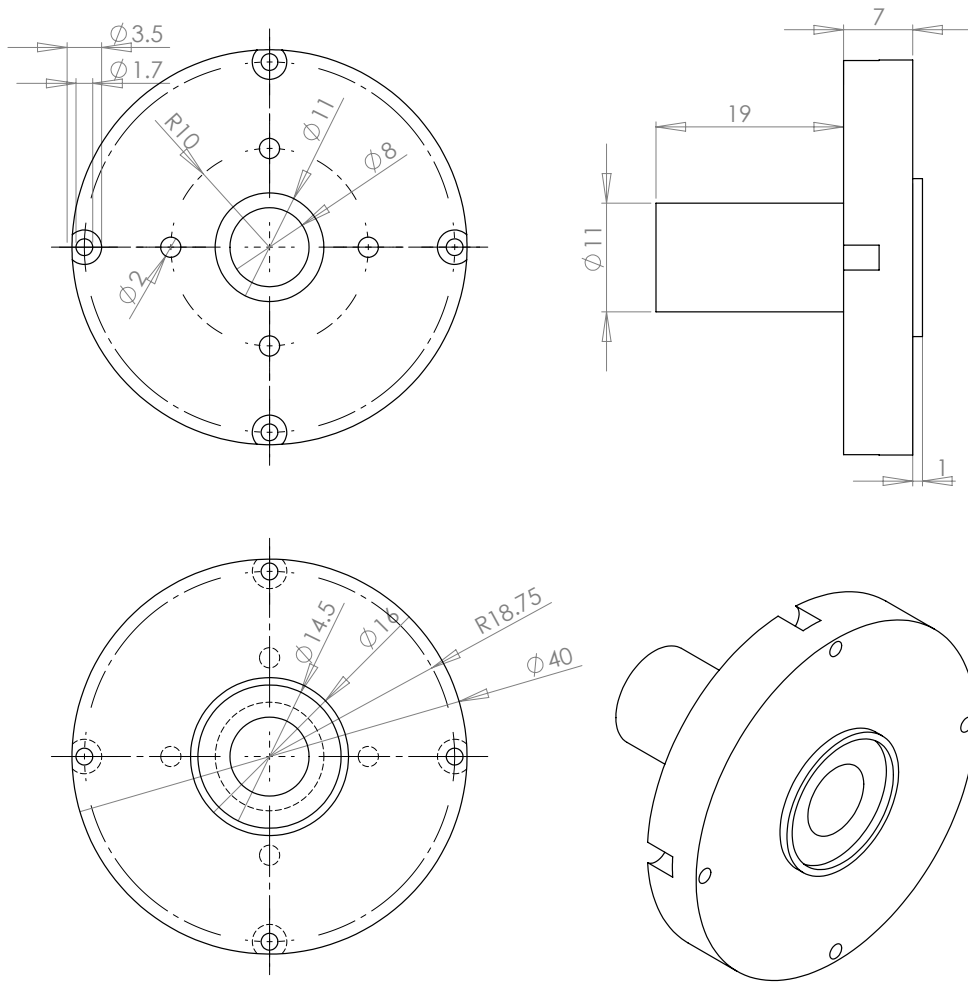


Figure A.4: Dimensions of the outer casing cap in [mm]

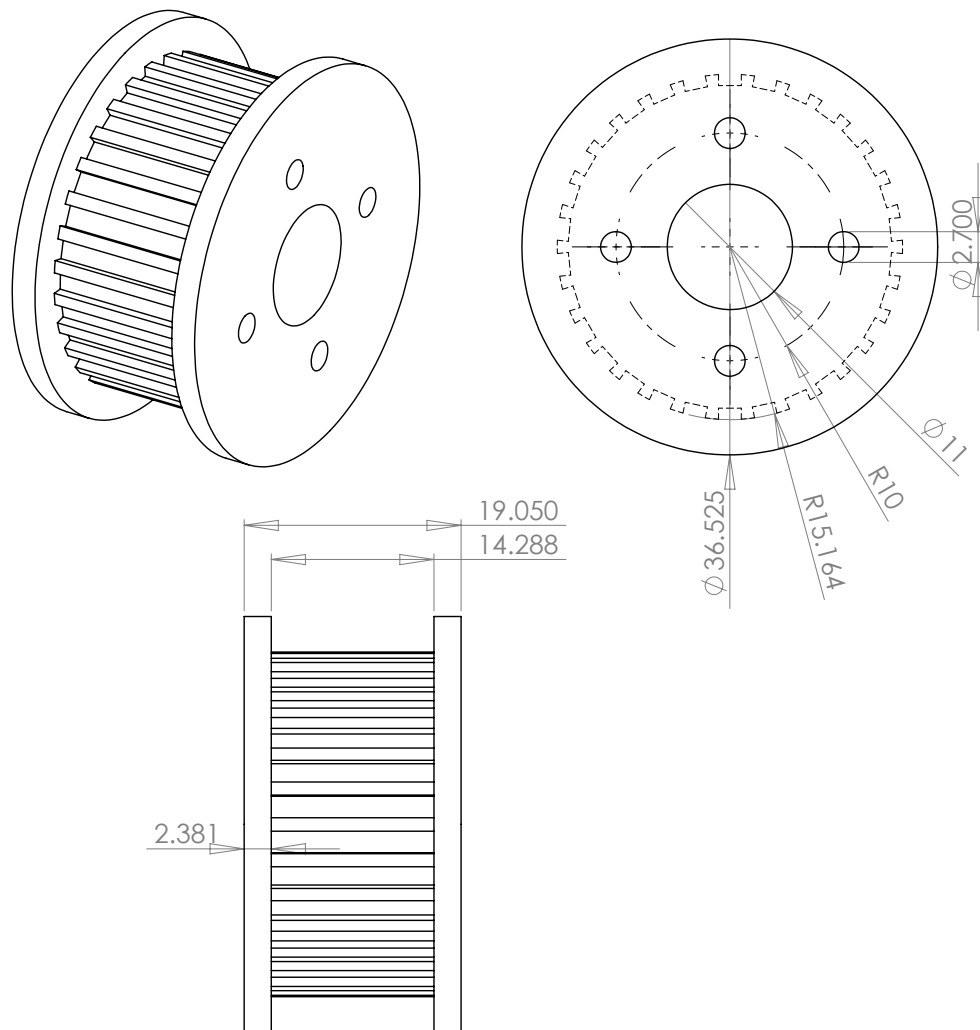


Figure A.5: Dimensions of the belt pulley in [mm]. Further Info: Fits 12.7 mm belt width, 36.52 mm outer diameter, 10 teeth, 1.94 inch pitch diameter, 9.52 mm pitch of the belt

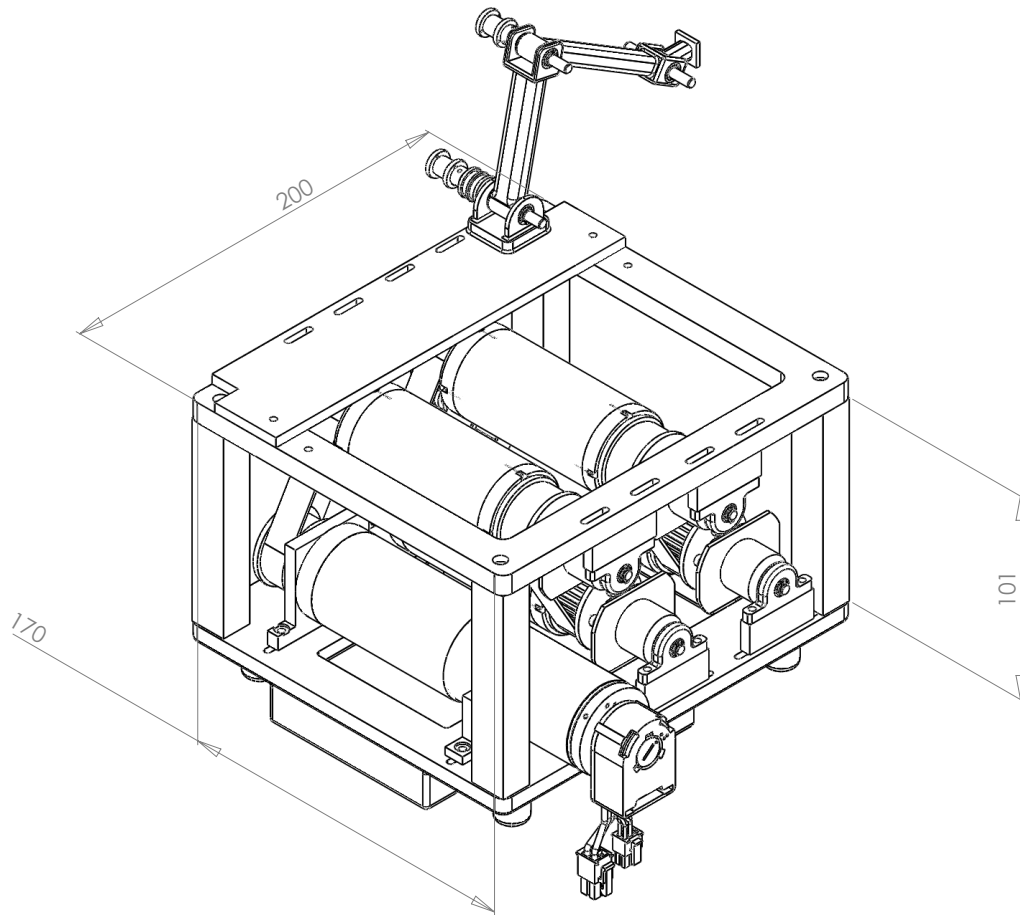


Figure A.6: Dimensions of the frames of the haptic interface in [mm]

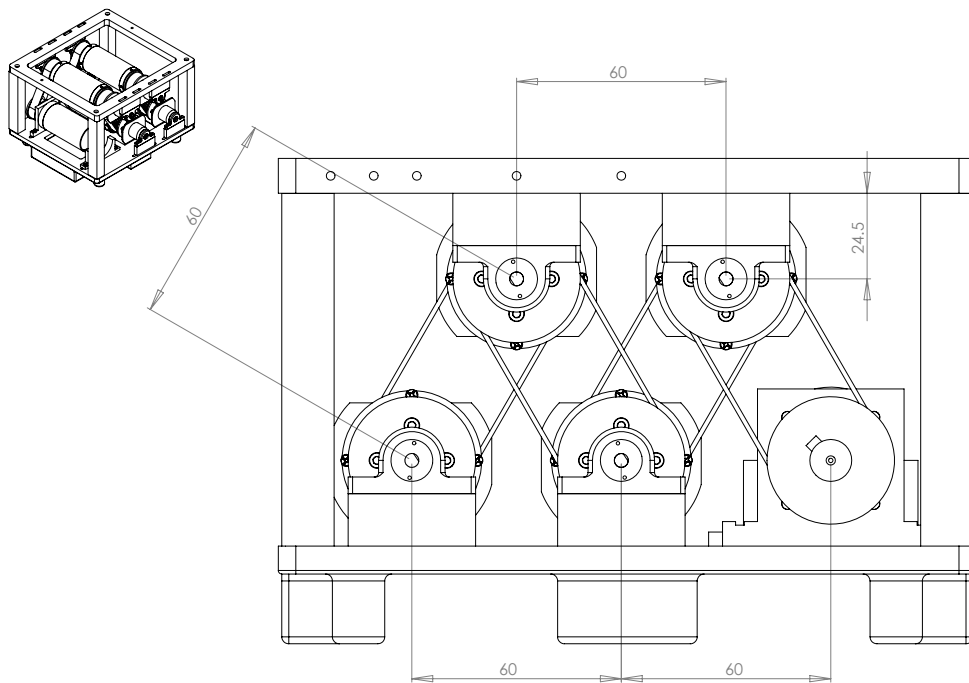


Figure A.7: Location of clutches with respect to each other in [mm]

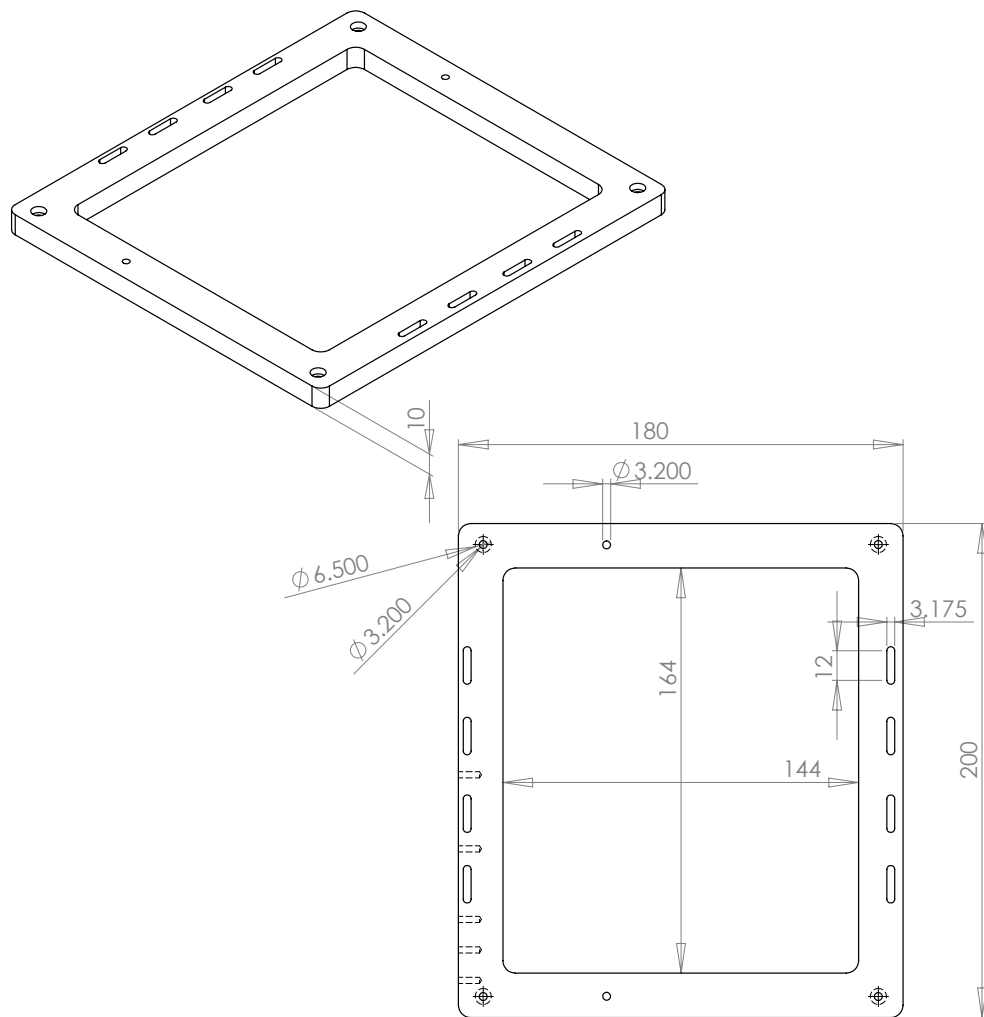


Figure A.8: Dimensions of the top frame in [mm]

Appendix B

Kinematics and Dynamics of the Haptic Handle

In this Appendix, the forward kinematics, inverse kinematics, Jacobian, and dynamic equations for the haptic handle are given. The frames assigned to this handle are shown in Fig. B. For this manipulator, l_i and m_i are the length and mass of the i -th link, respectively ($i = 1$ to 3). θ_i , $\dot{\theta}_i$, and $\ddot{\theta}_i$ are the angle, speed, and acceleration of the i -th joint. g is the gravitational acceleration.

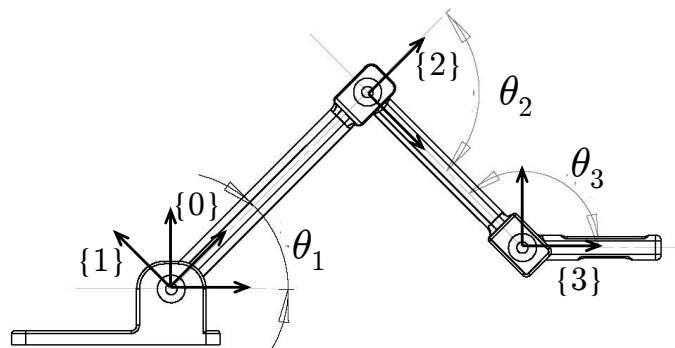


Figure B.1: Assigned frames to the haptic handle.

B.1 Kinematics

The Denavit-Hartenberg (DH) parameters of the haptic handle are given in Table B.1.

Table B.1: DH Parameters of Haptic Handle

i	1	2	3
Link Twist, α_{i-1}	0	0	0
Link Length, a_{i-1}	0	$l_1 = 0.100\text{m}$	$l_2 = 0.079\text{m}$
Link Offset, d_i	0	0	0
Joint Angle, θ_i	θ_1	θ_2	θ_3

The transformation matrices are as follows:

$${}^0_1T = \begin{bmatrix} \cos(\theta_1) & -\sin(\theta_1) & 0 & 0 \\ \sin(\theta_1) & \cos(\theta_1) & 0 & 0 \\ 0 & 0 & 1 & 0 \\ 0 & 0 & 0 & 1 \end{bmatrix} \quad (\text{B.1})$$

$${}^1_2T = \begin{bmatrix} \cos(\theta_2) & -\sin(\theta_2) & 0 & l_1 \\ \sin(\theta_2) & \cos(\theta_2) & 0 & 0 \\ 0 & 0 & 1 & 0 \\ 0 & 0 & 0 & 1 \end{bmatrix} \quad (\text{B.2})$$

$${}^2_3T = \begin{bmatrix} \cos(\theta_3) & -\sin(\theta_3) & 0 & l_2 \\ \sin(\theta_3) & \cos(\theta_3) & 0 & 0 \\ 0 & 0 & 1 & 0 \\ 0 & 0 & 0 & 1 \end{bmatrix} \quad (\text{B.3})$$

As a result, the planar position of the end effector (*i.e.*, origin of frame {3}) is given by,

$${}^0_3P = \begin{bmatrix} x \\ y \end{bmatrix} = \begin{bmatrix} l_2(\cos(\theta_1)\cos(\theta_2) - \sin(\theta_1)\sin(\theta_2)) + l_1\cos(\theta_1) \\ l_2(\sin(\theta_1)\cos(\theta_2) + \cos(\theta_1)\sin(\theta_2)) + l_1\sin(\theta_1) \end{bmatrix} \quad (\text{B.4})$$

B.2 Inverse Kinematics

The inverse kinematics of the manipulator, based on it's geometries is given by

$$\theta_2 = \pm \arccos\left(\frac{x^2 + y^2 - l_1^2 - l_2^2}{2l_1l_2}\right) \quad (\text{B.5})$$

and

$$\theta_1 = \begin{cases} \beta - \psi & : \theta_2 > 0 \\ \beta + \psi & : \theta_2 \leq 0 \end{cases} \quad (\text{B.6})$$

where,

$$\beta = \arctan\left(\frac{y}{x}\right) \quad (\text{B.7})$$

and

$$\psi = \arccos\left(\frac{x^2 + y^2 + l_1^2 - l_2^2}{2l_1\sqrt{x^2 + y^2}}\right) \quad (\text{B.8})$$

B.3 Jacobian

The Jacobian of the system with respect to the base frame {0} is given by

$${}^0J = \begin{bmatrix} -l_1 \sin(\theta_1) - l_2 \sin(\theta_1 + \theta_2) & -l_2 \sin(\theta_1 + \theta_2) \\ l_1 \cos(\theta_1) + l_2 \cos(\theta_1 + \theta_2) & l_2 \cos(\theta_1 + \theta_2) \end{bmatrix} \quad (\text{B.9})$$

B.4 Dynamics

The dynamics of the system are as follows:

$$\tau = M(\theta)\ddot{\theta} + V(\theta, \dot{\theta}) + G(\theta) \quad (\text{B.10})$$

where,

$$M(\theta) = \begin{bmatrix} m_2 l_2^2 + 2l_1 l_2 m_2 \cos(\theta_2) + (m_1 + m_2) l_1^2 & m l_2^2 + l_1 l_2 m_2 \cos(\theta_2) \\ m_2 l_2^2 + l_1 l_2 m_2 \cos(\theta_2) & m_2 l_2^2 \end{bmatrix} \quad (\text{B.11})$$

and

$$V(\theta, \dot{\theta}) = \begin{bmatrix} -m_2 l_1 l_2 \sin(\theta_2) \dot{\theta}_2^2 - 2m_2 l_1 l_2 \sin(\theta_2) \dot{\theta}_1 \dot{\theta}_2 \\ m_2 l_1 l_2 \sin(\theta_2) \dot{\theta}_2 \end{bmatrix} \quad (\text{B.12})$$

and

$$G(\theta) = \begin{bmatrix} m_2 l_2 g \cos(\theta_1 + \theta_2) + (m_1 + m_2) l_1 g \cos(\theta_1) \\ m_2 l_2 g \cos(\theta_1 + \theta_2) \end{bmatrix} \quad (\text{B.13})$$

Curriculum Vitae

Name:	Nima Najmaei	
Post-secondary Education and Degrees:	B.Sc, Shiraz University Shiraz Iran	2002-2006
	M.E.Sc, University of Western Ontario London, Ontario, Canada	2007-2009
	Ph.D., University of Western Ontario London, Ontario, Canada	2009-2014
Selected Honors and Awards:	NSERC Canada Graduate Scholarship (CGS-D)	2009-2012
	Ontario Graduate Scholarship (OGS)	2012-13
	Queen Elizabeth II Scholarship in Science and Technology	2012-13
	NSERC CREATE CAMI Program stipend Scholarship	2012-13
	Outstanding Presentation Award, ECE Graduate Symposium	2013
	Western GTA Union Academic Achievement Scholarship	2012
	Western GTA Union Outstanding Research Award	2011
	Western Graduate Thesis Research Award	2008,09,10,11
	3 rd place, Annual Iranian Students Research Competition	2007-2008
	Graduated with distinction from Shiraz University	2006
Related Work Experience:	Research Assistant Canadian Surgical Technologies and Advanced Robotics (CSTAR)	2009-2014
	Teaching Assistant University of Western Ontario	2007-2014
	Research Assistant University of Western Ontario	2007-2009
	Research Assistant Shiraz University	2005-2007

Publications:

Book Chapter:

– **Najmaei N.**, Kermani M.R., Pre-Collision Planning and Control Strategies for Physical Human-Robot Interactions, to appear in *New Development of Manufacturing Robotic Systems*, Bentham Science, ISBN: 978-1-60805-281-3, 2011

Journal Papers:

– **Najmaei N.**, Asadian A., Kermani M.R., Patel R.V., Design of a Haptic Interface for Medical Applications using MRF-based Actuators, *IEEE Transactions on Mechatronics*, submitted, 2014

– **Najmaei N.**, Kermani M.R., Patel R.V., Suitability of Small-Scale Magneto-Rheological Fluid Based Clutches in Haptic Interfaces for Improved Performance, *IEEE Transactions on Mechatronics*, in Press, 2014

– Azizian M., **Najmaei N.**, Khoshnam M., Patel R.V., Visual Servoing in Medical Robotics; Part II: Tomographic Imaging Modalities: Techn. and Apps., *International Journal of Medical Robotics and Computer-Assisted Surgery*, In Press, Accepted January 2014

– Azizian M., Khoshnam M., **Najmaei N.**, Patel R.V., Visual Servoing in Medical Robotics; Part I: Endoscopic and Direct Vision Imaging: Techn. and Apps., *International Journal of Medical Robotics and Computer-Assisted Surgery*, In Press, Accepted August 2013

– **Najmaei N.**, Mostafavi S.K., Shahbazi S., Azizian M., Image-Guided Techniques in Renal and Hepatic Interventions, *International Journal of Medical Robotics and Computer-Assisted Surgery*, Vol. 9(4), pp. 379-95, December 2013

– **Najmaei N.**, Kermani M.R., Al-Lawati M., A New Sensory System for Modeling and Tracking Humans within Industrial Work Cells, *IEEE Transactions on Instrumentation and Measurement*, Vol. 60(4), pp. 1227-1236, April 2011

– **Najmaei N.**, Kermani M.R., Applications of Artificial Intelligence in Safe Human-Robot Interaction, *IEEE Transactions on System, Man, and Cybernetics – Part B*, Vol. 41(2), pp. 448-459, April 2011

– **Najmaei N.**, Kermani M.R., On Superquadric Human Modeling and Risk Assessment for Safe Planning of Human-Safe Robotic Systems, *ASME Journal of Mechanisms and Robotics*, Vol. 2(4), November 2010

– **Najmaei N.**, Kermani M.R., A Streamlined Search Algorithm for Path Modifications of a Safe Robot Manipulator, *Paladyn Journal of Behavioral Robotics (Springer Verlag)*, Vol. 1(2), pp. 130-140, 2010

– Shames I., **Najmaei N.**, Zamani M., Safavi A.A., A New Intelligent and Adaptive Traffic Shaper for High Speed Networks, *International Journal of Information Science and Technology*, Vol. 5, 67-82, July 2007

Conference Papers:

– **Najmaei N.**, Asadian A., Kermani M.R., Patel R.V., Design and Evaluation of a Prototype Two-DOF Haptic Interface for Medical Applications based on Magneto-Rheological Actuation, Submitted to *IEEE International Conference on Robotics and Automation ICRA15*, Seattle WA, May

26-30, 2015

- **Najmaei N.**, Asadian A., Kermani M.R., Patel R.V., Magneto-Rheological Actuators for Haptic Devices: Design, Modeling, Control, and Validation of a Prototype Clutch, Submitted to IEEE International Conference on Robotics and Automation ICRA15, Seattle WA, May 26-30, 2015
- **Najmaei N.**, Yadmellat P., Kermani M.R., Patel R.V., Application of Magneto-Rheological Fluid Based Clutches for Improved Performance in Haptic Interfaces , IEEE International Conference on Robotics and Automation ICRA14, Hong Kong, June 1-4, 2014
- **Najmaei N.**, Kermani M.R., An Accurate and Computationally Efficient Method for Whole-Body Human Modeling with Applications in HRI, IEEE International Conference on Robotics and Automation ICRA11, Shanghai, China, May 9-13, 2011
- **Najmaei N.**, Kermani M.R., Prediction-Based Reactive Control Strategy for Human-Robot Interaction, in Proc. of IEEE International Conference on Robotics and Automation ICRA10, Anchorage AL, USA, May 3-8, 2010
- **Najmaei N.**, Kermani M.R., Superquadric Obstacle Modeling and a Danger Evaluation Method with Application in Human-Safe Industrial Robots, in Proc. of the 2nd Annual IEEE International Conference on Technologies for Practical Robot Applications TePRA09, Woburn MA, USA, November 9-10, 2009
- **Najmaei N.**, Kermani M.R., Optimal Safe Planning Using a Danger Evaluation Method, in Proc. of the 14th IASTED International Conference on Robotics and Applications RA09, Cambridge MA, USA November 21-24, 2009
- Shames I., **Najmaei N.**, Zamani M., Safavi A.A., Application of Reinforcement Learning in Development of a New Adaptive Intelligent Traffic Shaper, in Proc. of the 5th IEEE International Conference on Machine Learning and Applications ICMLA06, Pittsburgh PA, USA, June 25-29, 2006
- Shames I., **Najmaei N.**, Zamani M., Safavi A.A., A New Intelligent Traffic Shaper for High Speed Networks, in Proc. of 18th IEEE International Conference on Tools with Artificial Intelligence IC-TAI06, Washington DC, USA, November 13-15, 2006